Interrogating the function of chromatin modifying enzymes in TRAIL response of GBMs

by

İbrahim Çağrı Kurt

A Thesis Submitted to the
Graduate School of Sciences and Engineering
in Partial Fulfillment of the Requirements for
the Degree of

Master of Science
in
Molecular Biology and Genetics

Koç University

June 2015

ABSTRACT

Glioblastoma multiforme (GBM) is an aggressive brain cancer with very limited treatment options. Average survival rate of the patients diagnosed with GBM is around 12 months. The invasive nature of GBMs and the presence of the blood brain barrier (BBB) that limits the delivery of therapeutic agents are among the obstacles for the poor prognosis of GBMs. Surgical resection of the intracranial tumors are also limited due to safety concerns. Tumor-necrosis-factor related apoptosis-inducing ligand (TRAIL) is a promising therapeutic bioagent that can target invasive GBM cells in the brain when delivered locally, and program tumor cells for cell death while leaving healthy cells untouched. However, a major obstacle against TRAIL-based therapies is that different tumor cells of a single tumor tissue or different tumors, exhibit differential sensitivity against TRAIL. This highly versatile behavior of the tumor cells is believed to be due to differential regulation of apoptosis mediators.

Emerging evidence suggests that TRAIL-resistance is associated with the aberrant expression of the key components of the apoptotic program. However, how these components are regulated at an epigenetic level is not understood. Since transcription levels of all genes are tightly regulated under the control of master transcription factors in concert with epigenetic modifying enzymes, we conducted a short-hairpin RNA (shRNA) screen to assess the function of chromatin modifying-enzymes and aimed to identify novel chromatin-based mechanisms regulating the TRAIL response. We employed 2-3 shRNAs/gene to interrogate the role of 47 genes in DNA and histone modification pathways. Accordingly, we tested shRNAs targeting DNA-methyltransferases (DNMTs), Histone-Methyltransferases (HMTs), Histone demethylases (HDMs), Methyl-DNA binding proteins, and Polycomb complex members (PrC). Upon infection with individual shRNAs, GBM cells were tested for their TRAIL response using viability assays.

As a result, we identified KDM2B and RING1A, an H3K36-specific demethylase and a E3 ubiquitin-protein ligase of H2AK119 respectively, as novel regulators of TRAIL response. We then focused our studies on KDM2B. Accordingly, silencing of KDM2B significantly enhanced TRAIL sensitivity, and activated caspase-8, caspase-3, caspase-7. Also, KDM2B knockdown accelerated the apoptosis process, as revealed by live cell imaging and real-time cell analyses. Moreover, simultaneous knockdown of the methyltransferases responsible for catalyzing the reverse modification of KDM2B significantly recovered the cell death phenotype observed with KDM2B inhibition. In order to decipher the downstream molecular pathways regulated by KDM2B, we examined the expression levels of apoptosis-related genes by RNA-seq and quantitative RT-PCR and observed de-repression of pro-apoptotic

genes HRK, caspase-7, DR4 and repression of anti-apoptotic gene Mcl-1 upon KDM2B silencing. We also observed that KDM2B-silenced tumors exhibited slower growth compared to controls *in vivo.*

Taken together, our findings suggest a novel mechanism, where the key apoptosis components are under epigenetic control of KDM2B in GBM cells. Therefore, identifying the direct DNA targets of KDM2B might provide a new understanding of apoptosis response in GBMs and aid in the design of successful pro-apoptotic therapies.

ÖZET

Glioblastoma multiforme (GBM), çok kısıtlı tedavi opsiyonları olan agresif bir beyin kanseridir. GBM hastalarının yaşam süreleri tanı sonrası 12 ay civarındadır. GBM, invaziv doğasından ve kan beyin bariyerinin (KBB) teröpatik ajanlara karşı limitli geçirgen yapısından dolayı zayıf bir prognoz sergilemektedir. Intrakranial tümörlerin cerrahi rezeksiyonu da güvenlik kaygıları nedeniyle sınırlıdır. Tümör-nekroz-faktör ilişkili apoptoz indükleyici ligand (TRAIL), sağlıklı hücrelere zarar vermeden sadece tümör hücrelerini hedef alarak programlı hücre ölümünü tetiklediği için ümit verici bir teröpatik ajandır. Buna rağmen, TRAIL-bazlı tedavilerde karşılaşılan büyük engellerden biri farklı tümör doku hücrelerinin TRAIL'a karşı farklı duyarlılık göstermeleridir. Tümör hücrelerinin bu yüksek değişken davranışı, TRAIL direncinde farklı seviyelere yol açan, apoptozda rol alan elemanların farklı düzenlenmesinden kaynaklanmaktadır.

Ortaya çıkan sonuçlar, TRAIL-direnci ile apoptotik programın temel bileşenlerinin anormal ifadesi arasında bir ilişki olduğunu göstermektedir. Bununla birlikte, bu komponentlerin epigenetik seviyede nasıl düzenlendikleri henüz tam olarak bilinmemektedir. Bütün genlerin transkripsiyon düzeyinde sıkıca kontrol edilmeleri, epigenetik modifiye edici enzimler ile uyum içerisinde çalışan ana transkripsiyon faktörlerinin denetimi altında olduğu için, kromatin modifiye-edici enzimlerin fonksiyonlarını değerlendirmek ve TRAIL yanıtını düzenleyen kromatin-bazlı yeni mekanizmaları tanımlamak amacıyla bir "short-hairpin RNA" (shRNA) taraması gerçekleştirildi. DNA'da ve histon modifikasyon yolağındaki 47 genin rolünü sorgulamak için 2-3 shRNA/gen kullanıldı. Buna dayanarak; DNA-metiltransferazları (DNMTs), Histon-metiltransferazları (HMTs), Metil-DNA bağlayıcı proteinleri ve Polikomb kompleks üyeleri (PrC) test edildi. Birbirinden farklı shRNA'ların enfekte edilmesi ile, U87MG hücrelerinde TRAIL cevabı canlılık deneyleri ile test edildi.

Sonuç olarak, sırasıyla bir H3K36-spesifik demetilaz ve bir H2AK119'un E3 ubikitin-protein ligazı olan KDM2B ve RING1A'yı TRAIL cevabında yeni bir düzenleyici olarak tanımlandı. Çalışmalarımızda KDM2B'ye odaklanıldı. Buna göre, KDM2B'nin susturulması TRAIL duyarlılığını, kaspaz-8, kaspaz-3, kaspaz-7 ve kesilmiş PARP'ı anlamlı bir biçimde artırdı. KDM2B susturulmasının apoptotik süreci hızlandırdığı canlı hücre görüntüleme ve gerçek zamanlı hücre analizi deneyleri ile ortaya konuldu. Ayrıca, eş zamanlı olarak KDM2B'nin tersine modifikasyonunun katalizlenmesinden sorumlu metiltransferazların susturulmasının, KDM2B inhibisyonuyla gerçekleşen fenotipi geri döndürdüğü gözlendi. KDM2B tarafından düzenlenen moleküler yolağı deşifre etmek amacıyla, apoptozla ilişkili genlerin ekspresyon seviyelerini RNA-sekanslama ve kantitatif RT-PCR ile test edildi ve

KDM2B'nin susturulması ile pro-apoptotik genler olan HRK, DR4 ve kaspaz 7'nin arttığı ve anti-apoptotik gen Mcl-1'in baskılandığı gözlemlendi. İmmün-baskılanmış farelere yapılan deri altı susturulmuş-KDM2B ve kontrol hücre enjeksiyonları da KDM2B'nin tümör büyümesini ve anjiyogenezi anlamlı şekilde etkilediğini gösterdi.

Birlikte ele alındığında, bulgularımız GBM hücrelerinde yeni bir mekanizmayı; apoptozun kilit bileşenlerinin KDM2B'nin epigenetik kontrolü altında olduğunu önermektedir. Dolayısıyla, KDM2B'nin doğrudan DNA hedeflerinin belirlenmesi, GBM'lerde apoptoz yanıtının anlaşılmasında ve başarılı bir pro-apoptotik terapi tasarımının yardımında yeni bir anlayış sağlayabilir.

ACKNOWLEDGEMENTS

He always helped me. I can never mention enough to pay back.

None of these data and information in this thesis would be possible without unending support of my outstanding advisor Dr. Tuğba Bağcı-Önder. She, not only clearly exemplified how to be a careful and organized scientist, but also taught me how to survive in the competitive environment of science by multi-tasking. She truly behaved me as if I was her son both in my personal and scientific life, especially during PhD applications. I will always remember and be grateful for her utmost guidance.

I would like to express my gratitude to Drs. Stephan Knierer and Ertugrul Ozbudak. Without their initial momentum, this unpolished stone wouldn't have rolled this far. Second, being the wise and patience fatherly figure with good humor in my lovely Santa Cruz life, I want to thank Dr. David Feldheim for everything he taught me about life and science.

Dr. Nathan Lack deserves a special thanks for enduring my everlasting scientific, and sometimes unscientific, inquiries and trying to satisfy my monstrous hunger by his answers. Dr. Tamer Onder always welcomed me into his office and clarified my blurry vision with his calm and wise advices. From the moment I met till the end of my days in Koç University, Dr. Gülayşe İnce-Dunn constantly answered my questions with a smile on her face. Dr. Mazhar Adlı was too kind to accept me into his lab to teach me new techniques and give me precious advices. Drs. İhsan Solaroğlu, Cory Dunn, Halil Kavaklı, Nurhan Özlü, Serçin Karahüseyinoğlu, Nuray Ulusu and Nihal Gülseren Çakmakçı always appreciated my small successes. I will always be indebted to them for making my life easier during sometimes-can-be-very-overwhelming Master's studies.

M. Haroon Qureshi defined me the honest meaning of brotherhood. He made his name equivalent to sacrifice, altruism and generosity in my heart and mind. Sleep-deprived, he coached and helped me at every step of my life and PhD applications. I do not bear a single doubt that we will be together in both worlds. Thus, I am not in a time crunch to show him my appreciation.

Tolerating my moody life, Derya Kabacaoğlu, my soul friend, did more than she can do to support me physically and mentally. Ömer Faruk Ağca always had the time and energy to meet me in other realms whenever I needed. Without their encouragement and good wishes, I would be one big piece missing.

This thesis is exclusively dedicated to the Kurt family. Words lack the meaning to demonstrate my gratitude to them. My parents Drs. Cemile and Necmi Kurt, my siblings

Serdar Kurt, Dr. Kübra Neslihan Kurt and Melike Kurt have never let their love down for a single second. They were always understanding and polite towards their odd and reckless son and brother. I love them.

Last but not the least, transforming my Master's life into a fantastic experience, I appreciate even the presence of my following colleagues: Zeynep Kahya, Hakan Cengiz, Ahmet Cingöz, Fatma Özgün, Pelin İspir, Ezgi Kaya, my roommate Uğur Gatfar, Zeynep Kaya, Filiz Şenbabaoğlu, Selena Kazancıoğlu, Burcu Özçimen, Deniz Uğurlu, Anıl Kaplan, Elifnur Erdem, Kubilay Kaymaz, Nur Zeynep Ay, Sencer Göklemez, Mehmet Uğur Girgin, Alp Erkent, Gülnihal Kavaklıoğlu, Hilal Saraç, Gizem Nur Şahin, Gizem Güzelsoy, Cansu Akkaya, Ayyub Ebrahimi, Kerem Fidan, Fidan Şeker, Ezgi Özyerli, Nil Grünberg, Gülben Gürhan, Ceren Şeref, Nazlı Ataç, Gamze Bildik, Elif Nurtop, Nastaran Langarizadeh, Levent Elmas, Aslı Azizoğlu, Eda Süer, Can Aztekin, Merve Özgür, Duygu Payzın, Eylem Külköylüoğlu, Sibel Çal, Gülkız Baytek, Bahriye Erkaya, Ekin Güney, Emel Akdoğan, Esra Ünsal, Erdem Sanal, Deniz Çonkar, Büşra Harmanda, Gökhan Güner, Sina Mojtahedi, Ahmet Kocabay, Görkem Özyurt and Bihter Borak.

Throughout these 2 years, TÜBİTAK 2210-E "Doğrudan Yüksek Lisans Burs Programı" and Koc University School of Medicine financially supported me.

It wouldn't be possible to end my acknowledgement without mentioning the humble heroes behind the curtain, who were always there ready for help. I want to thank Emine Büyükdurmuş, Gözde Şirin, Gizem Işık, Pınar Yazıcı Yaman and Merve Çiğdem Atsu for constructing bridges between graduate students and the administration. I want to thank Gülizar Batu and Zöhre Şahin for their underrecognized crucial roles in our academic lives.

"*Just because you can't see something, doesn't mean it doesn't exist Ibrahim.*" said my first post-doc supervisor in the lab, while I was trying to see plasmids in a tube. I dedicate this thesis to my family and to people who believe in the *unseen* to help humanity.

TABLE OF CONTENTS

List of Tables xii

List of Figures xiii

Nomenclature xvi

Chapter 1: Review of the Literature 1

1. Brain cancers and glioblastoma multiforme 1
2. Chemotherapeutic treatment and resistance 3
3. Apoptosis and TRAIL resistance 5
4. Epigenetics and chromatin modifying enzymes 8
5. KDM2B as a chromatin modifying enzyme 15

Chapter 2: Materials & Methods 22

1. Cell culture 22
2. Production of TRAIL in 293T cells 22
3. TRAIL ELISA 22
4. Cloning of the shRNA constructs 23
5. Production of viral supernatants 27
6. shRNA-screen for TRAIL response 27
7. Cell viability 27
8. Caspase activity assays 28
9. Quantitative real-time PCR 28
10. Histone extraction 31
11. Western blotting 31

12. Real-Time Cell Growth Analysis 32

13. Live-cell microscopy 33

14. RNA-seq library preparation and sequencing analysis 34

15. Statistical and functional analysis of the RNA-seq data and differentially expressed gene identification 34

16. In vivo experiments 35

17. Immunohistochemistry 36

18. Beta-galactosidase staining 36

19. Flow cytometric analysis of cell cycle with propidium iodide 37

20. Chromatin Immunoprecipitation 37

21. Statistical analysis 39

Chapter 3: Results 40

1. shRNA screen reveals KDM2B and RING1A as modulators of TRAIL-induced apoptosis in GBM cells 40
2. shRNAs can knockdown their targets efficiently 43
3. KDM2B can be successfully silenced at both transcriptional and translational levels 44
4. Knockdown of KDM2B does not affect the expression of other KDM family members 45
5. Loss of KDM2B cooperates with TRAIL to reduce GBM cell viability 46
6. KDM2B loss accelerates TRAIL-induced cell death 47
7. Silencing of KDM2B does not affect healthy human fibroblasts 49
8. Silencing KDM2B sensitizes GBM cells to TRAIL-induced apoptosis 50
9. Inhibition of caspases protects cells from TRAIL induced cell death 51
10. RNA-seq analysis of shControl vs shKDM2B cells 52
11. KDM2B regulates expression of apoptosis related genes 59

12. Loss of Harakiri partially reverses the shKDM2B phenotype 61

13. Co-silencing of H3K36-specific HMTs partially rescues the phenotype 62

14. Loss of KDM2B slows down cell proliferation in vitro in long-term 65

15. Loss of KDM2B attenuates tumor growth in vivo 65

Chapter 4: Discussion 68

Appendix I 74

1. Cloning and validation of KDM2B overexpression constructs 74
2. Generation of RNAi resistant and domain deleted KDM2B overexpression vectors 80
3. CRIPR-induced knock-out of KDM2B in GBM cells 81

Appendix II 84

1. Validation of RING1A as another hit in the shRNA screen 84

Appendix III 86

1. KDM2B interacts with CpG Islands of HRK 86

Appendix IV 87

1. Bcl-2 protects shKDM2B cells from TRAIL induced apoptosis 87

Appendix V 88

1. KDM2B and its regulation of senescence induced morphology 88

Appendix VI 90

1. MS-275 treatment downregulates KDM2B and upregulates HRK 90

Bibliography 91

Vita 100

LIST OF TABLES

Table 1. List of genes targeted in the shRNA screen 23

Table 2. List of primers used in q-RT-PCR and their sequences 28

Table 3. List of primary antibodies used 32

Table 4. Custom gene list of the differentially expressed apoptosis-related genes from RNA-Seq data 58

Table 5. List of gRNA cloning and diagnosing primers and their sequences 82

LIST OF FIGURES

Figure 1. Tumorigenesis of primary and secondary GBMs 2

Figure 2. MRI of a GBM patient 3

Figure 3. IDH1 → 2-OG → TET → DNA demethylation axis 5

Figure 4. Intrinsic and extrinsic apoptosis pathways 7

Figure 5. Miregulated extrinsic apoptotsis pathway in cancer 8

Figure 6. Selected KDM family members and their activities on selected histone tails 11

Figure 7. Epigenetic regulating proteins dysregulated in cancers 12

Figure 8. Clinical and preclinical drugs targeting chromatin modifying enzymes 13

Figure 9. List of KDM family proteins and their expressional regulations in malignancies 15

Figure 10. Protein diagrams of KDM2 members displaying domains and isoforms 17

Figure 11. Diagram showing canonical and non-canonical (variant) PRC1 complexes interacting with KDM2B 21

Figure 12. Experimental setup for the shRNA screen in U87MG cells 39

Figure 13. Percent viability analysis of the untreated cells after shRNA infection 40

Figure 14. The analysis strategy for the shRNA screen 41

Figure 15. Percent change in viability analyses of the infected cells upon TRAIL treatment 41

Figure 16. Top shRNA hits as TRAIL sensitizer 42

Figure 17. q-RT-PCR analysis of the top-hit target genes 43

Figure 18. q-RT-PCR and western analysis of KDM2B in shKDM2B transduced cells 44

Figure 19. q-RT-PCR analysis of KDM family members in shKDM2B transduced cells 45

Figure 20. Viability analyses of GBM cells after KDM2B knockdown 46

Figure 21. Real-time viability analysis of the shKDM2B cells upon TRAIL treatment 47

Figure 22. Images of shKDM2B cells at different time points after TRAIL treatment and real-time quantification of apoptotic bodies 47-48
Figure 23. Viability analysis of KDM2B silenced healthy human BJ fibroblasts 49
Figure 24. Caspase 3/7 and 8 activity analysis, and western blotting analyses of apoptotic hallmark proteins in shKDM2B cells 50
Figure 25. Viability analysis of caspase inhibitor treated shKDM2B cells after TRAIL treatment 51
Figure 26. Quality check of the RNA samples for RNA-seq 52
Figure 27. Representative quantification of the quality of one of the RNA samples for RNA-seq 53
Figure 28. Quality check of the RNA libraries of the RNA-seq samples 54
Figure 29. Representative quantification of the quality of one of the RNA libraries for RNA-seq 55
Figure 30. A list of the diseases and functions that changed significantly upon KDM2B knockdown 56
Figure 31. q-RT-PCR validation of the deregulated apoptosis-related genes from the selected apoptosis genes 59
Figure 32. Viability analyses of HRK and KDM2B knockdown cells upon TRAIL treatment 60
Figure 33. Viability analysis of KDM2B, SMYD2, NSD1, ASH1L and SETD2 knockdown cells 62
Figure 34. Long-term in vitro real-time growth analysis of shKDM2B cells 64
Figure 35. Bioluminescence analysis of labeled shKDM2B cells in vitro and long-term growth analysis of shKDM2B tumors in vivo 65
Figure 36. Immunohistochemistry analysis of the removed shKDM2B tumors 66
Figure 37. Schematic representation of H3K36 methylation and demethylation cascade 66
Figure 38. Plasmid map of pCAG-hKDM2B 72
Figure 39. q-RT-PCR analysis of pCAG-hKDM2A and pCAG-hKDM2B constructs in transfected 293T cells 73
Figure 40. q-RT-PCR analysis of pLenti-KDM2B constructs in 293Ts 73
Figure 41. Western blot analysis of KDM2B constructs transfected in 293T cells 74

Figure 42. q-RT-PCR and western blot analysis of pLenti-KDM2B constructs infected into U87MG cells 75
Figure 43. Plasmid map of pLenti-PGK-Puro-DEST vector with KDM2B cloned in it 76
Figure 44. Plasmid map of retroviral pBabe-puro-KDM2B vector 77
Figure 45. Western blot analysis of pBabe-KDM2B constructs in U87MG and 293T cells 77
Figure 46. Brightfield images of KDM2B knocked-down and overexpressing U87MG cells 78
Figure 47. Viability analysis of U87MG and LN18 cells overexpressing KDM2B by the pBabe construct 79
Figure 48. Western blotting analysis of KDM2B by anti-FLAG antibody 80
Figure 49. Reverse-PCR strategy for domain deletions in KDM2B 80
Figure 50. Genomic map of KDM2B and gRNAs targeting exons 81
Figure 51. Plasmid map lentiCRISPR vector 81
Figure 52. Diagnostic cut of exon 4 at day 10 after gRNA infection 82
Figure 53. Western blot analysis in different time points of gRNA infected U87MG cells 82
Figure 54. q-RT-PCR analysis of RING1A in shRING1A U87MG cells 83
Figure 55. Viability analysis of RING1A and KDM2B knocked-down U87MG cells 84
Figure 56. ChIP-qPCR analysis of CGIs of HRK against KDM2B 8
Figure 57. Viability analysis and fluorescent images of Bcl-2 overexpressing shKDM2B cells 86
Figure 58. Representative images of X-gal staining of shKDM2B cells 87
Figure 59. Cell cycle analysis of shKDM2B cells by flow cytometry 88
Figure 60. q-RT-PCR analysis of KDM2B and HRK in MS-275 treated U87MG cells 89

NOMENCLATURE

2-HG	2-hydroxyglutarate
2-OG	2-oxoglutarate
APAF-1	Apoptotic protease activating factor 1
BBB	Blood-Brain-Barrier
BCL2	B-cell lymphoma 2
Caspase	cysteine-aspartic proteases
CGI	CpG islands
CME	Chromatin modifying enzyme
CNS	Central Nervous System
DCR	Decoy receptor
DNMT	DNA methyltransferase
DR4/5	Death receptor 4/5
EZH2	enhancer of zeste 2
FDA	Food and Drug Administration
Fluc	Firefly luciferase
FMC	Fluc-mCherry
GBM	Glioblastoma multiforme
H&E	Hematoxylin and eosin
H2AK119ub	Histone 2A Lysine 119 mono-ubiquitin
H3K27me3	Histone 3 Lysine 27 trimethyl
H3K36me3	Histone 3 Lysine 36 trimethyl
HAT	Histone acetyltransferase
HDAC	Histone deacetylase
HDMT	Histone demethylase
HMT	Histone methyltransferase
HRK	Harakiri
IAP	Inhibitor of Apoptosis
IDH	Isocitrate dehydrogenase
Ink4/Arf	Ihibitors of CDK4
JmjC	Jumonji C
KDM2B/FBXL10/JHDM1B/NDY1	Lysine (K)-Specific Demethylase 2B
LRR	Leucine-Rich Repeat
LSD	lysine (K)-specific demethylase
MEF	Mouse embryonic fibroblast
mESC	Mouse embryonic stem cell
miRNA	microRNA
MOMP	Mitochondrial outer membrane permeabilization
MoMuLV	Moloney Murine Leukemia Virus
NOD/SCID	Nonobese diabetic/severe combined immunodeficiency
PARP	Poly [ADP-ribose] polymerase
PRC	Polycomb repressive complex
q-RT-PCR	Quantitative real-time PCR
RING1A/B	ring finger protein 1
RNA-seq	RNA sequencing
shRNA	short-hairpin RNA

Smac/DIABLO	Second Mitochondria-Derived Activator Of Caspase
TMZ	Temozolomide
TNF	Tumor necrosis factor
TRAIL	TNF-related apoptosis inducing ligand
TSS	Transcription start site
VEGF	Vascular endothelial growth factor
ZnF-CxxC	Zinc finger, CXXC-type

Chapter 1

Review of the Literature

Brain cancers and glioblastoma multiforme (GBM)

Every year around the globe approximately 7 individuals out of 100,000 will be diagnosed with brain tumors [1]. Brain tumors are categorized as primary or metastatic tumors. Metastatic tumors are the tumors that originate outside of the central nervous system (CNS) and then spreads into CNS. The most common cancers that metastasize into CNS are breast, bladder, lung, kidney, lymphoma and melanoma. A 2014 review published in Nature reveals that 7-14 brain metastasis will occur per a population of 100,000 in USA [2].

On the other hand, primary tumors originate in CNS and there are numerous common and rare types. The common ones are namely gliomas, meningiomas and schwannomas. Meningiomas originate from meninges, the membrane surrounding spinal cord and brain, whereas schwannomas originate from the helper schwann cells. Meningiomas are more common than schwannomas [3].

77% of all malignant primary brain tumors are gliomas [4]. Gliomas are the generic name given to tumors originate from certain glial cells, as classified first time 89 years ago [5]. These are namely all 4 different stages of astrocytomas (originate from astrocytes), oligodendrogliomas (originate from oligodendrocytes) and oligoastrocytomas (mixture of astrocytes and oligodendrocytes) [6]. Astrocytomas, according to the World Health Organization, graded into 4: Grade I bening astrocytoma, Grade II low-grade astrocytoma, Grade III anaplastic astrocytoma and Grade IV glioblastoma multiforme (GBM) [7].

GBM can form in two ways: either de novo or by gradual tumorigenesis from lower stages by accumulation of further mutations. The former is defined as primary and latter is defined as secondary GBMs (**Figure 1**).

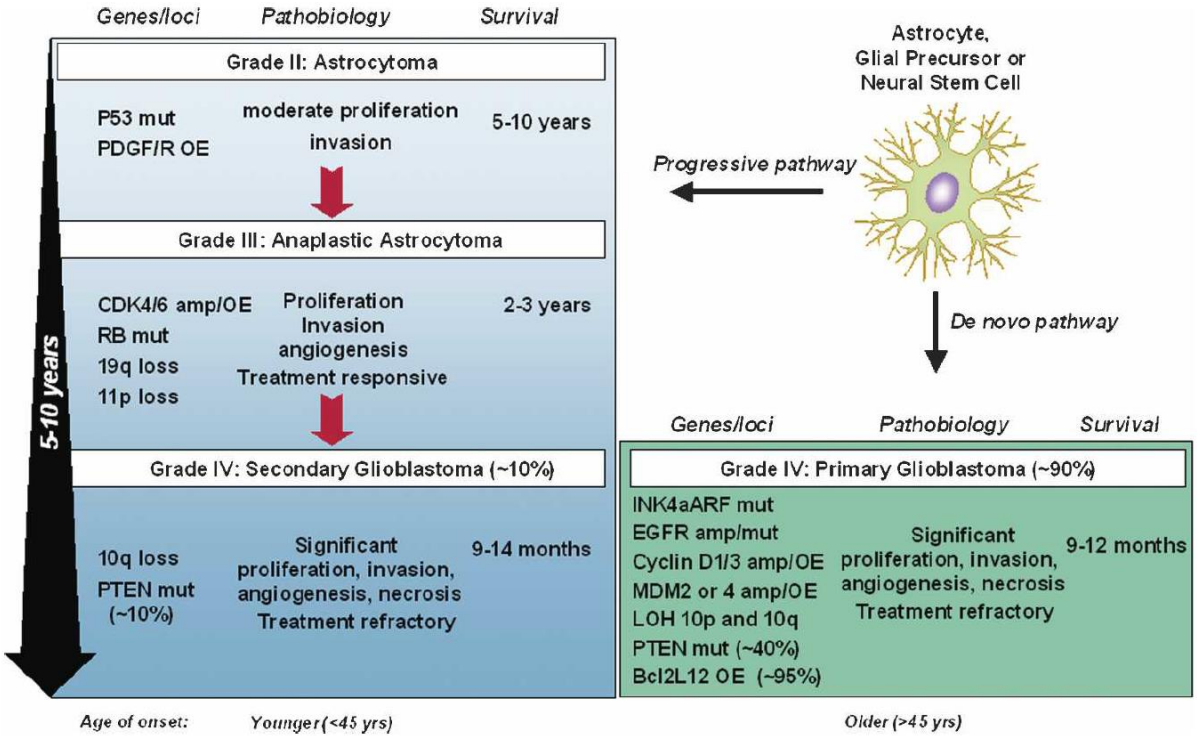


Figure 1. Diagram illustrating development of primary and secondary GBMs. The progressive pathway shows the common acquired mutations by astrocytes during tumorigenesis to GBM [1].

Regardless of being primary or secondary, GBMs being the last stage astrocytic tumors, display invasive and aggressive phenotype. Its mitotic index is dramatically enhanced, compared to its previous grades, which leads to massive proliferation and thus formation of a necrotic core in the middle of the tumor, as one of GBM's hallmarks [8]. One another hallmark of GBM is also related to its increased proliferation. Due to generation of hypoxic environment in the middle parts of the tumor, GBMs starts to demonstrate promoted angiogenic activity. Other hallmarks of GBMs are resistance to drugs, diffuse invasion into parenchyma of brain, genomic instability and resistance to apoptosis [1]. GBM owes its nickname multiforme to its intrinsic morphologic, genetic and epigenetic heterogeneity of intratumor cancer cell populations [9].

In adults, GBM is not only the most common primary brain tumor, but also is the most lethal one [10], due to the 12 months median overall survival of the patients diagnosed with GBM [11]. GBM owes its lethality to its several enabling nature. First, GBM, being a diffuse tumor, can aggressively spread within parenchyma and form microfoci tumors (satellite tumors) that can go undetected by most of current imaging techniques [12]. This fact elevates the rates of recurrent or secondary tumors (**Figure 2**).

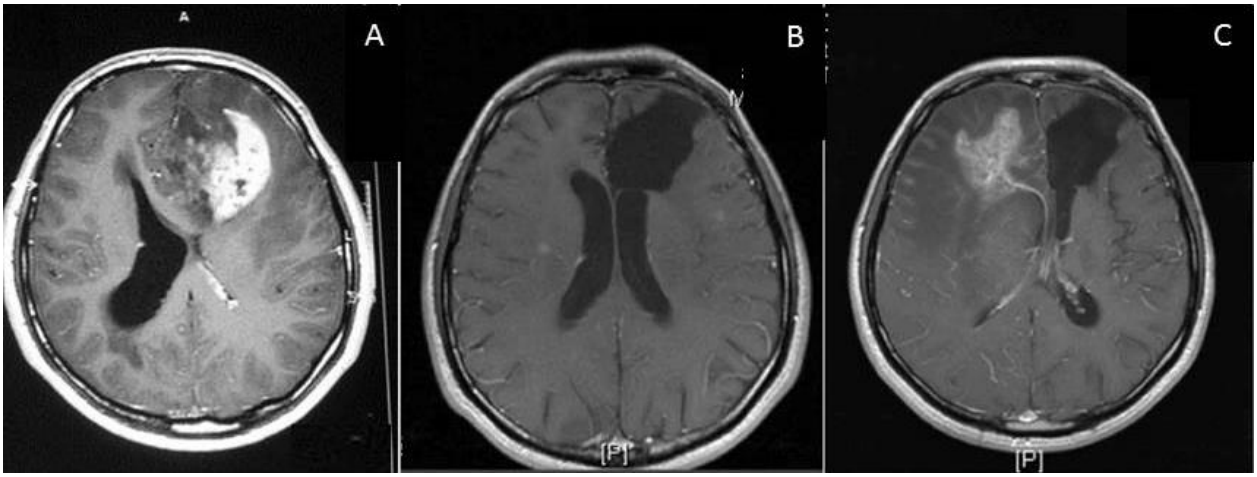


Figure 2. MRI of a GBM patient. A. Before surgery B. After surgery C. Recurrence of tumor after 18 months of therapy (MRI scan, kindly provided by Prof. Dr. Ihsan Solaroglu)

Therapeutic approach for treating GBM generally starts with maximum safe resection, if possible. Although recent advances in specific fluorescent labeling of cancer cells by 5-aminolevulinic acid improves surgeons' accuracy, it is still not possible to eradicate the tumor by surgery, especially without causing damage to the nervous system [13]. Surgery is usually followed by radiotherapy and chemotherapy as adjuvant therapies, though they all fail to improve prognosis significantly [14].

Chemotherapeutic treatment and resistance

Endothelial cells constituting the blood capillaries innervating brain are unusually tightly contacted with each other. On top of that, endothelial cells are further fortified by glial cells and pericytes surrounding them from outside (brain side). Unlike the other veins innervating rest of the body, these veins therefore do not allow leakage of majority of molecules. This security check point is called the blood-brain-barrier (BBB) and its presence is the biggest obstacle hindering discoveries of novel anti-cancer drugs against brain tumours [15]. BBB strictly reduces transfer of ions and any molecules above 200 daltons [16]. A molecule needs to have lipophilic properties and should be free of carrier proteins in the serum, to be able to pass through intracranial endothelial cells. Moreover, the endothelial cells constituting BBB has been shown to express active transporters (p-glycoprotein and multidrug resistance protein) pumping the chemotherapeutic agents out [17].

One of the rare chemotherapeutic agents that can pass BBB and is clinically in use is Temozolomide (TMZ), approved by FDA in 2005 [18]. TMZ is a DNA alkylating agent

methylating the oxygen n 6th position of guanine in DNA. O-6-methylguanine-DNA methyltransferase (MGMT) is a self-sacrificing DNA repair enzyme with capacity to irreversibly transfer the methyl group onto one of its cysteine groups. This is followed by ubiqutination of the used MGMT and proteosomal degradation [19]. When CpG islands of MGMT's promoter are hypermethylated, the gene is silenced [20]. Thus, damaged DNA, in the absence of MGMT, leads to pronounced genomic instability, acquired mutations and eventually cancer cell death. As another hallmark of GBMs, the global hypomethylation of genome but hypermethylation of certain tumor suppressor proteins, such as MGMT, regulates the response of GBMs to TMZ [21]. It has been shown that response of GBMs against TMZ is strongly correlated with hypermethylation status of MGMT gene, while unmethylated MGMT results in poor response to TMZ [22,23]. Unfortunately, GBM recurrence and acquired TMZ resistance are not the only obstacles.

There is also the other side of the coin. Although literature suggests that TMZ increases overall survival for glioma patients, a recent, 2014, meta-mutational analysis of 23 primary gliomas of patients carried out by a UCSF group has forced us to rethink the pros and cons of TMZ. They demonstrated that more than half of the secondary GBMs, which are recurred upon removal of the primary gliomas along with adjuvant TMZ therapy, obtained 20-60 times more mutations, compared to ones that did not receive TMZ therapy. In paper, authors further show that the newly acquired additional mutations carry pre-known TMZ signatures. TMZ is shown to induce clonal selection of cancer cells with somatic mutations in MGMT and abnormal methylation profiles. Leading to TMZ-resistance Therefore, the data clearly suggests that treating lower grade gliomas with TMZ upon resection does increase tumor burden via accumulation of more and alternative mutations [24].

Interestingly, hypermethylation of promoter of MGMT can be regulated by adjusting the balance of available substrates for chromatin modifying enzymes. One such incidence is the recent discovery that around majority of low grade gliomas and some secondary GBMs carry either IDH1 or IDH2 mutation, but never both together [25]. IDH genes code for isocitrate dehydrogenase enzymes which are responsible for production of 2-oxoglutarate (2-OG). 2-OG serves as a co-substrate along with Fe2+ for certain DNA and histone demethylases, such as TET and JmjC domain containing proteins. Mutated IDH enzymes starts generating 2-hydroxyglutarate (2-HG), instead of 2-OG [26]. Hence, upon mutation of IDH1 or IDH2, cytosolic levels of 2-OG reduces and instead 2-HG increases. It has been shown that this results in global hypermethylation, due to inhibition of demethylases requiring 2-OG, and good response correlation against TMZ, due to hypermethylation of MGMT [27,28] (**Figure 3**).

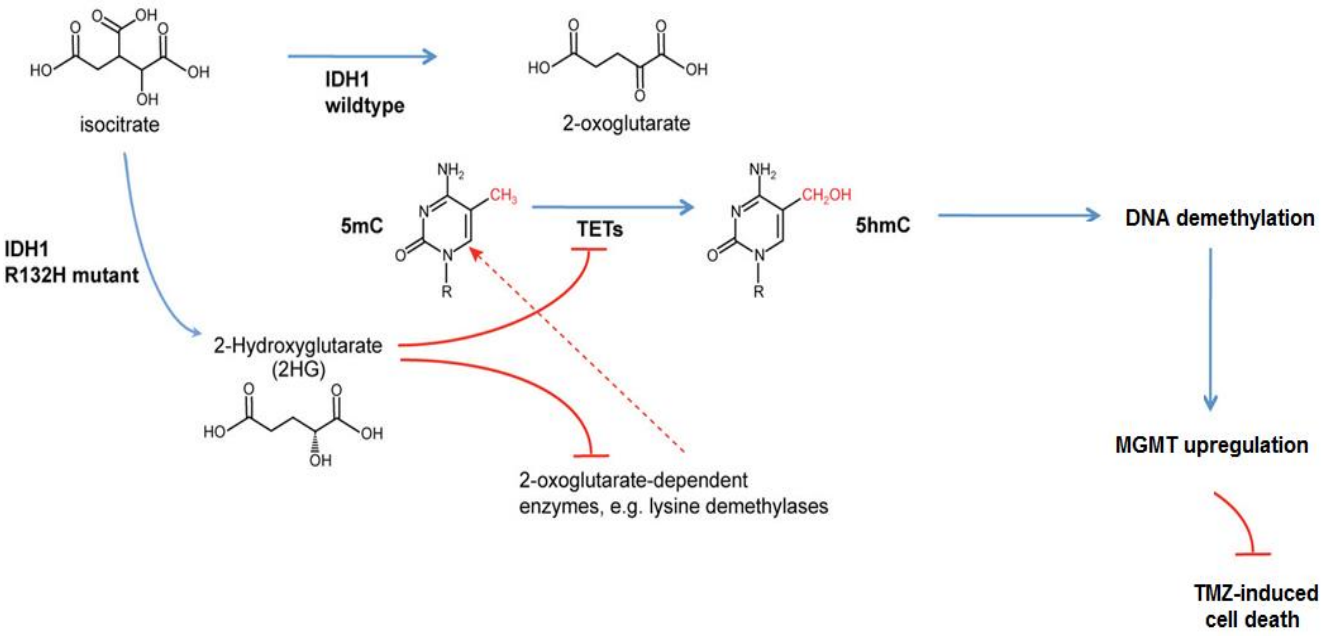


Figure 3. Schema representing IDH1 wildtype versus mutant enzymatic activities. Mutant cascade leads accumulation of 2-HG, leading to depletion of available 2-OG and inhibition of TETs and other 2-OG dependent demethylases. This leads to global DNA hypermethylation, suppression of MGMT and better therapeutic response to TMZ. Image adapted from [29].

Apoptosis and TRAIL resistance

Programmed cell death, or apoptosis, is a cellular process in which cells commit themselves to die in an organized and “cleaner” manner, as compared to necrosis [30]. Apoptosis is an indispensable phenomenon for maintenance of homeostasis of organisms at almost any stages [31]. For example, during developmental stages, redundant cells are eliminated by apoptosis. Respectively genetically blocked apoptosis specifically in neuron cells in mice displays enlarged brain size [32]. Development of human hands rely on apoptosis as well, via clearing the inter-digital cells during prenatally [33]. Apoptosis is the crucial player for many human diseases as well. That is why its balance is critical and strictly regulated. Uncontrolled and extensive cell death due to viral or intracellular reasons can develop into diseases such as AIDS and neurodegenerative disorders, due to loss of immune and neuron cells respectively [34,35]. Whereas inefficient and disabled apoptotic machinery has the potential to kill 8.2 million people in a single year world-wide (Cancer Research UK). Cell that cannot be killed or that can evade apoptosis is one of the main hallmarks of tumorigenesis [36].

There are two main pathways regulating and leading to apoptosis: intrinsic and extrinsic (mitochondrial). There are both common and distinct players in these cascades. Cysteine serine proteases (caspases) are the overarching common molecules both initiating and executing the ultimate programmed cell death [37]. The intrinsic apoptosis pathway can be initiated by cytotoxic stimuli and cellular stresses. Cytotoxic agents can induce DNA damage and DNA damage can promote p53 activation. p53 in return overexpresses players of pro-apoptotic machinery, such as Puma and Noxa, which can activate apoptosis [38]. Or the cytotoxicity can directly damage mitochondria. In both cases the downstream gatekeeper is the BH-3 containing apoptotic proteins regulating mitochondrial outer membrane (MOM). Pro-apoptotic proteins Bax and Bak have multiple BH-3 domains and can dimerize to form pores on MOM. Bcl-2, Bcl-xL and Mcl-1 on the other hand, sequester them to keep MOM intact. The constant battle between these molecules is regulated by single BH-3 containing pro-apoptotic proteins of HRK, Bim, Bid, Bik, Bad, Bmf, Puma and Noxa [39,40]. By cross-interaction with Bcl-2, Bax and Bak, these molecules sequester anti-apoptotic molecules on MOM and leads to MOM permeabilization (MOMP). MOMP leads to leakage of cyctochrome c and Smac/DIABLO normally found in intermembrane space of mitochondria. Cyctochrome c interacts with APAF-1 and forms apoptosome, which recruits initiator pro-caspase 9 and promotes its activation by cleavage [41]. Smac/DIABLO, on the other hand, interacts with inhibitors of apoptosis proteins (IAPs) which in normal conditions keep caspases inactive, thus sets caspases free [42]. Activated caspase-9 starts cleaving free executor pro-caspase 3 and 7. Activated caspase 3 and 7 have several downstream targets, such as PARP, nuclear lamina and inhibitor of caspase-activated DNAse (ICAD), so that CAD can chop down genomic DNA in nucleus [43].

The extrinsic pathway works through pro-apoptotic death receptors found on cellular membrane. Tumor-necrosis-factor (TNF) family of proteins are TNF-alpha, Fas and TNF-related apoptosis-inducing ligand (TRAIL). Each one of them has its own receptors. TRAIL can bind to death receptor 4 (DR4), death receptor 5 (DR5), decoy receptor 1 (DcR1), decoy receptor 2 (DcR2), and osteoprotegerin (OPG). Fas can bind to Fas receptor (FasR). TNF-alpha binds to TNF-receptor. DRs, unlike DcRs, have intact and functional death domains on their intracellular sides. DRs are the key initiators that trimerize upon ligand binding, in order to recruit initiator pro-caspase 8 in close proximity to each other, just like apoptosome. Activated zymogen caspase 8 then further relays the cascade downstream via cleavage of Bid into truncated-Bid (tBid) or of caspase 3 and 7. Via tBid, extrinsic pathway can join the intrinsic pathway and thus the cascade pronounces [44] (**Figure 4**).

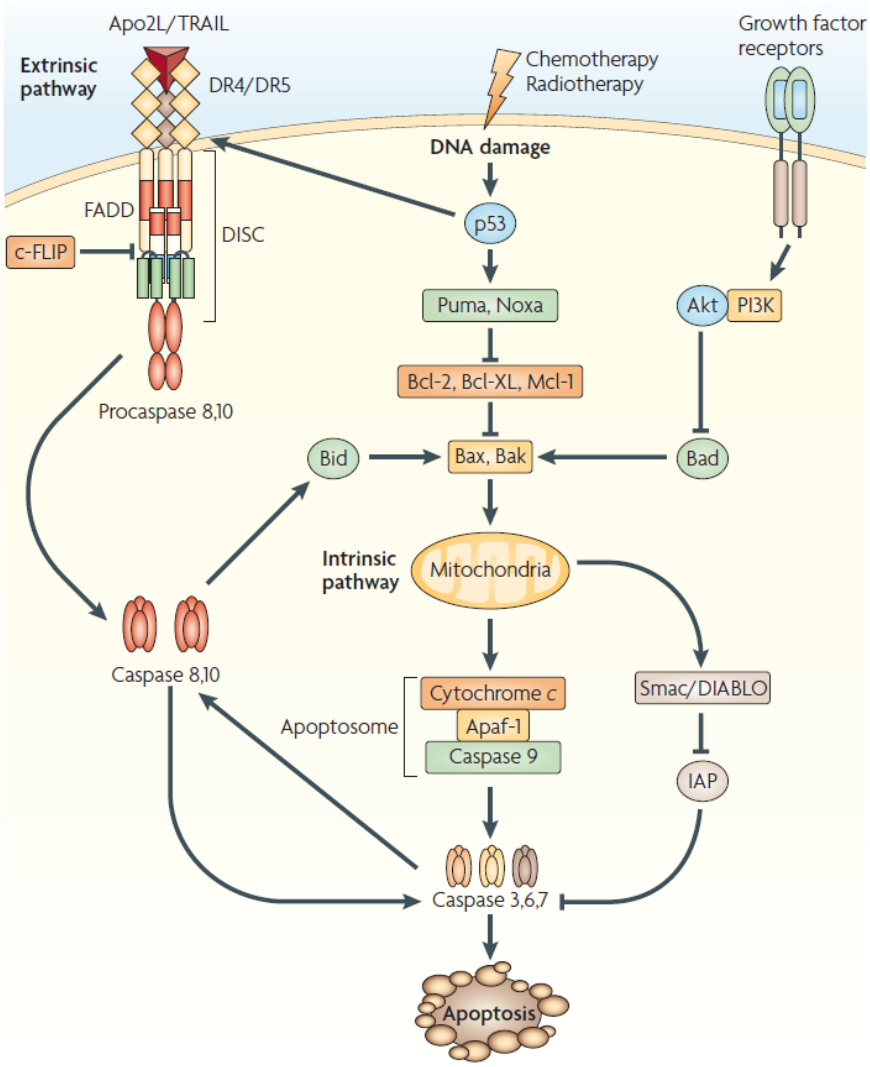


Figure 4. Representation showing intrinsic and extrinsic apoptosis pathways and cross-talk between them [44].

Apoptosis can be induced in healthy cells by several different factors. Cytotoxic immune cells via TRAIL pathway can kill tumor cells. Serum and essential growth factor deprivation can start apoptotic cascade. Cytotoxic anti-cancer agents inducing DNA damage or dysregulating mitochondrial molecular dynamics can directly initiate the intrinsic apoptotic pathway. However, there is mounting evidence showing that cells, by acquiring mutations, can evade the programmed cell death [45]. These mutations can lead to both genetic and epigenetic changes. For example, DcR upregulation, thus diluting the effective concentrations of DRs on cellular membranes could allow cells to evade TRAIL-induced apoptosis [46]. Deregulation of the apoptotic machinery, by upregulation of c-FLIP (a protein that can inhibit pro-caspase 8 activation) or Bcl-2 has been all reported [45]. In summary, downregulation or complete loss of pro-apoptotic proteins and upregulation of anti-apoptotic

proteins allows cancer cells to evade apoptotic stimuli. Tumors display intra and inter tumor heterogeneity in terms of their response to the same pro-apoptotic stimuli. There is accumulated evidence in the literature that the heterogeneity could be due to misregulations of chromatin modifying enzymes, which in return would aberrantly de-pattern the epigenetic landscape of the cells [47]. Abnormal epigenome would result in massive transcriptional changes. As an exemplifier, miRNAs targeting anti-apoptotic Bcl proteins are shown to be downregulated in many cancers [48,49]. Further, expression of DRs in cancer is also suppressed by DNA hypermethylation [50,51] (**Figure 5**).

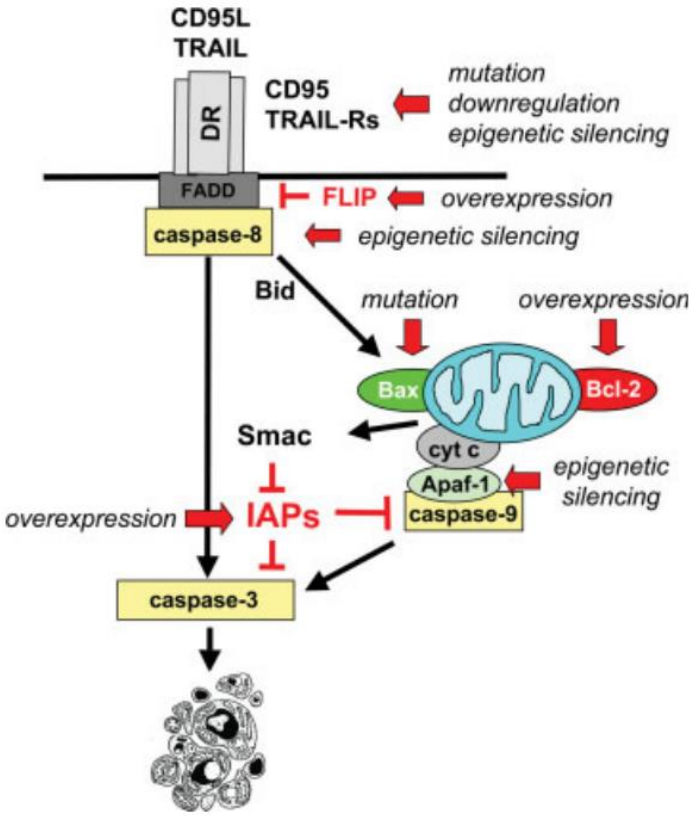


Figure 5. Schematic displaying the extracellular apoptotic pathway, its components and observed genetic and epigenetic dysregulations reported in cancer research [45].

Epigenetics and chromatin modifying enzymes (CMEs)

Epigenetics is the field that studies what lies above the naked sequences of base-pairs of DNA. Although the stretches of four different base pairs already offer high complexity, having “epi” layers regulating how and when these stretches (genes) are going to be available to transcription regulators confer cells more flexible to adapt and differentiate. Even though interest in epigenetic alterations in the context of molecular pathophysiology

started to be appreciated later, compared to genetic changes, it is now emerging as a dominating field, especially in the cancer biology [52]. Epigenetic abnormalities in cells have the power to exert genome-wide effects. Thus it has the potential to emerge as a single hallmark to rule all the other identified hallmarks of cancer [53].

There are mainly two types of epigenetic modifications that eventually lead to either a more permissive (euchromatin) or a more tightly packed (heterochromatin) chromatin state: 1) DNA methylation, 2) Histone modifications. The former is the well-characterized methylation of the C5 position of cytosine residues in CpG dinucleotides by DNA methyltransferases (DNMT). Interestingly, around 50% of the promoter regions of all human genes have the stretches of DNAs consisting of 60% or more CpG dinucleotides, called CpG islands (CGI) or CpG shores. These regions acting as promoters and enhancers are shown to be directly responsible for the transcription of their downstream genes. More interestingly, hypermethylated CGIs are well-correlated with the transcriptionally inactive genes. Aberrant global hyper- or hypomethylation of CGIs are also observed in many cancer cells [54]. Addition of a hydroxyl group to the methyl, called hydroxymethylation, is believed to prime methylated CpGs for demethylation and its significance in transcriptional regulation is also under investigation [29].

The latter, histone modifications are versatile. Every 147 bp piece of DNA is found wrapped around histone octamers. N-termini tails of histones are available to numerous modifications carried out by chromatin modifying enzymes. Lysine and arginine residues can be methylated up to three times and these modifications are catalyzed by histone demethylases (HDM) and histone methyltransferases (HMT). Lysine residues can also be acetylated by histone acetyltransferases (HAT) and these residues can be removed by histone deacetylases (HDAC). Moreover, serine and threonine residues can be phosphorylated and dephosphorylated by kinases and phosphatases. Lysine residues further can be modified by addition of ubiquitin, SUMO, ADP-ribose, among many others that are under investigation.

Although the number of possible combinations of different modifications, that are present on the histone tails in a single nucleosome at a given time, looks overcomplicated, there are number of modifications that are well characterized in terms of their overall effects on transcriptional regulation. Acetylation of the positively charged lysine residues on the tails of histones are thought to be acting as neutralizing forces by reducing the electrostatic interactions between negatively charged phosphate backbone of DNA, leading to less tightly packed nucleosomes, thus chromosome. One well characterized other modification is H3K27me3 accumulated on and around transcriptional start sites (TSS) of the inactive

genes. This modification is carried out by one of the polycomb group (PcG) proteins called EZH2.

Histone demethylations are carried out by two main group of enzymes: 1) FAD-dependent amine oxidases 2) Fe(II) and 2-OG (alpha-keto glutarate) dependent dioxygenases. LSD-1 (KDM1A) and LSD-2 (KDM1B) are first discovered members of the FAD-dependent amine oxidases. Both LSD-1 and LSD-2 can demethylate H3K4me2/me1 and in addition, LSD-1 can demethylate H3K9me2/me1. H3K9 methylation is associated with transcriptional repression, whereas H3K4 methylation is associated with transcriptional activation [55]. But one must note that these associations are highly contextual. Fe(II) and 2-OG dependent JmjC-domain containing family of proteins consist of around 30 members (**Figure 6**). 18 out of these 30 members in humans are shown to be lysine demethylases. In contrast to LSD family [56], some of the JmjC-domain containing proteins can catalyze demethylation of the trimethylated lysine residues as well. KDM2A and KDM2B can demethylate H3K36me2 and me1 and H3K4me3; in addition, although controversial, KDM2B is believed to carry out demethylation of H3K36me3 as well [57–59]. H3K36me3 found along gene bodies are generally deemed as an active mark and has been shown to take place in regulation of alternative splicing, transcriptional elongation [60]. Some other members of KDM family are KDM4, KDM5 (JARID1), KDM6A (UTX). UTX catalyzes the opposite activity of EZH2, removing 1 or 2 methyl groups from H3K27me3. It is found mutated in multiple cancers. KDM4 catalyzes demethylation of H3K36me3/me2 and H3K9me3/2, whereas JARID1 can demethylate H3K4me3/me2. Both of them are shown to be deregulated in multiple different cancers [61].

Mutations and deregulated expression levels of chromatin modifying enzymes found in cancer cells initiated a new field called epigenetic therapy as an attempt to reverse the abnormalities [61]. There are now tens of different small compounds known to inhibit different chromatin modifying enzymes [62]. One interesting pattern between these therapeutic small drugs is that both HDAC and DNMT inhibitors have shown therapeutic potentials in different cancer cells. DNMT inhibitor results in global hypomethylation of CGIs, and HDAC inhibitor results in global accumulation of acetylated histones. Both of the acquired features of epigenome can lead to derepression of hundreds of genes, some of which might be critical for tumor maintenance. More interestingly, proving that the postulated idea is context dependent, EZH2 overexpression or UTX loss-of-function deregulations in cancer cells, which will lead to abnormal global accumulation of H3K27me3 marks, would lead to suppression of hundreds of genes, again, that might be important for cancer progression. These evidences indicate that epigenetic changes and their phenotypical outcomes are very contextual and vary between cell types.

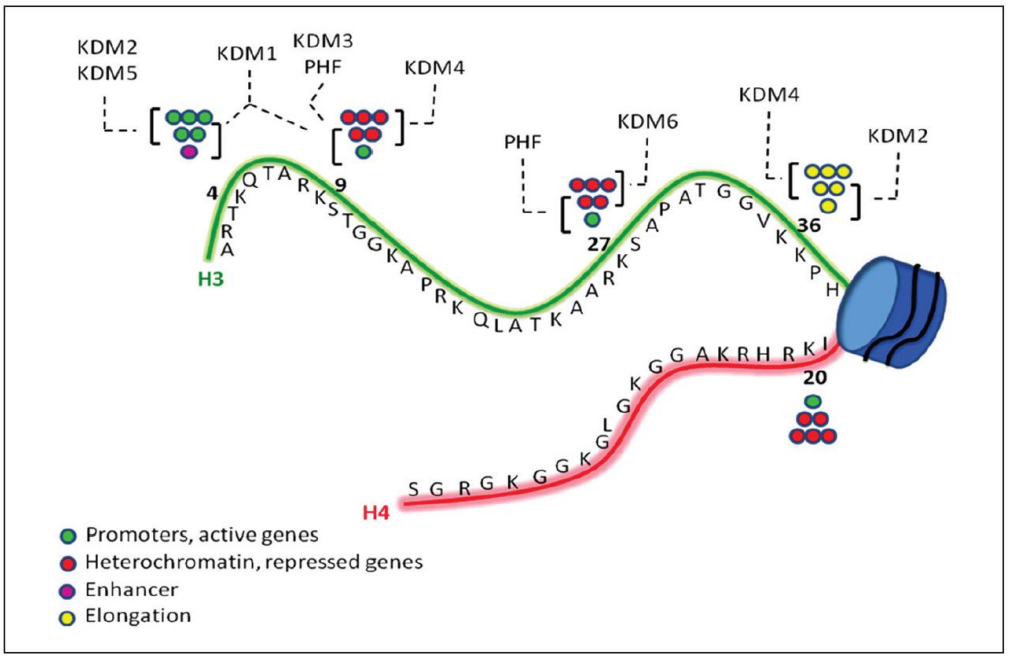


Figure 6. Diagram illustrating N termini tails of H3 and H4 along with most studied KDM family members, their corresponding modifications and studied regulatory roles of these modifications [63].

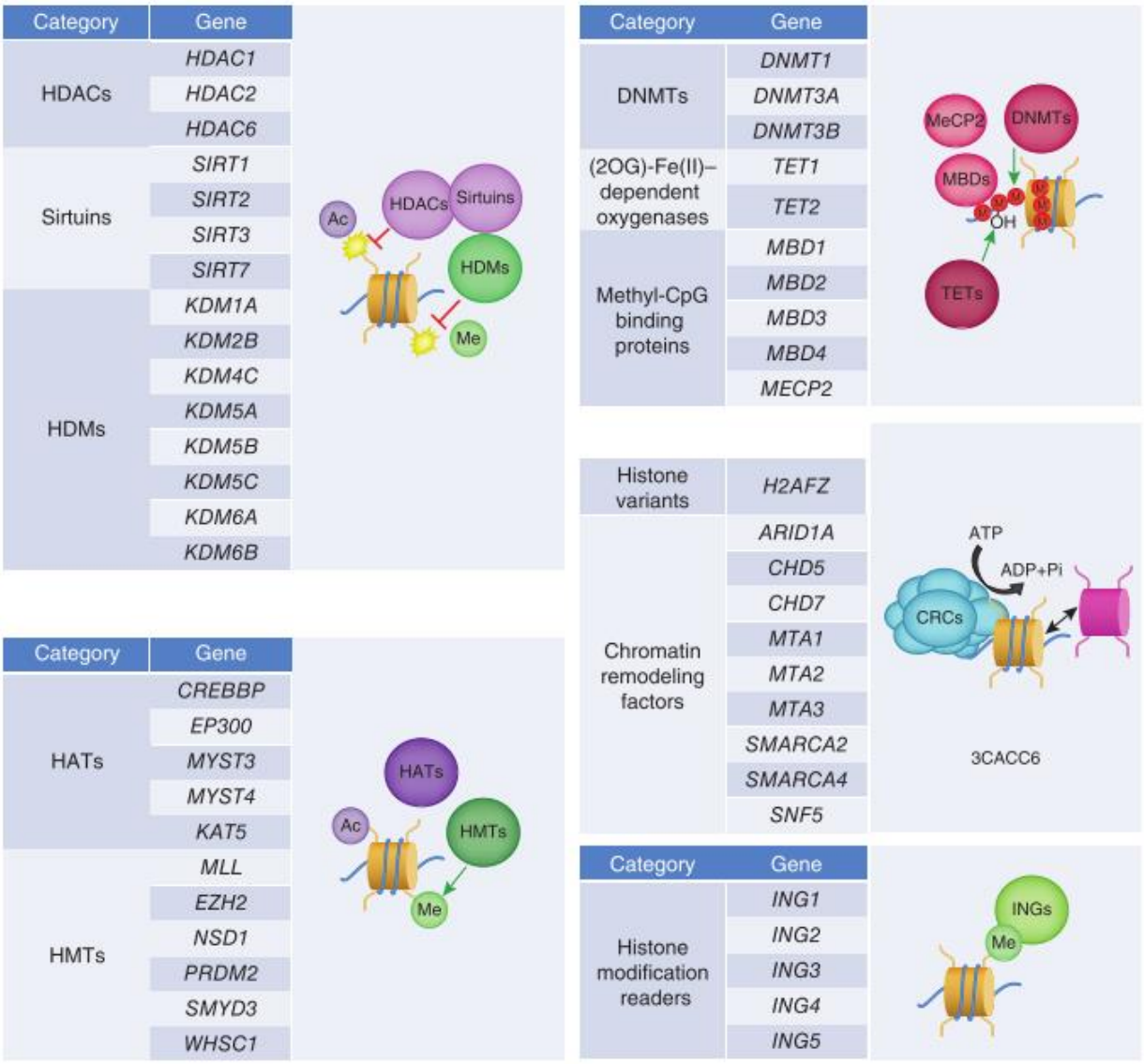
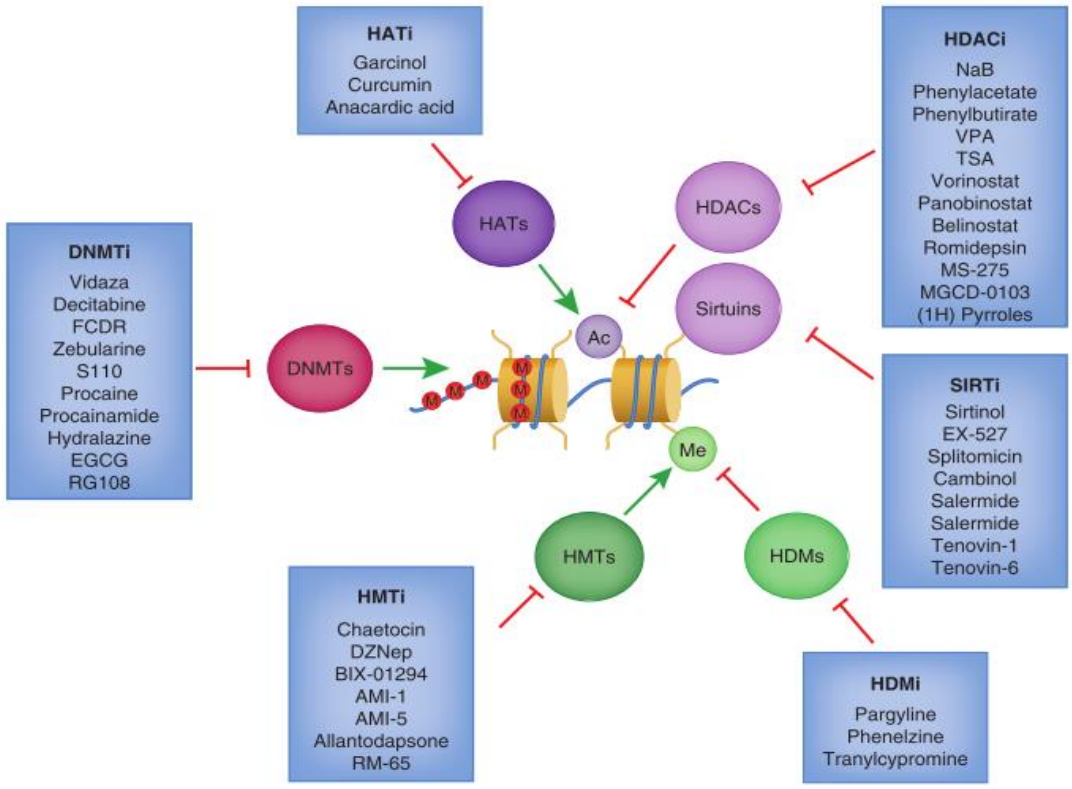


Figure 7. List of chromatin modifying and interacting (readers) proteins that are either mutated, deleted or transcriptionally deregulated in human tumors. Me, methylation. Ac, acetylation. [61]

Due to the recent advancements, targeting epigenetic modifying enzymes (writers, erasers and readers) that are commonly mutated in cancers (**Figure 7**) is now popular [63,64]. Small drug inhibitors against CMEs are promising novel therapeutics, some of them already being in clinical trials (**Figure 8**) [65–67].

.



Substance	Target structure	Clinical trial	Disease
SGI110	DNMT	Phase I/II	MDS, AML, ovarian and hepatocellular cancer
AGI-5198	Mutant IDH	Preclinical	Glioma
Pivanex (also known as AN-9)	HDAC	Phase I/II	CLL, small lymphocytic lymphoma, malignant melanoma and NSCLC
ACY-1215	HDAC6	Phase I/II	Multiple myeloma
Resveratrol (SRT501)	SIRT1 and SIRT5 activation	Phase I/II	Colorectal cancer, melanoma, multiple myeloma
	SIRT3 inhibition	Phases I–III	Metabolic and cardiovascular diseases
Curcumin	HAT	Phase I/II	Breast cancer, colorectal cancer and multiple myeloma
Tranylcypromine	KDM1A	Phase II	AML
EPZ-5676	DOT1L	Phase I	Advanced haematological malignancies and acute leukaemia with 11q23 or *MLL* abnormalities
EPZ-6438	EZH2	Phase I	NHL and breast cancer
GSK126	EZH2	Preclinical	Haematological malignancies, including NHL
GSK525762	BET bromodomain	Phase I	NMC
RVX-208	BET bromodomain	Phase II	Atherosclerosis
		Preclinical	Haematological malignancies
JQ1	BET bromodomain	Preclinical	NMC, AML and multiple myeloma
PFI-1	BET bromodomain	Preclinical	B cell acute lymphoblastic leukaemia

AML, acute myeloid leukaemia; BET, bromodomain and extraterminal family of proteins; CLL, chronic lymphocytic leukaemia; DNMT, DNA methyltransferase; DOT1L, DOT1-like histone H3 methyltransferase; EZH2, enhancer of zeste homologue 2; HAT, histone acetyltransferase; HDAC, histone deacetylase; IDH, isocitrate dehydrogenase; KDM1A, lysine-specific histone demethylase 1A; MDS, myelodysplastic syndrome; *MLL*, mixed-lineage leukaemia; NHL, Non-Hodgkin's lymphoma; NMC, NUT midline carcinoma; NSCLC, non-small-cell lung cancer; SIRT, sirtuin (a family of histone deactylases).

Figure 8. Diagram on top showing the most studied epigenetic drugs and categorized based on class of chromatin modifying enzymes they target. Table on bottom showing certain epigenetic drugs in preclinical or clinical trials. Adapted from [47,61].

Moreover, aggressive tumors like GBM are known for having an identifiable subpopulation of cancer stem cells (CSCs) that are refractory to chemotherapeutics. It has been reported that CSCs upon drug treatment enter a temporary resistant state that is reversible upon removal of the treatment. Hence, it is deemed that this temporary state is regulated by epigenetic modifications. It has been shown that KDMs can not only demethylate histones but also other important proteins that regulate proliferation and cell cycle regulations such as p53, Rb and E2F1. By demethylation of p53 by LSD proteins, p53's activity can be inhibited to protect cancer cell from apoptosis [68]. That's why recent research is also focused on KDM inhibitors to force cancer cells die (**Figure 9**) [69].

Cluster	Name	Expression in cancer types
KDM1	KDM1A	Overexpression in breast, small cell lung, colorectal, prostate, neuroblastoma, and bladder cancer
	KDM1B	N.R.
KDM2	KDM2A	Reduced expression in prostate cancer and colon cancer
	KDM2B	Overexpression in Leukemia and bladder cancer, low expression in brain tumors.
	KDM2C	N.R.
KDM3	KDM3A	Overexpression in renal cell carcinoma and colon cancer. Low expression in nasopharyngeal carcinoma.
	KDM3B	N.R.
	KDM3C	Low expression in breast cancer
KDM4	KDM4A	Overexpression in prostate cancer
	KDM4B	Overexpression in renal carcinoma
	KDM4C	Overexpression in esophageal squamous cell carcinoma and Metastatic lung sarcomatoid carcinoma
KDM5	KDM5A	Overexpression in gastric cancer
	KDM5B	Overexpression in Breast and prostate cancer
	KDM5C	N.R.
	KDM5D	N.R.
KDM6	KDM6A	Low expression in bladder cancer
	KDM6B	Overexpression in Hodgkin's Lymphoma and Prostate cancer
KDM8	KDM8	Overexpressed in breast cancer
		(N.R.-Not reported)

Figure 9. List of KDM family proteins and whether they are reported to be aberrantly expressed in cancers. Adapted from [67].

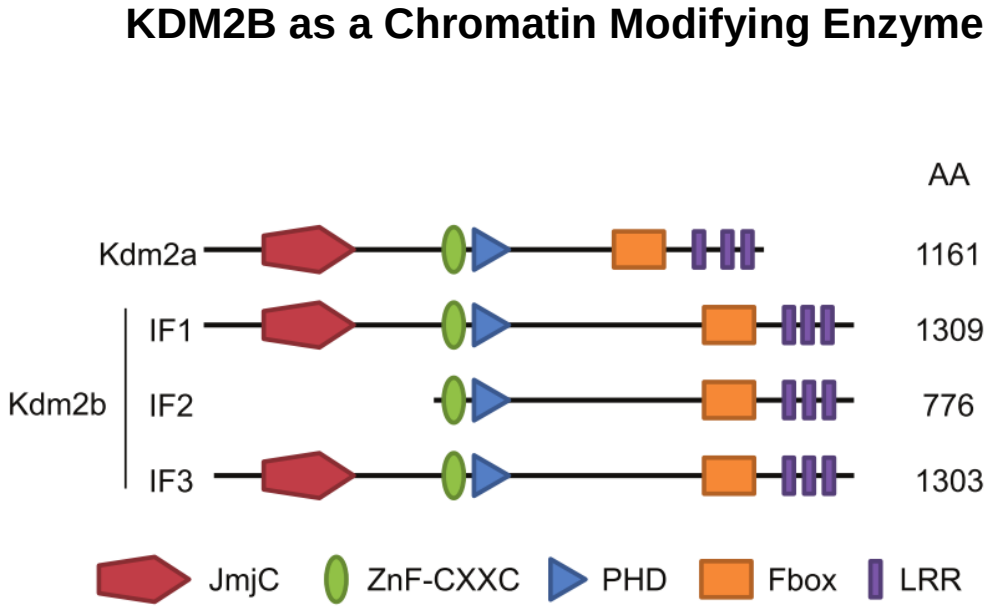


Figure 10. Illustration of KDM2 family members. KDM2A has one, whereas KDM2B has 3 distinct isoforms. The longest isoforom (IF1) is the main and mostly studied functional variant, while short isoform (IF2) lacks the enzymatic JmjC domain for demethylase activity. [70]

KDM2B has been shown to be capable of demethylating, by its JmJC domain in a Fe(II) and 2-OG dependent manner, H3K36me2 and it is specifically called H3K36me2-specific demethylase by many research groups. Though in different contexts it has been shown to catalyzye demethylation of H3K36me1, H3K36me3 and H3K4me3 as well (reviewed in Epigenetics and chromatin modifying enzymes section). By its PHD domain might enable KDM2B to recognize and bind to trimethylated H3K4. By its Fbox domain it can serve as a substrate specifier for E3 ubiquitin ligases such as RING1B as will be described in the next section. ZnF-CxxC domain enables it to recognize and bind to non-methylated CpG islands. Its leucine rich repeat (LRR) domain allows it to interact with various other proteins.

5.1. Protein interactions of KDM2B

RING1B is a RING finger E3 ligase which catalyzes mono-ubiqutination of H2AK119 and that is deemed as a suppressive mark on genome. However, for this to happen, RING1B requires the presence of a regulatory protein called Bmi1. It was interesting to see that in a high-throughput proteomics study conducted by Sachez et al. in 2007, KDM2B is first time

identified as a novel protein interacting partner of RING1B, the main catalytic member of PRC1. The novel complex formed together with RING1B and KDM2B also contained Bmi1, although whether KDM2B can dimerize with Bmi1 in the absence of RING1B yet remains to be elucidated. Hence, the complex is an active group of proteins that can catalyze the ubiqutination. More interestingly, one of the domains of KDM2B is the F-box domain (FBXL10/KDM2B) and it can serve as a substrate recognition complex for the ubiqutination activity of RINGB. When it is considered that H3K36 methylation is deemed as an active mark found on gene bodies, work of KDM2B to inactivate the genes can be perfectly coupled with recruiting RING1B, thus PRC1, to the same target loci to suppress further. [71]

In a profound bioinformatics study by Farcas et al. in 2012 and then by Wu et al. in 2013 closely analyzed CpG islands (CGIs) and their residents in mouse embryonic stem cels (mESCs) [72,73]. The papers confirm the recent challenge of the idea that PRC1 complex prerequisites H3K27me3 modification catalyzed by EZH2 of PRC2. It shows that KM2B, not KDM2A, occupies CGIs throughout genome and recruits PRC1 by forming a non-canonical PRC1 complex via direct interaction with RING1B. Thus, loss of KDM2B is shown to be leading to a global reduction in H2AK119ub levels. The data further displays that KDM2B could be priming and specifying the loci for RING1B to suppress the developmental genes in mESCs. It is concluded that PRC complexes indeed are always in a basal level of interaction with polycomb responsive elements throughout genome, however the delicate balance and constant battle between currently active transcriptional factors and activators versus PRCs determine the chromatin state of loci. KDM2B by having the residing capacity on non-methylated CGIs nominates as a strong candidate, in the light of the data, for regulating localization of PRCs, thus regulating cell fate. In a follow-up study by the same group then showed that variant-PRC1 recruited by KDM2B not only can work in a H3K27-independent manner, but it can also subsequently recruit, via H2AK119ub, PRC2 for H3K27 trimethylation [74] (**Figure 11)**.

In another interesting paper reflecting the research conducted in mESCs, KDM2B expression is found to be driven by Oct4 and Sox2 by direct interactions. The authors observes the same interactions between KDM2B and PRC1, by which PRC1 is recruited to developmental genes to be kept suppressed. However, upon KDM2B loss, these genes gets derepressed and starts driving differentiation of mESCs [75].

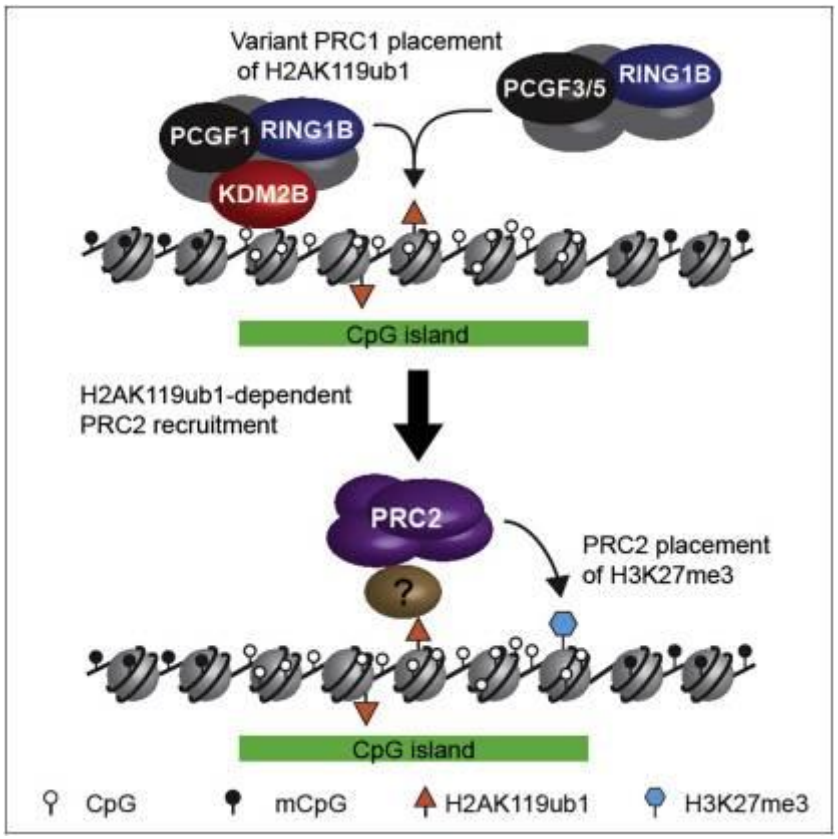


Figure 11. Diagram showing canonical and non-canonical (variant) PRC1 complexes interacting with KDM2B, by which they are recruited to nonmethylated CpG islands of genes. PRC2 might further recognize H2AK119ub1 and interact with the loci to place H3K27me3 [74].

5.2. KDM2B in malignancies

Both KDM2B and its homologue KDM2A are implicated in malignancies by several groups by the provirus integration screens of Moloney murine leukemia virus conducted in rats. Both alleles of KDM2B came out several times as a hotspot for proviral integration that results in retrovirus-induced rat lymphoma. However, it was interesting to see that some of these integrations did not result in any shitfts in open reading frame of KDM2B, suggesting that tumorigenic activity of KDM2B could be due to deregulation of its transcriptional levels. [76,77] While Pfau et al. displays that KDM2B could be a proto-oncogene, whose overexpression immortalizes mouse embryonic fibroblasts and whose inhibition leads to senescence, Suzuki et al. shows that KDM2B is a tumor suppressor gene that is usually mutated or downregulated in tumors. KDM2B is suggested to have tumor suppressor activities as regulator of DNA mismatch and repair systems.

As another parameter increasing the complexity of the context, KDM2B has been shown to colocalize in nucleolai regulating rRNA transcription. This observation was dependent on its H3K4me3 demethylase activity. H3K4me3 is a well-established active mark found on gene promoters. Thus, it is proposed that its demethylase activity on H3K4me3 of rRNA genes leads to suppression of ribosomal genes. Since ribosomal genes and their aberrant expression is implicated with tumorigenesis, this paper suggests also that KDM2B is a tumor suppressor gene [78]. They further conducted bioinformatics analysis and demonstrate that KDM2B expression is inversely correlated with grade of brain cancers.

In 2011 He et al. reported their findings linking their previous work, demonstrating that KDM2B is critical regulator of maintanence of proliferation in MEFs, to a human disesase, leukemia. In this paper, intrigued by the observation that KDM2B is upregulated in number of human leukemia, they confirm that KDM2B indeed drives leukemogenesis in vitro and in vivo. They specifically reveals that ectopic expression of KDM2B can induce tumorigenesis in healthy hematopoietic progenitors and its knockdown abrogate proliferation potential of leukemic stem cells. The mechanism that is demonstrated to be responsible behind the data is, as previously reported by them, KDM2B's direct suppression of p15/Ink4b locus by its demethylase activity on H3K36me2 [79].

In contrast, In 2013, Tzatsos et al. clearly illustrated that KDM2B drives pathogenesis of a deadly pancreatic cancer cell type. They demonstrated there is a linear correlation between grades of human pancreatic cancers and expression KDM2B, while metastatic ones having the highest expression levels. The seminal study described two interactions of KDM2B that lies behind the mechanisms of KDM2B in tumorigenesis. One, they revealed that KDM2B can bind to Polycomb group proteins to recruit them to suppress developmental genes, in a H3K27me3 (EZH2) dependent manner. Two, they reported that KDM2B can also activate metabolic genes' transcription by interacting with MYC oncogene and somehow stabilizing H3K4me3 levels. [80].

5.3. KDM2B regulating senescence and pluripotency

In 2008, new findings brought some light into the possible reasons why KDM2B has been implicated in tumorigenesis and cell-cycle regulation. It has been shown that KDM2B, in mouse embryonic fibroblasts, can directly interact with transcription-start-site of p15 (Ink4b) gene in the Ink4-Arf-Ink4b locus. This interaction has been shown to suppress the locus. Loss of KDM2B is shown to reduce proliferation and induce cellular senescence in p15

(Ink4b), pRb and p53 dependent manner. They display this by inhibiting both Rb and p53 pathways, via SV40 large T antigen, and failing to observe shKDM2B induced cellular senescence. It is worth to mark that RING1B, as a part of PRC1, is also shown to carry out the same suppression on the same locus, with similar and stronger outcomes upon knockdown. By utilizing a p53 null MEF cell line, He et al. also suggest that KDM2B synergizes with Ras oncogene to support oncogenic transformation [81]. Pfau et al. as well in 2008, upon identifying KDM2B and KDM2A as hotspots for MoMuLV [77], showed that both KDM2B and KDM2A overexpression is enough to immortalize MEFs. They further showed that ectopic KDM2B expression promotes activation of Rb and upregulates p53 and its downstream target p21. Although the latter is counterintuitive to what is expected, they present data suggesting that somehow NDY1 is able to suppress p21 induced senescence.

In 2009, Tzatsoz et al. reports that they also obtain the same results of KDM2B as the key bypasser of cellular senescence and immortalizer of MEFs through its demethylase activity on Ink4/Arf locus. They start their research by first demonstrating the gradual decrease of KDM2B and EZH2 as MEFs are passaged. They further display that ectopic KDM2B expression is sufficient to reverse EZH2's senescence induced reduction. Since EZH2 is the catalytic core of PRC2 conducting H3K27 trimethylation, well-characterized suppressive mark, they further shows that Ink4/Arf locus indeed becomes hypermethylated on H3K27 by KDM2B induced EZH2 upregulation. Another interesting remark is involvement of Bmi1 in this process. It is a known PRC1 member that is recruited to Ink4/Arf locus in senescence dependent manner. It can interact with RING1A/B and recruit it to carry out its H2AK119 ubiqutination. In this paper they show that KDM2B, EZH2 and BmiI works together to suppress Ink4/Arf locus. This clearly links PRC1, PRC2 and KDM2B. Although He et al. in 2008 clearly showed that KDM2B can help Ras-oncogene induced oncogenic transformation, Tzatsoz et al. here confirms and elaborates the observed phenomenon further. Unlike He et al. they do not use p53 null cell line, thus they show that Ras-oncogene induced premature cellular senescence in MEFs in normal conditions can be overcome with KDM2B overexpression, on top of KDM2B-Ras synergistic oncogenic transformation [82].

In 2011, Tzatsoz et al. describes another axis of KDM2B bypassing cellular senescence, besides the known KDM2B-Ink4/Arf axis [83]. Here, along with their previous findings on the relationship between KDM2B and EZH2, they show that KDM2B binds and regulates let-7 miRNA loci to keep it suppressed. As cells go through passages, KDM2B is gradually downregulated and let-7 miRNA correspondingly gets upregulated, which targets EZH2 mRNAs for degradation. They prove that let-7 is downstream of KDM2B but upstream of EZH2 by forced expression of let-7. As a new finding, authors utilize Ink4/Arf null cell lines to show that KDM2B overexpression can still influence their proliferation dynamics. Overall

data suggests that KDM2B not only regulates Ink4/Arf locus as previously well-defined, but also regulates miRNA loci which regulate other chromatin modifying enzymes. On top of these findings, in 2014, it has been showed that the information of KDM2B-let-7-EZH2 can be potentially exploited by therapeutically targeting EZH2 mediated H3K27me3 modifications by DZNep in patients with Myelodysplatic syndromes (MDS). Progressed MDS leads to acute myeloid leukemia (AML). It is known that hematopetic cells of MDS patients, compared to healthy cells, display aberrant hypermethylation throughout genome and histones. According to the data presented, 5-azacitidine, a DNA demethylation agent and potential pro-apoptotic chemical for the malignant hematopoietic cells can be supplemented with DZNep to pronounce the effects via EZH2-loss-induced upregulation of cyclin-dependent-kinase inhibitors, such as p16 [84].

Chromatin structure, thus epigenome, of the cells are the main barrier blocking or hindering reprogramming of somatic cells into induced pluripotent stem cells. KDM2B has been shown in mouse embryonic fibroblasts to increase efficiency of iPSC generation when overexpressed. Their data suggested that overcoming of the barrier by KDM2B is dependent on its demethylation and DNA binding activities. However, the paper shows that this promotion by KDM2B is not dependent on its senescence suppression activity. This looks counterintuitive considering the fact that suppression of the Ink4a/Arf senescence locus by itself is another promoter of iPSC generation. KDM2B has been shown to directly interact with early-responsive epithelial genes in the process of reprogramming and conduct H3K36me2 demethylation. The paper suggests that this catalytic activity on the genes lead to their upregulation, in concert with reprogramming transcription factors Oct4, Sox2 and Klf4. [70] Same group in 2013 also defines the Oct4-Sox2-KDM2B-PRC1 axis that KDM2B is directly regulated by Oct4 and Sox2 in mESCs and that KDM2B recruits PRC1 to the developmental genes' CGIs to keep them suppressed. Knockdown of KDM2B is shown to be leading to early differentiation of mESCs. [75]

In a separate 2013 study conducted by Gao et al. describes that KDM2A, as well as KDM2B, maintains proliferation capacity of mesenchymal stem cells (MSCs) by suppressing p15/Ink4B and p27/Kip1 loci by its H3K4me3 specific demethylase activity. KDM2A loss leads to accumulation of H3K4me3 and derepression followed by upregulation of p15/Ink4B and p27/Kip1. Furthermore, their data suggests that human stem cells from apical papilla (SCAP) displays G1/S-phase arrest upon loss of KDM2A. [85].

Recently, in 2014, the group of Tsichlis published another paper on KDM2B connecting its role in maintenance of pluripotency in stem cells and implications in cancer cells, via utilizing breast cancer stem cells [86]. This research pushed the balance towards

deeming KDM2B as a proto-oncogene rather than a tumor suppressor. This seminal work combined separate previous observations and defined that certain cancer stem cells could be targeted for KDM2B which can lead to differentiation and senescence. By analyzing numerous human samples they not only further confirmed previous finding that KDM2B-miRNA-PRC1/2-developmental genes axis also valid for cancer stem cells, but also showed that KDM2B expression levels in breast cancers can be used as a diagnostic biomarker.

In this thesis, we have shown that KDM2B can be functioning as a proto-oncogene in U87MG GBM cell line. This argument is supported by several lines of evidences. First, loss of KDM2B cooperated with TRAIL to reduce GBM cell viability. This was also evident from the augmented apoptotic response of shKM2B cells upon TRAIL treatment, as assessed from hallmarks of apoptosis. Accordingly, shKDM2B cells displayed elevated levels of caspase 3/7 and 8 activities, and pronounced cleavage of PARP. RNA-seq analysis of shKDM2B cells revealed that knockdown of KDM2B deregulates the extrinsic and intrinsic apoptotic machinery by upregulating pro-apoptotic genes DR4, Bim, Bak and HRK, and downregulating anti-apoptotic gene Mcl-1. Pro-apoptotic gene HRK was the top upregulated gene upon KDM2B loss. Data suggested that KDM2B could be directly interacting with HRK to regulate its expression. HRK loss recovered the phenotype. Moreover, silencing of KDM2B not only accelerated the TRAIL-induced apoptosis, but also reduced proliferation capacity of cells in long term both in vitro and in vivo. shKDM2B tumors resected from mice demonstrated reduced angiogenesis and increased basal level of apoptosis.

Chapter 2

Materials and Methods

1. Cell culture

U87MG cells were received and authenticated from ATCC, human BJ fibroblasts and 293T cells were kindly provided by Dr. Tamer Onder (Koç University, Turkey). All cells were cultured in DMEM medium (Gibco, USA) supplemented with 10% FBS (Gibco, USA) and 1% Penicillin-Streptomycin (Gibco, USA) at 37ºC in a humidified chamber with 5% CO2 as described [87]. Puromycin selection was applied at a final concentration of 1 ug/mL for 3-7 days. Neomycin (G418) (Life Technologies, USA) selection was applied at a final concentration of 400 ug/mL for at least 1 week.

2. Production of TRAIL in 293T cells

The extracellular portion of human TRAIL (aa 95-281) was cloned into lentiviral expression vectors and used to produce functionally active TRAIL as described [88,89]. Briefly, 293T cells were seeded as $2{,}5x10^6$ per 10 cm plate. Next day, 5 ug of TRAIL Vector DNA with 20 ul Fugene transfection reagent and 380 ul OptiMEM (Promega, USA) were transfected into the cells dropwise in afternoon. Next day in the morning, the medium was replaced with 8 mL serum-free medium. Around 48 hours post-transfection, the medium was collected and stored at 4ºC, and another 8 mL serum-free media was added. The collection was repeated the next day. The collected media was centrifuged for 5 minutes at 1500 RPM to get rid of cells and debris. TRAIL in the media was concentrated using spin filter columns filtering proteins above 15kD (Millipore, USA). The columns were spun at 4ºC at 3800 RPM for 20 minutes. The flow through was discarded and the remaining media at top was collected. The procedure wass repeated until the entire sample is concentrated. The concentrated TRAIL-enriched medium was aliquoted and stored at -80ºC. Quantification of TRAIL protein was performed by TRAIL ELISA.

3. TRAIL ELISA

Abcam's TRAIL Human ELISA Kit contains a monoclonal antibody specific for TRAIL which has been coated onto the wells of the provided microtiter strips. TRAIL detection is performed by comparing the desired sample to known TRAIL

concentration standards and control specimens. First, incubation is done with the standards or samples and a biotinylated monoclonal antibody specific for TRAIL. Afterwards the enzyme Streptavidin-HRP, that binds the biotinylated antibody is added. Finally, a substrate solution which acts on the bound enzyme to induce a colored reaction product is added. The intensity of this colored product is directly proportional to the concentration of TRAIL present in the samples. To detect the intensity of the colored product the read was performed at 540 nm by Synergy H1 Reader (Biotek, USA).

4. Cloning of the shRNA constructs

shRNAs targeting chromatin modifying proteins were designed using the RNAi Codex Program as 97-mer oligos (**Table 1**) The designed oligos were amplified with the following primers pair having compatible restriction ends with the backbone:

Forward: GATGGCTGCTCGAGAAGGTATATTGCTGTTGACAGTGAGCG,

Reverse: GTCTAGAGGAATTCCGAGGCAGTAGGC.

PCR products were gel purified, digested with EcoRI and XhoI and ligated into the retroviral pSMP vector as decribed [90]. Clones were verified by sequencing. shRNA targeting the firefly luciferase was used as a control.

shKDM2B-1:

TGCTGTTGACAGTGAGCGCCCTGAACCACTGCAAGTCTATTAGTGAAGCCACAG
ATGTAATAGACTTGCAGTGGTTCAGGTTGCCTACTGCCTCGGA,

shKDM2B-2:

TGCTGTTGACAGTGAGCGCTCAACCTGTCTGACTGCAATATAGTGAAGCCACAG
ATGTATATTGCAGTCAGACAGGTTGATTGCCTACTGCCTCGGA,

shRING1A-1:

TGCTGTTGACAGTGAGCGACCCTGCAACGTCCCATCTATATAGTGAAGCCACAG
ATGTATATAGATGGGACGTTGCAGGGCTGCCTACTGCCTCGGA,

shRING1A-2:

TGCTGTTGACAGTGAGCGACCAGCCAATAAGAGGACACAATAGTGAAGCCACAG
ATGTATTGTGTCCTCTTATTGGCTGGCTGCCTACTGCCTCGGA,

shSMYD:

TGCTGTTGACAGTGAGCGACGGAGGGCCAAGCACTATAAATAGTGAAGCCACA
GATGTATTTATAGTGCTTGGCCCTCCGGTGCCTACTGCCTCGGA,

shNSD1:

TGCTGTTGACAGTGAGCGACCAGCTCGTCTCCTGCAAGAATAGTGAAGCCACAG
ATGTATTCTTGCAGGAGACGAGCTGGCTGCCTACTGCCTCGGA,

shSETD2:
TGCTGTTGACAGTGAGCGCGCCATGTTACTTTGATCTTATTAGTGAAGCCACAGA
TGTAATAAGATCAAAGTAACATGGCATGCCTACTGCCTCGGA,
shASH1L:
TGCTGTTGACAGTGAGCGCCCAAAGAACTTGGAGAACTATTAGTGAAGCCACAG
ATGTAATAGTTCTCCAAGTTCTTTGGATGCCTACTGCCTCGGA

Source	*Gene name*	*Category*
Onder TT et al.	BMI1	PRC1 member
Onder TT et al.	BMI1	PRC1 member
Onder TT et al.	BMI1	PRC1 member
Onder TT et al.	RING1A	PRC1 member
Onder TT et al.	RING1A	PRC1 member
Onder TT et al.	RNF2	PRC1 member
Onder TT et al.	RNF2	PRC1 member
Onder TT et al.	YY1	TF
Onder TT et al.	YY1	TF
Onder TT et al.	EZH1	PRC2 member
Onder TT et al.	EZH1	PRC2 member
Onder TT et al.	EZH1	PRC2 member
Onder TT et al.	EED	PRC2 member
Onder TT et al.	EED	PRC2 member
Onder TT et al.	EZH2	PRC2 member
Onder TT et al.	EZH2	PRC2 member
Onder TT et al.	SUZ12	PRC2 member
Onder TT et al.	SUZ12	PRC2 member
New	NR6A1	Other
New	NR6A1	Other
Onder TT et al.	NR2F1	TF
Onder TT et al.	NR2F1	TF
New	NR2F2	TF
New	NR2F2	TF
New	NR2F2	TF
New	H2AFZ	Other
New	H2AFZ	Other
New	H2AFZ	Other
New	AHCY	Other
New	AHCY	Other
Onder TT et al.	MBD1	MCBP
Onder TT et al.	MBD1	MCBP
Onder TT et al.	MBD1	MCBP
Onder TT et al.	MBD2	MCBP

Onder TT et al.	MBD2	MCBP
Onder TT et al.	MBD2	MCBP
Onder TT et al.	MBD3	MCBP
Onder TT et al.	MBD3	MCBP
Onder TT et al.	MBD4	MCBP
Onder TT et al.	MBD4	MCBP
Onder TT et al.	MBD4	MCBP
Onder TT et al.	MeCP2	MCBP
Onder TT et al.	MeCP2	MCBP
Onder TT et al.	MeCP2	MCBP
New	DNMT3L	Other
New	TCF3	TF
New	TCF3	Tf
Onder TT et al.	DNMT3A	DNMT
Onder TT et al.	DNMT1	DNMT
Onder TT et al.	DNMT1	DNMT
Onder TT et al.	DNMT1	DNMT
New	LSD1/KDM1A	HDM
New	LSD1/KDM1A	HDM
New	LSD1/KDM1A	HDM
New	LSD2/KDM1B	HDM
New	LSD2/KDM1B	HDM
New	KDM2A	HDM
New	KDM2A	HDM
New	KDM2A	HDM
New	KDM2B	HDM
New	KDM2B	HDM
New	KDM2B	HDM
New	KDM3A	HDM
New	KDM3A	HDM
New	KDM3B	HDM
New	KDM3B	HDM
New	KDM3B	HDM
New	KDM4A	HDM
New	KDM4A	HDM
New	KDM4A	HDM
New	KDM4B	HDM
New	KDM4B	HDM
New	KDM4C	HDM
New	KDM4C	HDM
New	KDM4C	HDM
New	KDM4D	HDM
New	KDM4D	HDM

New	KDM5A	HDM
New	KDM5A	HDM
New	KDM5A	HDM
New	KDM5B	HDM
New	KDM5B	HDM
New	KDM5B	HDM
New	KDM5C	HDM
New	KDM5C	HDM
New	KDM5C	HDM
New	KDM6A	HDM
New	KDM6A	HDM
New	KDM6A	HDM
New	KDM6B	HDM
New	KDM6B	HDM
New	KDM6B	HDM
New	SET1A	HMT
New	SET1A	HMT
New	SET1A	HMT
New	ASH1L/ KMT2H	HMT
New	ASH1L/ KMT2H	HMT
New	ASH1L/ KMT2H	HMT
New	SETD2/KMT3A	HMT
New	SETD2/KMT3A	HMT
New	SETD2/KMT3A	HMT
New	NSD1/KMT3B	HMT
New	NSD1/KMT3B	HMT
Onder TT et al.	G9A/EHMT2	HMT
Onder TT et al.	G9A/EHMT2	HMT
Onder TT et al.	G9A/EHMT2	HMT
Onder TT et al.	G9A/EHMT2	HMT
Onder TT et al.	EHMT1	HMT
Onder TT et al.	EHMT1	HMT
Onder TT et al.	EHMT1	HMT
Onder TT et al.	DOT1L	HMT
Onder TT et al.	DOT1L	HMT
Onder TT et al.	SUV39H1	HMT
Onder TT et al.	SUV39H1	HMT
Onder TT et al.	SUV39H2	HMT
Onder TT et al.	SUV39H2	HMT
Onder TT et al.	SUV39H2	HMT
Onder TT et al.	SETDB1	HMT
Onder TT et al.	SETDB1	HMT
Onder TT et al.	SMYD2	HMT

Onder TT et al.	SMYD2	HMT
Onder TT et al.	SMYD2	HMT

Table 1. List showing the categories of the shRNAs and the genes targeted by them (Cloning of the new shRNAs are performed by Dr. Tamer Önder).

5. Production of viral supernatants

293T cells were seeded as $2{,}5x10^6$ per 10 cm plate. Next day in the afternoon, 250 ng VSV-G (envelope protein), 2250 ng GagPol (pUMVC for retroviral, 8.2dVPR for lentiviral packaging) and 2500 ng shRNA vectors were mixed with 20 ul Fugene transfection reagent and optiMEM up to final 400 ul (Promega, USA). Next day in morning, the media was replaced with 8 mL media. 48 hours after transfection, the virus containing media was collected and stored at +4^{o}C. 8 ml fresh medium was added for a second collection the next day. Combined collected media was centrifuged at 1500 RPM for 5 minutes to pellet cells and debris. The viral supernatant was filtered through 0.45 um filters (Millipore, USA) by syringe, aliquoted as 1 mL and stored at -80^{o}C. Everything that contacted viral supernatant was incubated with bleach for 15 minutes before discarding. (shRNA packaging was done with Zeynep Kahya, Dr. Nathan Lack, Duhan Toparlak and Dr. Tamer Önder)

6. shRNA screen for TRAIL response

U87MG cells were seeded as 2500 cell per well into black-bottom 96-well plates (Corning Costar, clear bottom black side). Next day, the cells were infected with 80 ul of viral supernatants with Protamine Sulfate (10 ug/mL). Next day the media was replaced with fresh media. Next day, fresh media with Puromycin (1 ug/mL) was added and the cells were selected for 3 days. Following Puromycin selection, old media was replaced with fresh media containing freshly diluted TRAIL (100 ng/mL) and cells were treated for 16-24 hours. Next day, cell viability was measured by CellTiter Glo Assay (Promega, USA). shRNA screen was performed by Zeynep Kahya and Dr. Tuğba Bağcı-Önder.

7. Cell viability

Viability of the cells in 96-well plates was measured using ATP-based assays with CellTiter Glo (CTG) (Promega, Madison, WI, USA). Media in the wells were withdrawn and 40 ul of CTG:media mix (1:10) per well was added by multichannel pipette. The plate was shaken for 2 minutes and incubated for an additional 8 minutes

in dark. Bioluminescence was measured by BioTek's Synergy H1 plate reader and Gen5 data analysis software. All experiments were performed in triplicates. In the experiments where caspases are inhibited, 20 uM final concentration of each inhibitor is used. Cells are co-treated with inhibitors and TRAIL for the same period of time. BD Pharmingen, Z-IETD-FMK, Caspase-8 Inhibitor: 550380, BD Pharmingen, Z-VAD-FMK, General Caspase Inhibitor, 550377, BD Pharmingen, Z-FA-FMK, Negative Control for Caspase Inhibitors, 550411, BD Pharmingen, Z-LEHD-FMK, Caspase-9 Inhibitor, 550381, Promega, Caspase Inhibitor Ac-DEVD-CHO (Caspase3/7)

8. Caspase activity assays

10,000 cells per well were seeded in a 96-well plate (Corning Costar, black-bottom). Next day the media was replaced with media containing 100 ng/mL TRAIL in 40 ul per well. 3 hours post-treatment, without removing media, 17 ul of CaspaseGlo 3/7 reagent or CaspaseGlo 8 reagent:MG-132 protease inhibitor (1:3 ratio) (Promega, Madison, WI, USA) were added in the wells. The plate was shaken for 30 seconds and incubated at room temperature for 30 minutes in dark. Bioluminescence was measured by BioTek's Synergy H1 plate reader and Gen5 data analysis software. All experiments were performed in triplicates.

9. Quantitative real-time PCR

NucleoSpin RNA isolation kit (Macherey-Nagel, Germany) was utilized for extraction of RNAs from cultured cells. Instructions of the manufacturer were followed. cDNAs were synthesized as the following: A 16,5 ul total volume of a reaction of 1 ug RNA, 2,5 ul of 2mM dNTP (Life Technologies, USA) and 2 ul of 25 A260 units/mL hexanucleotide mix (Roche, Switzerland) was assembled with water in a PCR tube. The mixture was incubated at 65^{o}C for 5 minutes and immediately transferred on ice. A reaction of 5 ul of 5X First Strand Buffer (Invitrogen, USA), 2 ul of 0.1M DTT (Invitrogen, USA) and 0,5 ul of RNAsin (Promega, USA) was assembled in a separate tube and then added on the RNA mix. The reaction was incubated for 10 minutes at room temperature. 1 ul of MMLV-RT enzyme (Invitrogen, USA) was added. The reaction was briefly vortexed, spun and incubated at 37^{o}C for 1 hour and then 70^{o}C for 15 minutes.. Finally, 75 ul of nuclease free water was added on the mix. Quantitative RT-PCRs was carried out using the primers in Table 2. 10 ul of 2X SYBR master mix (Roche, Switzerland), 7 ul of nuclease water, 1 ul of 5 uM primer mix and 2 ul of cDNA were mixed and assembled in a 96-well opaque white plate (Roche, Switzerland) and Roche's LightCycler 480 Instrument II is used to measure delta Ct

values of each sample. Majority of q-RT-PCRs were conducted by Selena Kazancıoğlu.

Gene	***Sequence***	
APAF1	F	5'-AATGGCAGGCTGTGGGAAGT-3'
	R	5'-TCCCCCTGGGAAACAACCTTCT-3'
ASH1L	F	5'-GGGAGACCCCCTAAGATGAGG-3'
	R	5'-GGTGAAGGAGAGTAAGGCATACC-3'
BAK1	F	5'-GTTTTCCGCAGCTACGTTTTT-3'
	R	5'-GCAGAGGTAAGGTGACCATCTC-3'
BCL10	F	5'-GCAGTTGTGAACCTTTTCCAGA-3'
	R	5'-TGGATGCCCTCAGTTTTTCAG-3'
BCL11B	F	5'-TGCAAGTGCAAGAGGCCAAG-3'
	R	5'-GCGGACTGGCTGGTTTCTTTA-3'
BCL2A1	F	5'-AGTGCTACAAAATGTTGCGTTC-3'
	R	5'-GGCAATTTGCTGTCGTAGAAGTT-3'
BCL2L11(BIM)	F	5'-TCCCTGCTGTCTCGATCCTC-3'
	R	5'GGTCTTCGGCTGCTTGGTAA-3'
BCL2L14	F	5'-ACATGACAGCCATTCCGTGG-3'
	R	5'-ATGTTGGGCCTGTGCCTTAGA-3'
BCL2L2	F	5'-GCGGAGTTCACAGCTCTATAC-3'
	R	5'-AAAAGGCCCCTACAGTTACCA-3'
BCL9	F	5'-TCCAGCCAAAGTGGTGTACGTG-3'
	R	5'-ATCTGTGTGTTCAGAGGCGCT-3'
BMF	F	5'-GAGCCATCTCAGTGTGTGGAG-3'
	R	5'GCCAGCATTGCCATAAAAGAGTC-3'
BNIP2	F	5'-GGAGGTCGGGATGTTATCACT-3'
	R	5'-CCAGGTCGCAAAAAGCAGG-3'
CARD16v1	F	5'-TGGGACTCTCAGCAGCTCTTCA-3'
	R	5'-GCTTGATTCTGCCTTCTGGGCT-3'
CARD16v2	F	5'-GCAGGTCCGATACCTGGAAATTAGC-3'
	R	5'-CCTGAAGAGCTGGGAAGGAAGAAAA-3'
CASP1	F	5'-TTTCCGCAAGGTTCGATTTTCA-3'
	R	5'-GGCATCTGCGCTCTACCATC-3'
CASP3	F	5'-CATGGAAGCGAATCAATGGACT-3'
	R	5'-CTGTACCAGACCGAGATGTCA-3'
CASP7	F	5'-CGGTCCTCGTTTGTACCGTC-3'
	R	5'-CGCCCATACCTGTCACTTTATCA-3'
DAPK1	F	5'-GACCACGGACGGAAAGACGG-3'
	R	5'-TTCTGTGTGGGTCGGAGCTG-3'
hGAPDH	F	5'-AGCCACATCGCTCAGACAC-3'
	R	5'-GCCAATACGACCAAATCC-3'
HRK	F	5'-AGGTTGGTGAAAACCCTGTG-3'
	R	5'-GCATTGGGGTGTCTGTTTCT-3'
KDM1A	F	5'-ACACCCCGCAAGAAAGAGC-3'

	R	5'-GACCCAGGCACGACAGTAG-3'
KDM2A	F	5'-GGGGTGGCTTGAGAGATCCT-3'
	R	5'-TCCCCACACACATTTTGACATC-3'
KDM2B	F	5'-CGCGGGTGCAGCCCAAATTC-3'
	R	5'-GGCTTCCTCGGGGCATCAAT-3'
KDM3A	F	5'-TTAGCTGAACGAAAGTCACCTG-3'
	R	5'-ATCTCCCAGAAAGCGAACAGA-3'
KDM3B	F	5'-AGATAAACCGCAACATTCGCT-3'
	R	5'-CTGCACCACCAGAGTCCTG-3'
KDM4A	F	5'-ATCCCAGTGCTAGGATAATGACC-3'
	R	5'-TCTTTTGGAGGAACAACCTTGG-3'
KDM4A	F	5'-GAGGAGCTAGAGGCCAAGC-3'
	R	5'-CTTCCAGGTCGGACCCTTC-3'
KDM4C	F	5'-AGCCTCTGACATGCGATTTGA-3'
	R	5'-GGGTCGGCCACATATTCATTC-3'
KDM4D	F	5'-CTGCAACCTGAACGCTATGAC-3'
	R	5'-TGCTCTCCTGGGTAACTGGAC-3'
KDM5A	F	5'-CCGTCTTTGAGCCGAGTTG-3'
	R	5'-GGACTCTTGGAGTGAAACGAAA-3'
KDM5B	F	5'-CCATAGCCGAGCAGACTGG-3'
	R	5'-GGATACGTGGCGTAAAATGAAGT-3'
KDM5C	F	5'-GTGGACAACTTCAGGTTACCC-3'
	R	5'-CGCCGTTCTACATTGGGAATCT-3'
KDM6A	F	5'-TTCCTCGGAAGGTGCTATTCA-3'
	R	5'-GAGGCTGGTTGCAGGATTCA-3'
KDM6B	F	5'-CTACCCCCTTCACATGGCAG-3'
	R	5'-CTCTGACTCGTACAGTTGCCC-3'
MCL1	F	5'-TGCTTCGGAAACTGGACATCA-3'
	R	5'-TAGCCACAAAGGCACCAAAAG-3'
NR2F2	F	5'CAACTGCCACTCGTACCTGTC-3'
	R	5'-GCAAATGTTCTCGATACCCATGA-3'
NSD1	F	5'-TCTGGGCAAAATTCAAGAGACG-3'
	R	5'-CCTCCGGTTGGAAACTTTCATT-3'
RING1A	F	5'-TCAGAACTCATGTGCCCTATCT-3'
	R	5'-GCAGGTAGGACACTCCTTGT-3'
SETD2	F	5'-GGAAAACACAACAACTGAACGAG-3'
	R	5'-TGAGTTTGCTTGTCTGGGTCT-3'
SMYD2	F	5'-GCCCTACAGTAAGCACTATCCT-3'
	R	5'-AGTCTCCCTAGCTTCAACCAC-3'
SUV39H2	F	5'-GGCTAAACAAAGGATAGCTCTGC-3'
	R	5'-TGAAAGAAGCAATCTGTGCATGA-3'
TNFAIP2	F	5'-TGACTTCAGCAAAGGCCACCT-3'
	R	5'-TAAGGGAAAATAGGGGCCGGGA-3'
TNFRSF10A	F	5'-ACCTTCAAGTTTGTCGTCGTC-3'
	R	5'-AACTCTCCCAAAGGGCTATGT-3'
TNFRSF11B	F	5'-GCGCTCGTGTTTCTGGACA-3'
	R	5'-AGTATAGACACTCGTCACTGGTG-3'

TNFRSF14	F	5'-ATGGGACCCTGGAGGAATGTCA-3'
	R	5'-TTTTCCGCTGGACGGAGACGAT-3'
TNFRSF1B	F	5'-ACCCAGGTGAAAAAGAAGCCCT-3'
	R	5'-CCTTATCGGCAGGCAAGTGA-3'
TRIAP1	F	5'-TCGCTGGTTCGCCGAGAAAT-3'
	R	5'-TTGCTTTCTGAACACACTGCTGG-3'
XAF1	F	5'-CAGCTCGGGAAAGGGGAAAGAAT-3'
	R	5'-TTCAGCAGCTTGACTTGGAAGAGA-3'

Table 2. List and DNA sequences of the primers used in q-RT-PCR experiments

10. Histone extraction

Abcam's protocol for histone extraction was modified and followed [91]. Cells were harvested and washed twice with ice-cold PBS. Cell pellets were resuspended in Triton Extraction Buffer (TEB: PBS containing 0.5% Triton-X-100 (v/v), 2 mM phenylmethylsulfonyl fluoride (PMSF), 0.02% (w/v) NaN3) at a cell density of 10^7 cells per ml and lysed on ice for 10 minutes. The lysate was centrifuged at 6,500 x g for 10 minutes at 4^{o}C to remove the supernatant and collect the nuclei at the bottom as pellet. The pellet was washed with half volume of TEB and centrifuged..The supernatant was removed and the pellet was resolubilized in 0.2N HCl as $4x10^7$ nuclei per ml. The solution was incubated at 4^{o}C overnight. Next day, 1/5 volume of 1M NaOH was added into the solution to neutralize the pH. The mixture was centrifuged at 6,500 x g for 10 minutes at 4^{o}C and the supernatant was collected. Protein quantifications of the lysates were performed by Pierce BCA Protein Assay Kit (Life Technologies, USA) by utilizing BSA control samples prepared in 0.2N HCl plus 1/5 volume of NaOH. The extracts were stored at -20^{o}C.

11. Western blotting

Cell lysates were prepared by harvesting cells from their culture vessels. Accordingly, cell culture medium was removed, adherent cells were washed with PBS, trypsinized, and collected by centrifugation at 1500 rpm for 5 minutes. The cell pellet was washed once with ice cold PBS. In few experiments that included TRAIL treatment, media of the cells was also collected and combined with the cell pellet. The cell pellets were lysed with NP40 lysis buffer (according to modified version of invitrogen's online available protocol) for 30 minutes, on ice, with brief vortexing at 10-minute intervals. Lysates were centrifuged at 13,000 rpm at 4^{o}C for 10 minutes. Supernatant was transferred and stored at -80^{o}C.

NP40 lysis buffer was prepared by constituting the following reagents with following final concentrations: 50 mM Tris (pH 7.4), 250 mM NaCl, 5 mM EDTA, 50 mM NaF, 1% NP40 and 0.02% NaN3. The buffer is aliquoted and stored at -20^{o}C. Lysis buffer was supplemented with protease inhibitor (Roche, Switzerland) and 1 mM final concentration of PMSF (0.3M stock in DMSO) before each use. Protein quantifications of the lysates were performed by Pierce BCA Protein Assay Kit (Life Technologies, USA) by utilizing BSA control samples prepared in NP40 lysis buffer. Lysates were mixed with 1x final concentration of 4x loading dye and boiled at 95^{o}C for 15 minutes. Loading dye was prepared by mixing 900 ul of 4X Laemmli sample buffer (Biorad, USA) with 100 ul of beta-mercaptoethanol (Biorad, USA). Boiled samples were stored at -20^{o}C.

For immunoblotting, 10-20 µg of whole-cell extract proteins or 1-2 ug of acid histone extract proteins were resolved on 4-15% gradient and 10% constant Mini-PROTEAN® TGX™ Gel (Biorad, USA), respectively, by using 1X TGS (Tris-glycine-SDS, Biorad, USA) as the running buffer. Proteins on gel were transferred to PVDF membrane by semi-dry Trans-Blot Turbo Transfer System. Transfer buffer used was 1X TGS (Tris-glycine-SDS, Biorad, USA) having 20% EtOH and the transfer program used was Biorad's pre-defined Standard SD transfer program (30 minutes 25V). After transfer, membrane was incubated at room temperature for 10 minutes covered with Ponceau S Red (Biorad, USA). Membrane was washed with ddH2O until the bands were clear enough to visualize the efficiency of transfer and equal loading. Membrane was blocked with 5% non-fat dry milk (Biorad, USA) in 1X TBS-T (from 10X TBS stock) for 1 hour at room temperature. 10X TBS stock was prepared by mixing 24 g Trizma Base and 88 g NaCl in 900 mL nanopure water. pH was adjusted to 7.6 w/ 12N HCl then stock was filled up to 1 liters. 1X TBS-T was prepared by diluting the stock and adding 0.1% Tween-20. Membrane was probed with the antibodies listed in Table 3 in primary antibody solution (2% BSA, 0.02%NaN3 in TBST) overnight at +4^{o}C. Next day, membrane was washed 3 times with TBST for 15 minutes each and incubated with HRP-conjugated secondary antibodies (1:5000) in blocking buffer for 1 hour at room temperature. Membrane was washed 3 times with TBST for 15 minutes each. Protein bands were detected by chemiluminescence system of Pierce ECL Western Blotting substrate (Life Technologies, USA) as instructed by the manual. Developed films were scanned as high DPI TIFF images. Quantification of the band intensities was carried out by ImageJ software (NIH Image, NIH Bethesda, USA). The images were uploaded to ImageJ and converted into 8-bit binary images. The values were normalized to alpha-tubulin band intensities of each sample.

Antibody	*Catalog Number*	*Brand*
α-Tubulin	T9026	Sigma-Aldrich
Cleaved Caspase-3	9664	Cell Signalling
Caspase-7	12827	Cell Signalling
Cleaved Caspase-8	ALX-804-242-C100	Enzo
Cleaved PARP	5625	Cell Signalling
JHDM1B/KDM2B	09-864	Millipore
H3K36me2	ab9049	Abcam
H3K36me3	4909	Cell Signalling

Table 3. List of the primary antibodies used in western blotting experiments

12. Real-Time Cell Growth Analysis

ACEA Biosciences' (USA) xCELLigence RTCA SP Station and Analyzer was utilized for real-time cell growth analysis. Single use, disposable E-Plate 96 plate was loaded with 100 ul of cell culture media per well and left for 30 minutes at room temperature to achieve the optimal equilibrium. The plate was inserted into RTCS SP Station, scanned by the software to measure the background impedance of blank cell culture The plate was removed and cell suspensions of 1000 or 5000 U87MG cells in 100 ul of cell culture media was added into the wells. The plate was reinserted. Impedance of the wells were scanned and quantified with 30 or 20 minute intervals for 24 or 202 hours.

13. Live-cell microscopy

All live-cell imaging experiments were carried out by Olympus Xcellence Pro inverted microscope with a 10X air objective in a chamber at 37^{o}C, supplied with 5% CO2. Time-lapse images were captured by ANDOR iXon3 EMCCD right after TRAIL treatment for 24 hours as 1440 frames/minute by 10X brightfield objective (DIC-40 contrast insert) with 100 ms exposure time and 2,1 volt transmission lamp. Arbitrarily identified 4 to 5 positions were recorded per sample/well. Time-lapse images were then converted into avi movies or TIFF image-stacks by using Xcellence RT 1.2 software. The numbers of apoptotic bodies were counted on each window by loading the avi movies on ImageJ (NIH Image, NIH Bethesda, USA) software. The frames were converted into binary image stacks. Particles having size (pixel^2) of 10 to infinity and circularity of 0.60 to 1.00 were denoted as apoptotic bodies on each frame.

14. RNA-seq library preparation and sequencing analysis

Total RNAs of shControl and shKDM2B cells were isolated using NucleoSpin RNA isolation kit (Macherey-Nagel, Germany). Construction and sequencing of RNA-seq library for each sample was carried out using TruSeq RNA-seq (polyA) Library Prep v2 based on protocols on Illumina HiSeq2500 to generate 50 bp single-end reads. RNA sequence data were generated from the sequencer and converted to FASTQ files using the Illumina CASAVA 1.8.2 pipeline at Weill Cornell Medical College (WCMC) epigenomics core. The reads that passed the quality control were aligned to human genome assembly hg19 using TopHat2 [92], which uses ultra-high-throughput short read aligner Bowtie as its core alignment engine and then analyzes the results to identify splice junctions between exons. The reads were annotated and counted for each transcript using Ensembl annotations available at the UCSC Genome Browser with R package GenomicFeatures [93]. The versions of the software used were TopHat2 v2.0.11, Bowtie v2-2.2.1 and Samtools v0.1.19.0. The RNA sequencing data from this study will be submitted to the NCBI Gene Expression Omnibus (GEO) (http://www.ncbi.nlm.nih.gov/geo/) and GSE numbers will be published. Around 18 million reads were acquired from sequencing of each sample that yielded in around 800 megabases. Around 83% of those reads passed filter (PF) quality check. Around 93% of those sequenced bases were equal or above Q score of 30. Mean quality score of the PF reads were around 37.

15. Statistical and functional analysis of the RNA-seq data and differentially expressed gene identification

Statistical and functional analysis of the RNA-seq data was carried out in collaboration with Dr. Zeynep Hulya Gumus (Mount Sinai Hospital, US). Accordingly, differentially expressed genes between shKDM2B and shControl cells were detected by DESeq [94], which controls for Type I Errors (false-positives) by modeling the count data with extended Negative Binomial distributions, and thereby allows for general, data-driven relationships between variance and mean, and provides an effective algorithm for fitting the model to data. Note that each paired comparison, genes with mean read count in both sets of samples with fewer than 10 were filtered out; for the remaining genes, if the read count was 0 in either set (but not both of them), the read count was set to be 1 before input to R DESeq package for differential expression calculation. Significant differentially expressed genes for each pairwise comparison were selected with multiple-testing correction to maintain False

Discovery Rate (FDR) at 5%. Genes with expression values that changed by a factor of 1.5 fold were deemed significant.

To relate the results to cell physiologic mechanisms, the complex biological processes induced by shKDM2B as compared to control were examined in the context of functional groups with Ingenuity Pathways Analysis (IPA), a web-delivered commercial application. Transcript identifiers were uploaded to IPA, each identifier was mapped to its corresponding gene object in the IPA Knowledgebase (www.ingenuity.com), which was searched for categories statistically enriched in the differentially expressed gene set, and the likelihood of perturbations in each category was scored.

16. *In vivo* experiments

All *in vivo* experiments were approved by the institution review boards of Koç University (HADYEK#2014-22) and carried out by certified researchers according to the guidelines.

U87MG cells that stably stably express shControl or shKDM2B vectors were used for in vivo experiments. These cells were transduced with lentiviral vectors encoding Firefly Luciferase (Fluc) and mCherry as described [88]. First, mCherry expression was verified under fluorescence microscopy, and Fluc activity was verified with *in vitro* luminescence assays. Accordingly, increasing number of cells (0-50.000/well) were seeded on 96-well plates and incubated with D-Luciferin (10 ug/ml) for 10 min. Bioluminescence was measured by BioTek's Synergy H1 plate reader and Gen5 data analysis software.

6-8 week old SCID mice, housed in appropriate conditions of Koç University Animal Facility, were used for tumor implantation experiments. $2.5x10^6$ cells that stably expressed Fluc and mCherry cells were injected in 50 ul PBS subcutaneously into 7 SCID mice. Starting from 1 day after injection, tumor cells were visualized by Fluc imaging using IVIS Lumina III equipment by injecting mice with 150 ug/g body wt. of D-luciferin (Biotium) intraperitoneally. The tumor progression was monitored with sequential Fluc bioluminescence activity over time for a period of 1 month. All Fluc imaging experiments were carried out on mice anesthesized by isoflurane. Following data acquisition, the mean, standard deviation, and sum of the photon counts in the regions of interest were calculated and plotted. At the end of the experiments, the tumors of these mice were dissected and further analyzed with immunohistochemistry

17. Immunohistochemistry

Tumor histology experiments were performed in collaboration with Dr. Sercin Karahuseyinoglu (Koc University). Accordingly, samples were fixed by 4% paraformaldehyde for 24 hours followed by 20% and 30% (wt/vol) sucrose treatment for cryosectioning. Consecutive cryosections (10 µm) were used for a routine hematoxylin/eosin staining and fluorescent stainings. Vascular endothelial growth factor (VEGF) followed by fluorescent conjugated secondary antibody of Alexa fluor 488 GAM was used for evaluation of vascular structures. Alexafluor 488 conjugated annexin V (Dead Cell Apoptosis Kit, Life Technologies, USA) was used for assessment of apoptotic activity. Dilutions were used as 1:50 for primary antibodies and 1:100 for the secondary antibody. All antibodies were incubated at 37°C for 2 hours. Hoechst (1µg/ml) was used in mounting medium. All antibodies were purchased from abcam. Images were taken under a Nikon Eclipse 90i confocal microscope and a Zeiss axioscope.

18. Beta-galactosidase staining

100,000 cells per well were seeded in 6-well plates. and cultured for 24-hours X-gal staining solution is prepared as following. 40 mg of X-gal is dissolved in 1 mL DMSO and then filtered to reduce formation of crystals in the wells upon staining. The rest of the components of X-gal staining solution if shown in the following table:

Reagent	Final Concentration	Stock Concentration	Vol required for 10 ml
X-Gal	1 mg/ml	40 mg/ml	250 µl
NaCl	150 mM	5 M	300 µl
$MgCl_2$	2 mM	1 M	20 µl
$K_3Fe(CN)_6$	5 mM	100 mM	500 µl
$K_4Fe(CN)_6$	5 mM	100 mM	500 µl
NaP (pH 6.0)	40 mM	1 M	400 µl
Water			8030 µl

When the desired cell confluence was reached, the media was aspirated, cells were washed with 1X PBS and fixed by 0.2% gluteraldehyde for 5 minutes at room temperature. Fixation media was removed followed by washing with 1X PBS. PBS was aspirated and cells were stained with X-gal staining solution at 37^{o}C until blue

colored cells started to appear. When the perinuclear staining started to appear, staining was stopped by removing X-gal solution and washing once with PBS. The wells were covered with 50% glycerol solution and then plates were stored at 4^{o}C. Images were captured with an inverted Nikon Eclipse TS100 microscope with CFI Plan Fluor Series objectives integrated with Nikon DS-Fi2 high-definition color camera.

19. Flow cytometric analysis of cell cycle with propidium iodide

300,000 cells per well were seeded in 6-well plates. On the second day, cells were harvested by trypsin and transferred to 5 ml polystyrene flow tubes (BD Biosciences, USA). Following centrifugation for 5 minutes at 1500 RPM, cell pellets were washed once with 1 mL PBS at room temperature by resuspending. Tubes were centrifuged again. Supernatant was aspirated carefully, leaving some PBS in the bottom. Cells were fixed by dropwise addition of 1 mL ice-cold 70% ethanol on cells as they were gently being vortexed.. The tubes were incubated for 30 minutes at 4^{o}C. Tubes were centrifuged at 850xg for 5 minutes this time to maximize pelleting out of EtOH. Pellets were washed twice in 1 mL PBS at room temperature and centrifuged. The pellets were treated with ribonuclease for 15 minutes at room temperature by addition of 50 ul of 100 ug/mL stock of RNase A. 200 ul of 50 ug/mL Propidium Iodide (PI) (Sigma Aldrich, USA) was added into tubes and incubated at room temperature for 30 minutes. Next, 200 ul of room temperature PBS was added and cell suspensions were filtered through filtered caps of BD Falcon 5 mL polystyrene tubes.. Samples were inserted into BD Accuri C6 flow cytometer (BD Biosciences, USA) and run at slow speed. Signals from PI were analyzed on FL2-A channel.

20. Chromatin Immunoprecipitation (ChIP)

All buffers and reagents in this protocol were prepared as described previously [95]. 10x10^{6} adherent cells were collected with trypsin and pelleted by centrifugation. Media was aspirated as leaving 1 mL at the bottom. The tube was flicked several times rigorously to ensure achieving uniform cell suspension. The cell mix was filled up to 5 mL by fresh media. Proteins in the cells were cross-linked to DNA by treating with Formaldehyde (37%) to media to a final concentration of 1%. The cells were incubated at 37^{o}C cell culture incubator, inverting the tube two times in 5th minute. Cross-linking was quenched by adding Glycine (2.5M) to a final concentration of 0.125M and incubating at 37^{o}C for 5 minutes. 5 mL ice cold PBS was added and then

cells were harvested by centrifuging at 1500 RPM for 5 minutes. Media was aspirated and cells were washed with 5 mL ice cold PBS by resuspending. Cells were pelleted and lysed in 1 mL lysis buffer (LB), and immediately put on ice. 1 mL was divided into 2 eppendorf tubes as 500 ul and immediately put at -80^{o}C until sonication. For sonication, one tube at a time was transferred from -80^{o}C to room temperature. Tube was thawed by keeping in palm of a hand until white SDS becomes clear. Upon fully thawing and flicking once, tube was left at room temperature for 10 minutes for lysis. After 10 mins, 500 ul of ice-cold chip dilution buffer (CDB) supplemented freshly with protease inhibitor was added in mix. Branson 250 Digital sonifier machine was used for sonication, programmed to 0.7 s 'On' and 1.3 s 'Off' pulses at 40% power amplitude for 9 minutes. Probe of the sonicator was adjusted to optimal depth within tube such that it neither touched wall of tube nor sprayed cells out. Cells were immediately sonicated in tube kept in wet-ice filled bucket during sonication, achieving optimal 200-700 bp fragmentation of chromatin. Tip of the probe was cleaned with ddH2O in between samples. Right after sonication, the tube was centrifuged at 4^{o}C at max speed for 10 minutes. A dark pellet and insoluble SDS should form at the bottom and walls of the tube. 50 ul of supernatant was transferred and stored as whole cell extract (WCE). WCE was stored at -20^{o}C. Remaining ~900 ul of supernatant was transferred into 2 mL tube and mixed with ice-cold 900 ul of CDB supplemented freshly with protease inhibitor. This ensures that high concentration of SDS in LB is diluted 10 times with CDB before incubating with antibodies. 2 ug antibody (JHDM1B, 09-864 Millipore) was added into the mix and incubated at 4^{o}C overnight in a rotator at medium speed. Next day, Dynabeads (Life technologies, USA) protein A and G were removed from 4^{o}C to and gently vortexed. A mixture of 15 ul from each was prepared. The mixture was washed with twice the volume of CDB and then placed in a magnetic rack to collect the beads out of solution. Supernatant was aspirated and the wash step was repeated. The beads were then reconstituted in 20 ul of CDB. Mix was added into overnight incubating antibody mix. The final mix was incubated at the same rotator at the same speed for 2 hours at 4^{o}C. After incubation, by using the magnetic rack, the beads were collected and then washed consecutively twice with ice-cold 1 mL of low-salt wash buffer, ice-cold 1 mL lithium chloride wash buffer and ice-cold 1 mL TE buffer. In between each wash and collection of beads, supernatant was aspirated, except the last TE buffer washes, whose supernatant was withdrawn by a 1 mL micropipette. A final elution buffer is prepared by mixing 5 ul of 1M DTT with 1 mL elution buffer (EB). Beads collected in the last step were reconstituted in 125 ul of EB and then incubated at 65^{o}C for 15 minutes. WCE from previous day was thawed and mixed with 200 ul of

EB. WCE was incubated at 65ºC as well along with the ChIPed sample. After 15 minutes, beads were harvested by the magnetic rack and EB was transferred into a new tube. The beads were reconstituted once again in 125 ul of new EB and incubated at 65ºC for 15 minutes. After 15 minutes, the beads were collected again and EB was combined with the previous 125 ul of EB. 250 ul of WCE and EB were incubated at 65ºC for at least 5 hours (up to overnight) in a water-bath. After incubation, tubes were minispinned and cooled down to RT. 5 ul of 20 mg/mL proteinase K was added into each, followed by a short vortex and a minispin. Samples were left 2 hours or overnight at 37ºC preferentially in a water-bath or in a cell culture incubator. Next day, 250 ul of ice-cold ultrapure IPC (Phenol:Chloroform:Isoamyl Alcohol 25:24:1) was added on each sample. Samples were vortexed thoroughly for 30 secs and centrifuged at maximum speed for 10 minutes at 4ºC. The top aqueous layers were carefully transferred into tubes filled with 500 ul of 100% EtOH, 25 ul of 3M NaAc and 1 ul of 20 mg/ml glycogen. The tubes were vortexed for 30 seconds and stored at -80ºC for 2 hours. The tubes were then centrifuged for 30 minutes at 4ºC at maximum speed. The supernatant was discarded carefully without losing the pellets. The pellet was washed with 1 mL of 70% EtOH by simple addition on top of the pellet and centrifuged for another 10 minutes at maximum speed. Ethanol was discarded carefully without disturbing the pellets. The pellets were air dried for 10-15 minutes and reconstituted in 50 ul of nuclease free water and 1 ul of 20 mg/mL RNAse A. The tubes were incubated at 37ºC for 30 minutes. DNA in the tubes were quantified utilizing Qubit dsDNA High-Sensitivity Assay Kit (Life technologies, USA). q-RT-PCR were conducted using minimum of 180 picogram DNA per well. Primers used for ChIP-qPCR are listed in Table 2. Data showed in the thesis are acquired in Dr. Mazhar Adlı's lab at University of Virginia, with help of Dr. Cem Kuscu.

21. Statistical analysis

Data were analyzed by Student t-test when comparing two groups. Data were plotted as mean ± SEM and differences were considered significant at $p < 0.05$ or $p<0.01$. *, **, *** denotes $P<0.05$, $p<0.01$, $p<0.001$ on the figures.

Chapter 3

Results

shRNA screen reveals KDM2B and RING1A as modulators of TRAIL-induced apoptosis in GBM cells

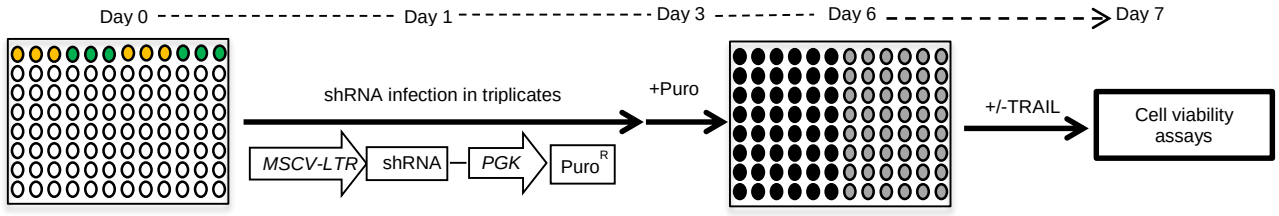


Figure 12. Schematic diagram of the experimental setup for the shRNA screen in U87MG GBM cells. Cells were individually infected with 125 different shRNAs targeting 48 different chromatin modifying enzymes in triplicates. Cell Titer Glo assays (Promega) were conducted after 100 ng/ml TRAIL treatment for 24 hours. An shRNA targeting Firefly Luciferase was utilized as control (shControl). (Conducted by Zeynep Kahya and Dr. Tuğba Bağcı-Önder)

In order to identify the key chromatin modifying enzymes (CME) regulating the apoptotic response of GBM cells, we employed 125 shRNAs in pSMP retroviral backbone targeting 48 different chromatin modifying enzymes. Each gene was targeted by 2 or 3 separate shRNAs. Among these enzymes, there were DNA methlytransferases (DNMTs), histone methyltransferases (HMTs), histone demethylases (HDMs), methylated DNA binding proteins, polycomb-group proteins (PRCs) and few transcriptional factors. U87MG cells were infected separately by each shRNAs in triplicates, followed by TRAIL treatment (**Figure 12**) (**Table 1**).

We first assessed the effects of shRNAs alone on GBM cell viability, since this would allow us to reveal the false-positive shRNAs displaying intrinsic toxicity leading to cell death without TRAIL treatment. Accordingly, 15 out of 125 shRNAs lied out of 2 standard deviation (SD) borders when compared to shControl (**Figure 13**). This suggested that majority of the knockdowns did not significantly alter the proliferation capacity of the cells. 2 of the 125 shRNAs, which caused ~100% cell death after Puromycin selection possibly due to viral packaging problems, were eliminated from further analyses of the screen. We then continued with the analysis of percent change in cell viability after TRAIL treatment.

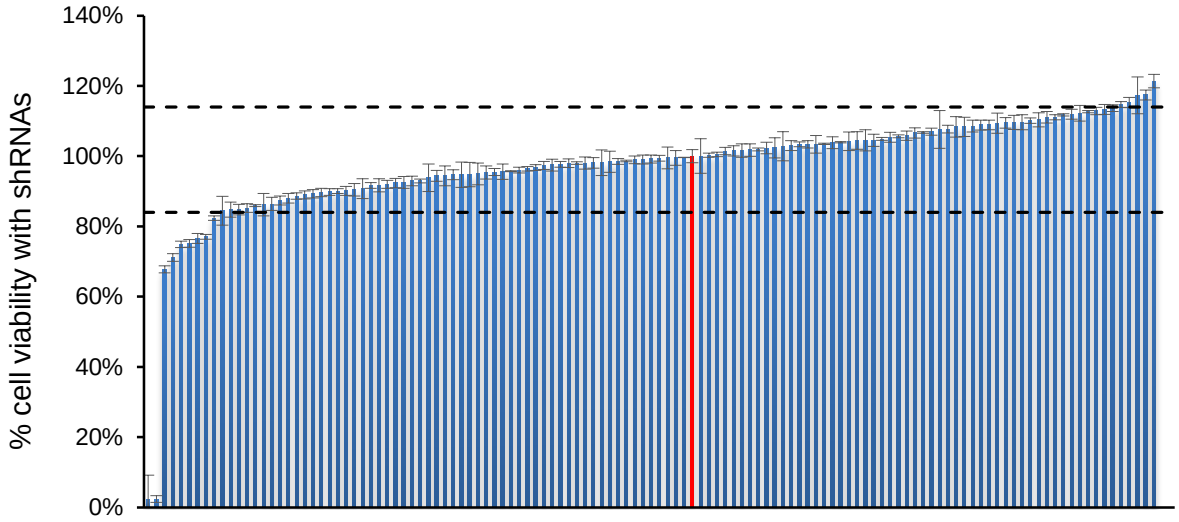


Figure 13. Percent viability analysis of the untreated wells after shRNA infection. Data were normalized to the shControl cells. Red bar indicates shControl. Dotted lines denote the significance limits based on 2 standard deviations (SD) below and above of shControl.

We wished to graph the percent change in cell viability of the transduced and TRAIL treated cells, as compared to their transduced only control cells. There were three possible outcomes for the alterations of the TRAIL response upon silencing of a CME gene. Silencing of a CME gene could make GBM cells more resistant or sensitive to TRAIL-induced apoptosis, or have no effect. Therefore, we plotted the percent change in TRAIL-induced decrease of cell viability upon silencing of target CMEs by 125 shRNAs to identify shRNAs that caused a more TRAIL-sensitive or -resistant phenotype (**Figure 14**).

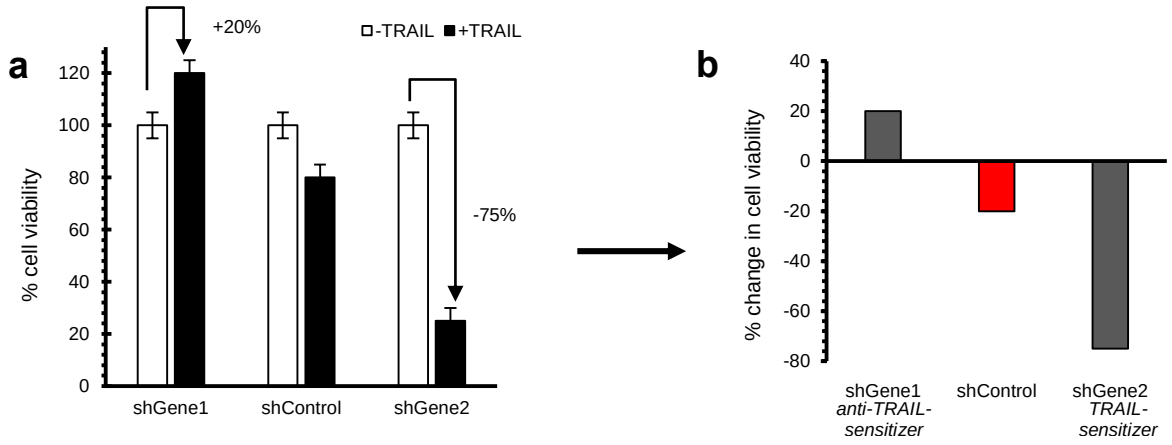


Figure 14. The analysis strategy for the shRNA screen. (a) Viability analysis as representative graph showing possible outcomes of TRAIL response upon silencing of two genes. (b) Graph reflecting percent change in cell viability upon silencing of each gene rendered from data in figure a.

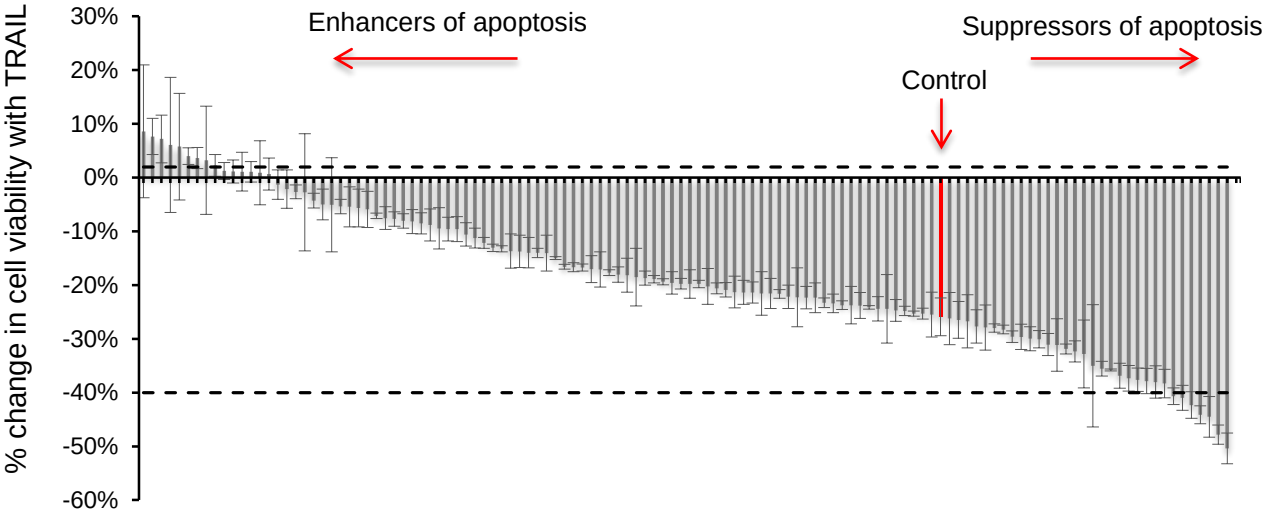


Figure 15. Percent change in viability analyses of the infected cells upon TRAIL treatment. Red bar indicates shControl. The effects of shRNAs below and over that of shControl were classified as suppressors and enhancers of apoptosis respectively. Dotted lines denote the significance limits based on 2 standard deviations (SD) below and above of shControl.

Assessing the percent change in the cell viability of the transduced cells after TRAIL treatment resulted in a wide range of responses (**Figure 15**). Accordingly, we categorized CMEs into two groups based on the phenotype observed upon their silencing compared to shControl cells :1) suppressors of apoptosis, if their knockdown sensitized the cells to TRAIL, or 2) enhancers of apoptosis, if their knockdown conferred cells more resistance to TRAIL.

We focused on the genes whose (of which) silencing sensitized the cells to TRAIL-induced apoptosis more than 2 SD. Among these 5 genes (**Figure 16**), we continued with the consistent genes/hits whose (of which) at least 2 out of 3 shRNAs sensitized GBMs to TRAIL.

As a result, we identified KDM2B and RING1A, an H3K36-specific demethylase and a E3 ubiquitin-protein ligase of H2AK119 respectively, as novel regulators of TRAIL response. We decided to focus on KDM2B and continued our further experiments to characterize the effects of KDM2B loss and mechanisms behind its regulatory role in apoptotic response of GBM cells.

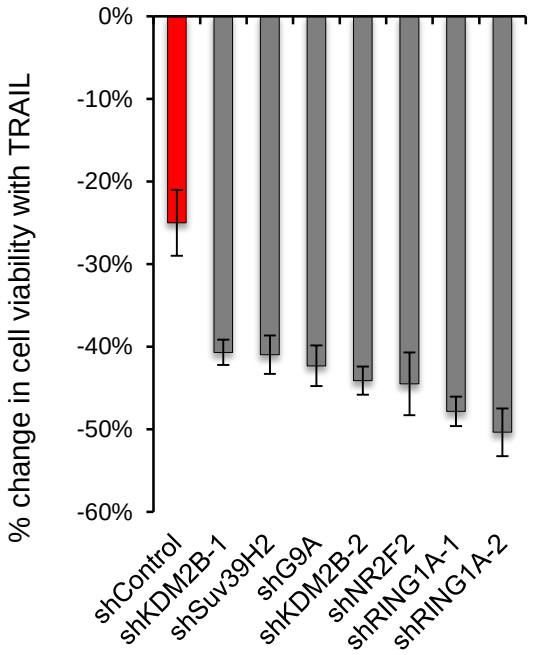


Figure 16. Graph showing the top hits, below 2 SD of shControl, as suppressors of apoptosis. shKDM2B and shRING1A were identified twice by two independent shRNAs.

shRNAs can knockdown their targets efficiently

In order to check the efficiency of the shRNAs used in the screen, we quantified the levels of knockdowns of the individual shRNAs targeting the top sensitizer hits. As assessed by q-RT-PCR experiments, we have observed silencing of the target genes down to at least ~40% in each shRNA (**Figure 17**).

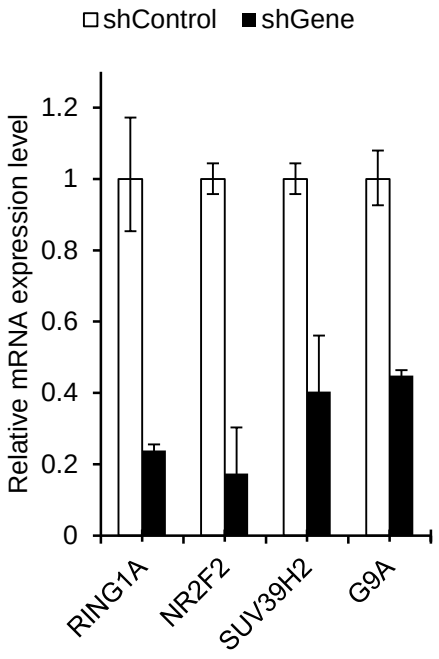


Figure 17. q-RT-PCR analysis of the top-hit target genes in shControl and shGene transduced U87MG cells. mRNA levels of the target genes relative to GAPDH mRNA levels were measured and relative expression was determined with ΔΔCt method. (Conducted by Selena Kazancıoğlu)

KDM2B can be successfully silenced at both transcriptional and translational levels

Analysis with two separate shKDM2Bs demonstrated that both shRNAs reduce KDM2B mRNA levels down to ~50% (**Figure 18a**). Knockdown to similar levels at protein level was only achieved with shKDM2B-2 (**Figure 18b**), although both could silence at mRNA level.

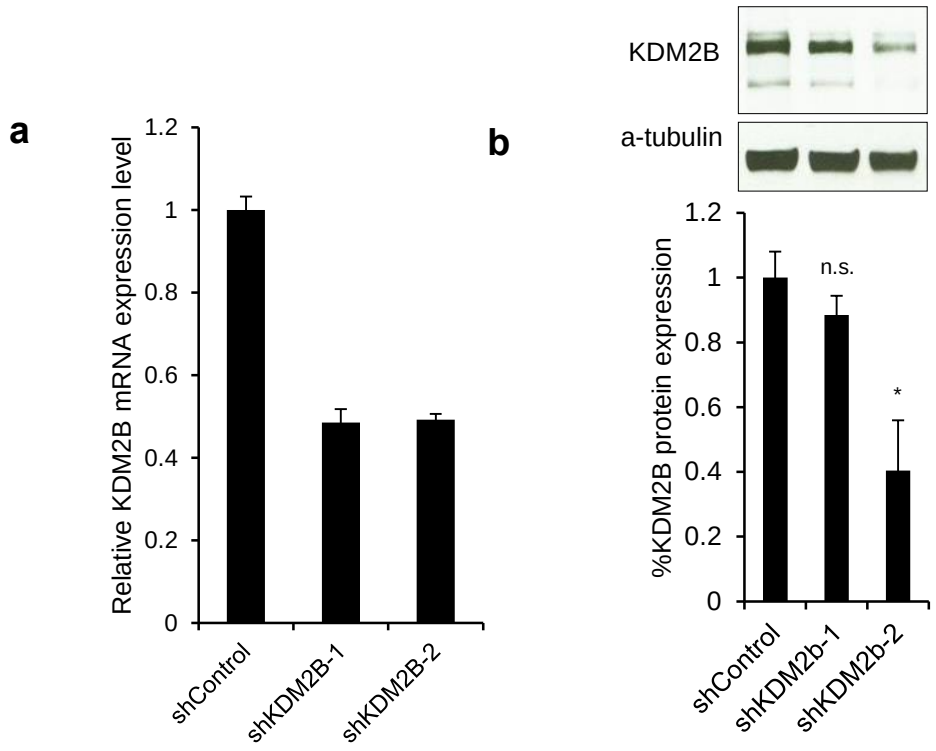


Figure 18. (a) qRT-PCR analysis of KDM2B in shControl and shKDM2B transduced U87MG cells. KDM2B mRNA levels relative to GAPDH mRNA levels were measured and relative expression was determined with DDCt method. (b) Western blot analysis of KDM2B in whole-cell lysates of U87MG cells infected with shControl, shKDM2B-1 and shKDM2B-2. Western blots were scanned and band intensities were determined using ImageJ. (*,**,*** denotes $P<0.05$, $p<0.01$, $p<0.001$, t-test)

Knockdown of KDM2B does not affect the expression of other KDM family members

One common issue with the RNAi technology is the possible compensation mechanisms in the cells to balance the change upon knockdown. One gene that is knocked-down could be compensated by upregulation of closely related other genes conducting same or similar enzymatic activity within same family, or unrelated genes taking role in the same pathway [96–98]. To see whether any compensatory regulations upon knockdown of KDM2B happens within KDM family and also to check whether the shRNA targeting KDM2B is specific, we conducted q-RT-PCR experiments and checked the mRNA levels of other known KDM family members (**Figure 19**). We did not observe major changes in the levels of KDM family members, except for slight upregulation of KDM3A, KDM4B, KDM5A, KDM5B and KDM6B expression, which were considered non-significant as the fold changes were all below 1.5. These results suggested that knockdown of KDM2B is specific.

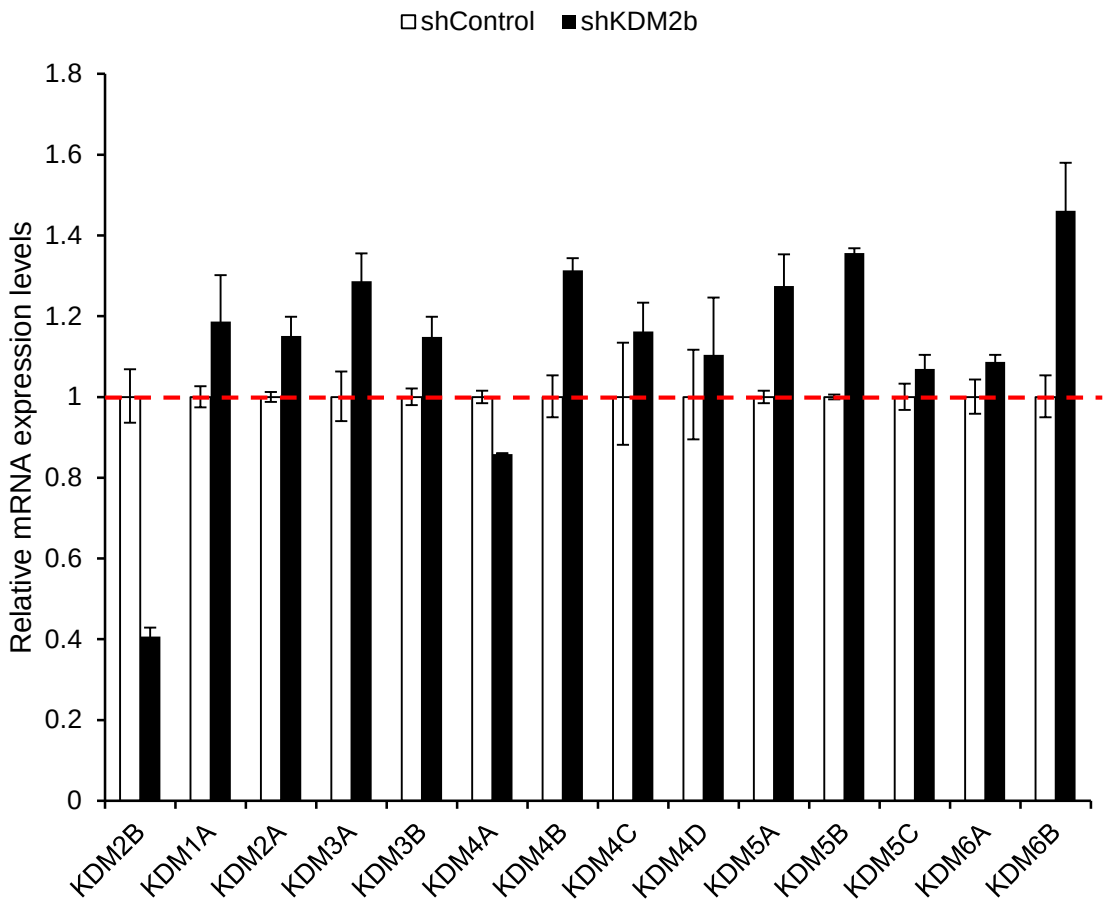


Figure 19. q-RT-PCR analysis of the KDM family members in shControl and shKDM2B transduced U87MG cells. mRNA levels of the target genes relative to GAPDH mRNA levels were measured and relative expression was determined with ΔΔCt method. (Conducted by Selena Kazancıoğlu)

Loss of KDM2B cooperates with TRAIL to reduce GBM cell viability

The screen results suggested that silencing of KDM2B could cooperate with TRAIL in reducing cell viability. To validate this further, we repeated the cell viability measurements and observed that shKDM2B cell viability was lower upon TRAIL treatment compared to shControl cells (**Figure 20**). As expected based on the knockdown efficiency (Figure 10), shKDM2B-2 cells responded better to TRAIL. Thus, we chose shKDM2B-2 as our major shRNA for future experiments.

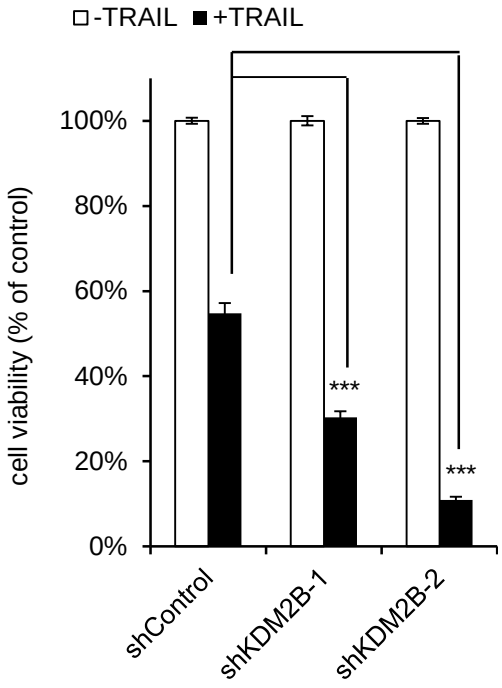


Figure 20. Viability analyses of U87MG cells after KDM2B knockdown by two separate shRNAs and 100 ng/mL TRAIL treatment. (*,**,*** denotes P<0.05, p<0.01, p<0.001, t-test)

KDM2B loss accelerates TRAIL-induced cell death

In order to observe the differences in cell death in shControl vs shKDM2B cells in further detail, we employed an assay that measures cell growth in real-time. In this assay, cells are seeded in a specialized plate that can measure electrical impedance in each well. The wells are covered with micro-electrodes covering 80% of the surface area at the bottom of each well. By applying small voltages, the impedance of adherent cells are quantified and transformed into cell index. This analysis in shControl and shKDM2B cells for 24 hours upon TRAIL addition revealed that silencing of KDM2B not only augments TRAIL response but also accelerates the process of cell death (**Figure 21**). There was no observable difference between untreated cells, showing that shKDM2B has no significant effect on short-term (24 hour) proliferation dynamics.

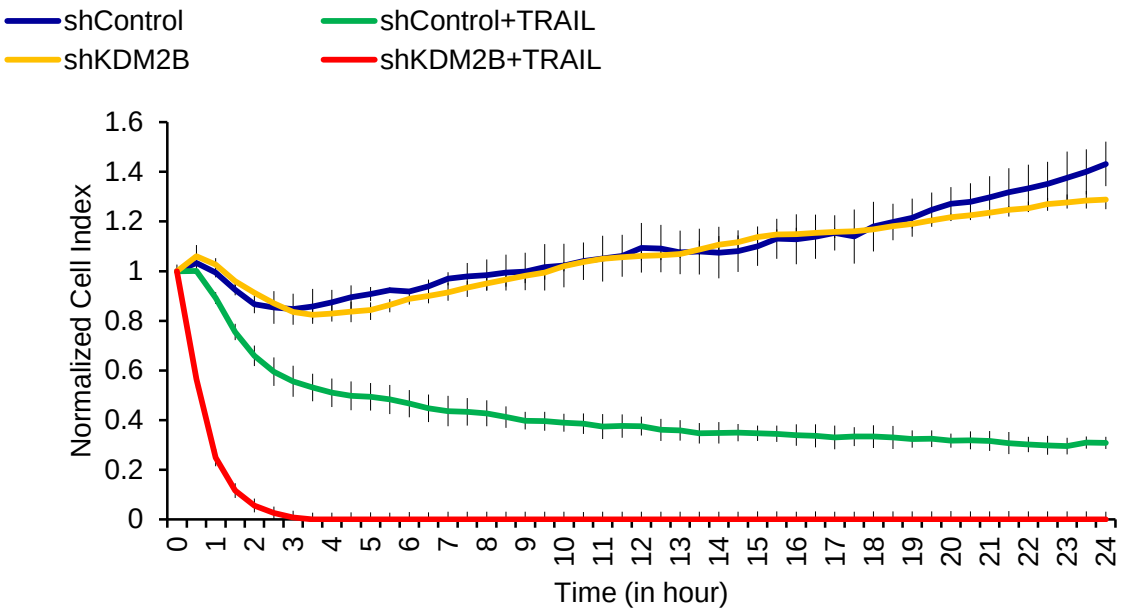
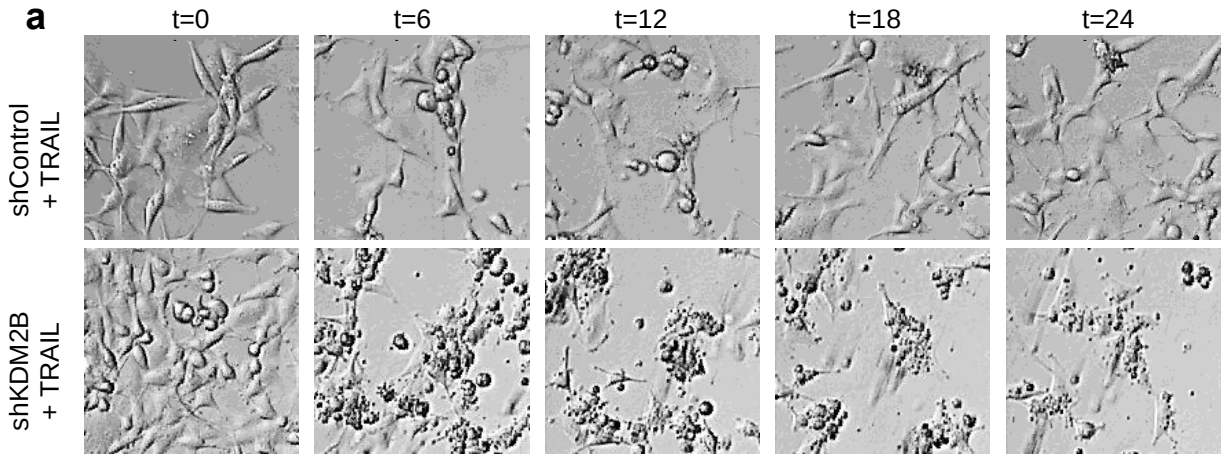


Figure 21. Real-time viability analysis of the shControl and shKDM2B cells upon TRAIL treatment by xCELLigence system (Roche). Cell index is normalized to the time of TRAIL addition.

This phenotype was also validated by live-cell imaging experiments, where the morphology of individual cells as well as apoptotic processes can be observed in real-time under a staged microscope (**Figure 22a**). As shown by automated quantification of the number of apoptotic bodies per frame during the 24 hours period right after TRAIL addition, the process of apoptosis was accelerated in shKDM2B cells compared to controls (**Figure 22b-c**). Presence of apoptotic particles reaches its maxima around 6 hours after the treatment in shKDM2B cells, earlier and in significantly higher numbers than shControl cells.



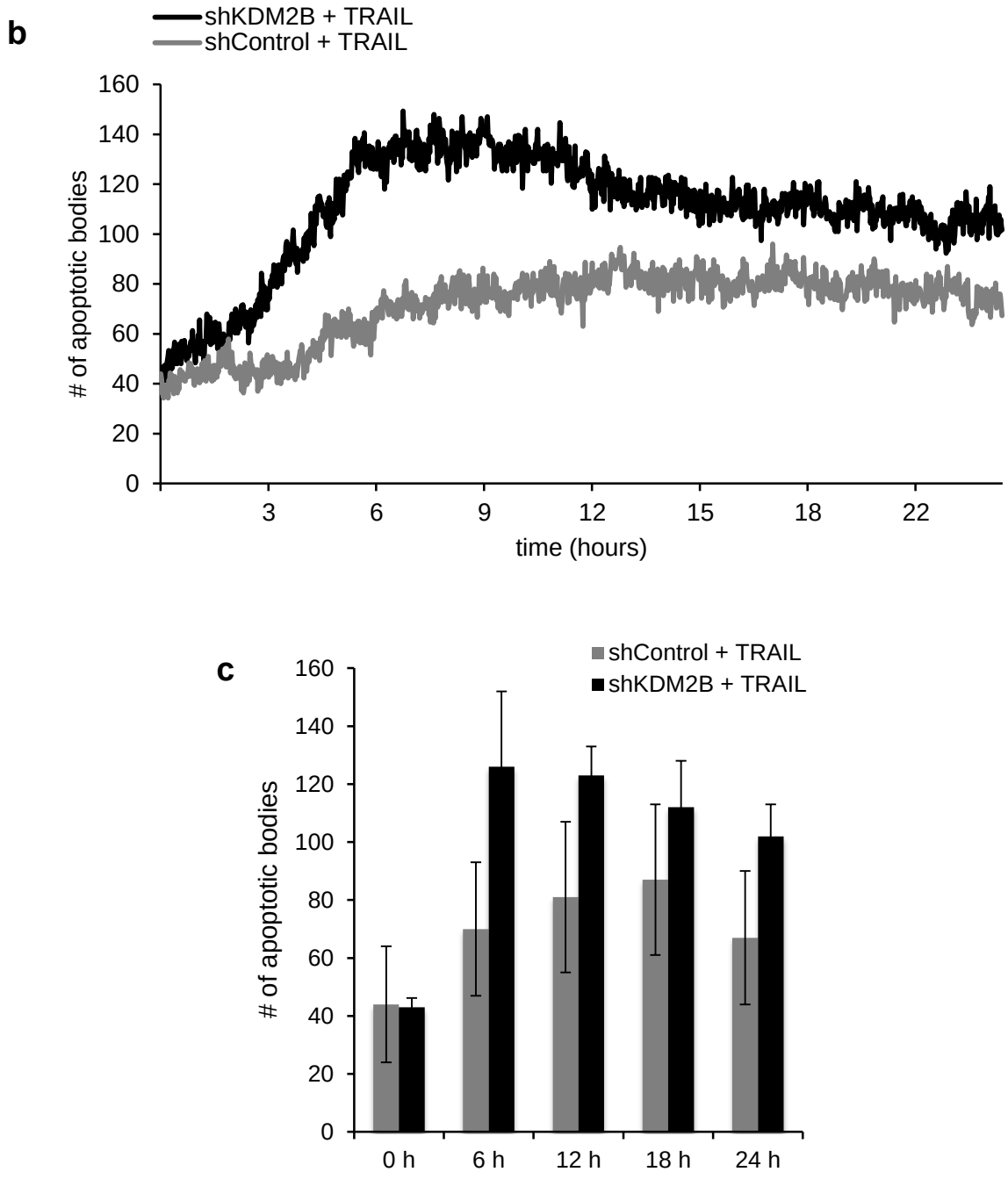


Figure 22. (a) Representative images of shControl and shKDM2B cells treated with TRAIL for 24 hours, taken by inverted live cell light microscopy (10X magnification). Number of apoptotic bodies per frame was determined using ImageJ (b-c).

Silencing of KDM2B does not affect healthy human fibroblasts

For future therapeutic implications, it is important to assess whether silencing of shKDM2B is toxic to non-malignant human cells. To this end, we employed healthy human BJ fibroblasts and checked the alterations in their TRAIL response upon shKDM2B infection.

We did not observe a significant change (**Figure 23**), suggesting that BJ cells were not as much affected by loss of KDM2B.

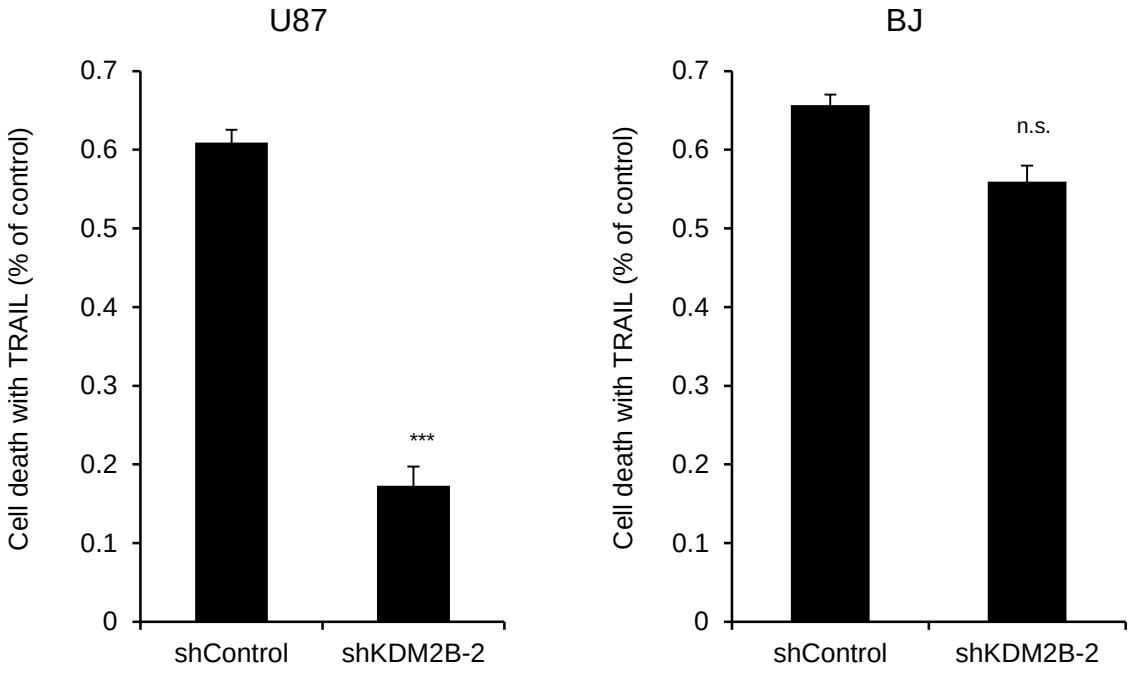


Figure 23. Viability analyses of U87MG and BJ human fibroblast cells after KDM2B knockdown and 100 ng/mL TRAIL treatment. (*** and n.s. denotes $p<0.001$ and $p>0.01$, t-test)

Silencing KDM2B sensitizes GBM cells to TRAIL-induced apoptosis

To gain more insight on how loss of KDM2B leads to reduced viability and increased cell death, we assessed the deregulated components of the apoptotic machinery in shKDM2B cells. We measured the active caspase-3/7 and caspase-8 levels respectively during TRAIL induced apoptosis. We observed ~3 fold increase in caspase-3/7 and ~2,5 fold increase in caspase-8 activities (**Figure 24a-b**). Western blot analysis of the whole cell lysates of shControl versus shKDM2B cells revealed that caspase-7 is indeed upregulated in shKDM2B cells (**Figure 24c**). Importantly, we observed that there is a significant increase in levels of cleaved PARP, caspase-3, caspase-7 and caspase-8, all of which are hallmarks of apoptosis.

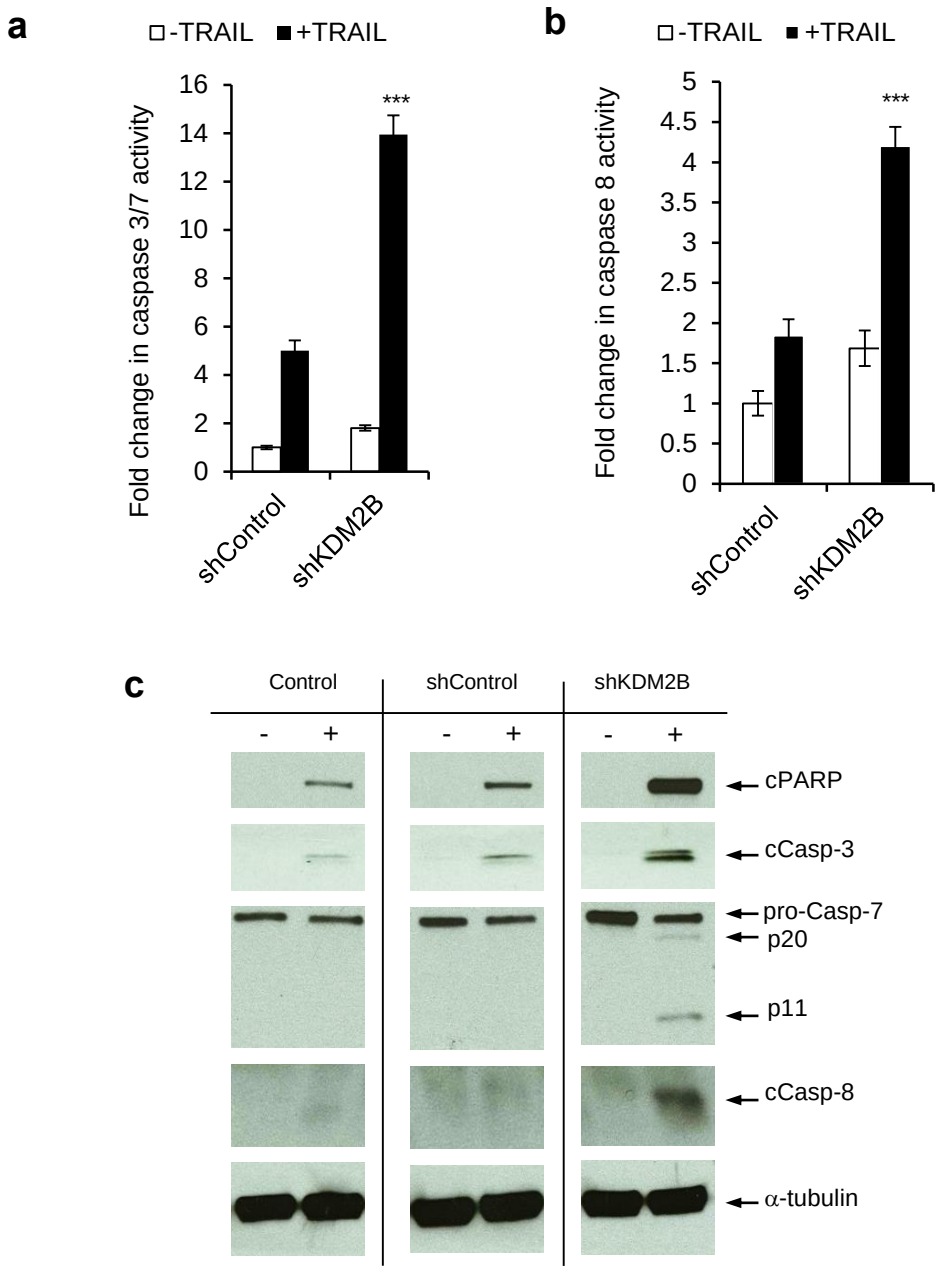


Figure 24. (a) Caspase3/7 and (b) Caspase 8 activity analyses of shControl and shKDM2B cells after 3 hours treatment of 100 ng/mL TRAIL, assesed by Caspase-Glo assays (Promega). (c) Western blot analyses of cleaved-PARP, cleaved-caspase-3, caspase-7 and cleaved–caspase-8 in whole-cell lysates of TRAIL treated and untreated control, shControl and shKDM2B cells. 100 ng/mL TRAIL treatment is applied for 6 hours.

Inhibition of caspases protects cells from TRAIL induced cell death

There are two main apoptotic pathways found in cells: extrinsic and intrinsic [99]. Initiator caspases Caspase-8 and -10 are activated by the extrinsic arm, whereas the Caspase-9 is activated in the intrinsic arm, together culminating in the activation effector

caspases Caspase-3 and -7. To test whether Caspase activation played functional role in shKDM2B-mediated apoptotic sensitization, we employed specific inhibitors for caspases-8, -10 (Z-IETD-FMK), and Caspase-9 (Z-LEHD-FMK). In addition, we used a general caspase inhibitor that targeted caspase-8, 10, 9, 3 and 7 (Z-VAD-FMK), and a negative caspase inhibitor (Z-FA-FMK). In both shControl cells and shKDM2B cells, inhibition of all caspases abolished the TRAIL response, suggesting that the observed augmented apoptotic response in shKDM2B cells was dependent on both intrinsic and extrinsic arms of apoptosis pathways (**Figure 25**).

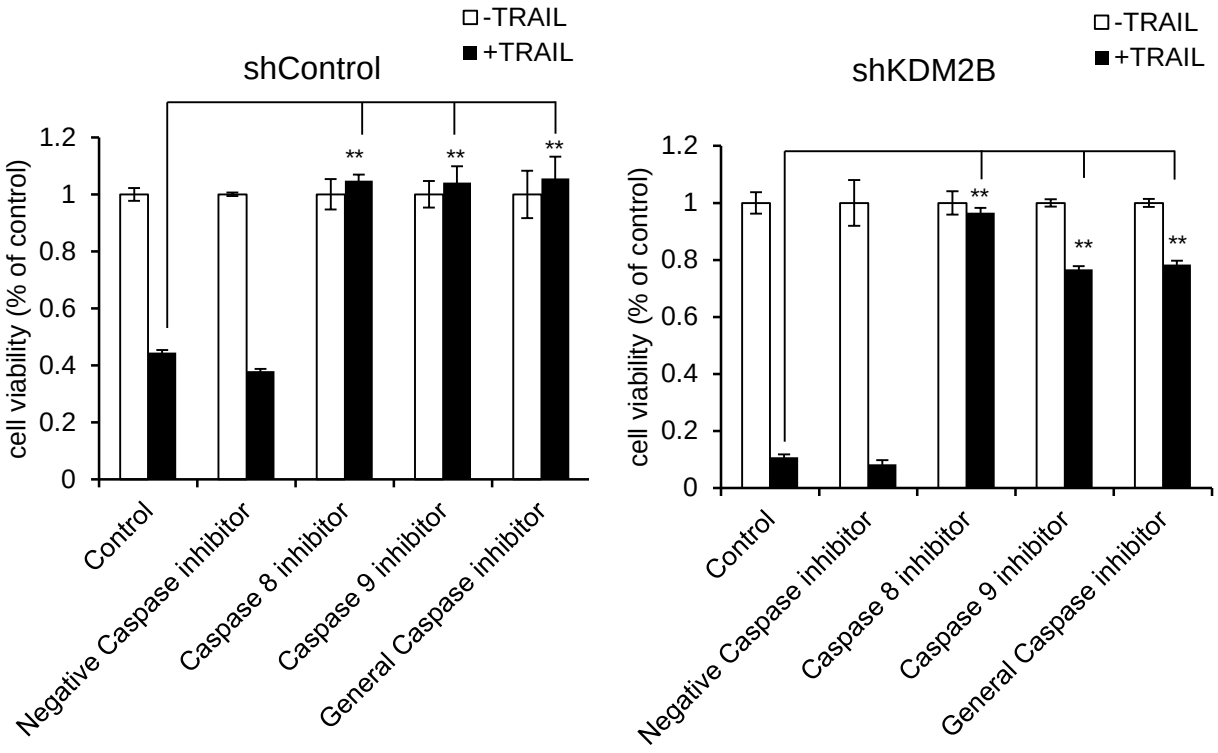


Figure 25. Cell viability analyses of shControl and shKDM2B cells after co-treatment with 100 ng/mL TRAIL and negative, caspase-8, caspase-9 or general caspase inhibitors. (*,**,*** denotes P<0.05, p<0.01, p<0.001, t-test) (Conducted by Selena Kazancığlu)

RNA-seq analysis of shControl vs shKDM2B cells

KDM2B can bind throughout genome, by its CxxC binding domain. This domain allows KDM2B to recognize and bind preferentially to non-methylated CpG islands (CGI) [100]. Knockdown of such chromatin modifier gene would result in broad alterations in the transcriptional machinery. To elucidate further the mechanism behind the observed sensitization to TRAIL, we decided to conduct RNA-seq analysis between shControl and

shKDM2B cells. First, the collected RNA samples from cultured cells were assessed for quality control by Bioanalyzer chip. 2 biological replicates were used.

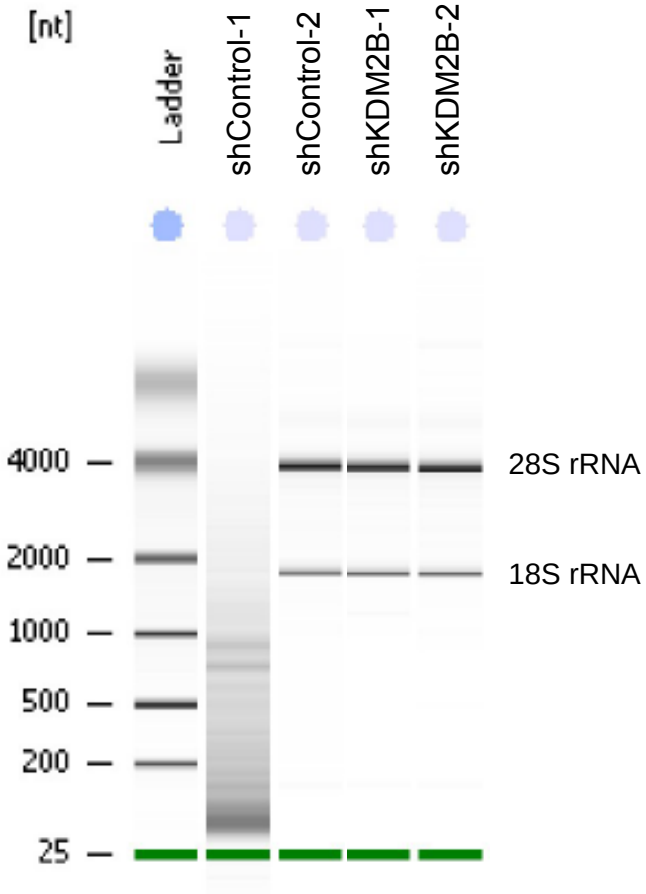
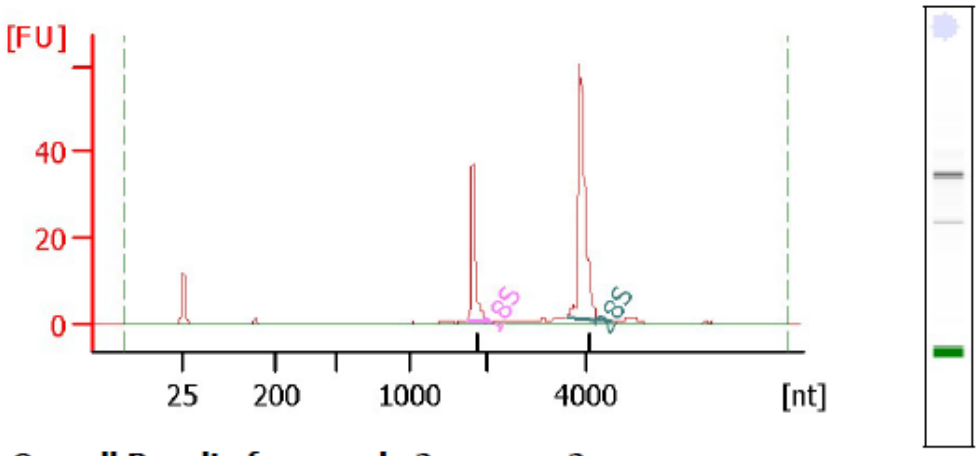


Figure 26. Quality check of the RNA samples sent for RNA-seq by Bioanalyzer electrophoresis run. (Conducted at Weill Cornell Medical College epigenomics core)

An eukaryotic RNA sample run on a Bioanalyzer electrophoresis chip ideally yields in two dominant bands corresponding to most abundant two ribosomal-RNAs (rRNAs). 28S and 18S eukaryotic rRNAs are transcribed from the same region as polycistronic mRNA. This ensures that they are transcribed at exactly the same level. Since 28S rRNA is 5070 bases and 18S rRNA is 1869 bases in length, in ideal conditions, within a total RNA sample, the ratio of the flourescent band signal is around 2.7 [101,102]. In the first run, except for one of our samples (**Figure 26**), all other three displayed perfect quality. Two more independent runs with the problematic sample solved the issue, as they have resulted in perfect quality (data not shown).



Overall Results for sample 2 : 2

RNA Area:	134.5
RNA Concentration:	74 ng/µl
rRNA Ratio [28s / 18s]:	2.3
RNA Integrity Number (RIN):	10 (B.02.08)
Result Flagging Color:	
Result Flagging Label:	RIN:10

Fragment table for sample 2 : 2

Name	Start Size [nt]	End Size [nt]	Area	% of total Area
18S	1,767	2,098	29.4	21.9
28S	3,589	4,503	67.9	50.5

Figure 27. Representative quantification of the quality check of shControl-2 RNA sample by Bioanalyzer electrophoresis run. (Conducted at Weill Cornell Medical College epigenomics core)

Band intensities of each sample, along with the background smear, are quantified and analyzed by the software and yielded in rRNA ratio and RNA Integrity Number (RIN) (**Figure 27**). Any rRNA ratio above 2 is considered good quality, and above 2.3 is considered perfect quality for in vitro cultured cells. RIN is the ultimate quality score as calculated by the software, considering all the parameters. It ranges from 0 to 10, 10 being the best score [101,102]. Our samples scored 10, hence we decided to continue with RNA-sequencing.

TruSeq RNA library preparation kit v2 was utilized for generating the RNA-seq library. This kit first uses polyA selection system to filter mRNAs out of the total RNA samples. It further fragments the mRNAs chemically and then converts single-stranded RNAs into double-stranded cDNAs for adaptor and index DNA blunt-end ligations. A critical checkpoint during the library preparation is to ensure optimized fragmentation, thus optimal single-end 50-bp reads. The optimal range for single end run for Illumina HiSeq 2500 system is between

300-500 bps [103]. As assessed by Bioanalyzer chip run, all of our samples displayed fragmentation between 250-600 bps (**Figure 28**).

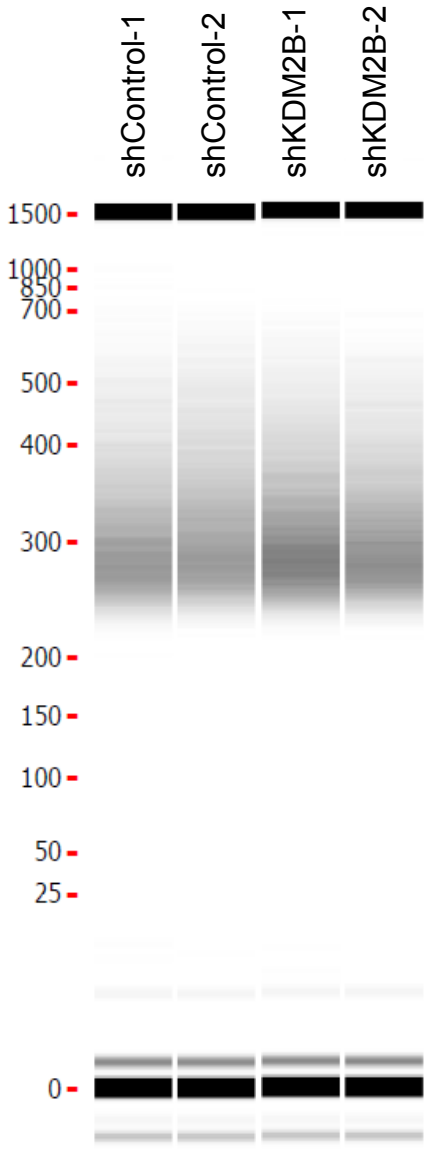


Figure 28. Quality check of the RNA libraries of the samples by Bioanalyzer electrophoresis run. (Conducted at Weill Cornell Medical College epigenomics core)

Software analysis of the lanes further revealed that the peak of the fragments were around 300 bps (**Figure 29**). Hence, we continued to next generation sequencing (NGS).

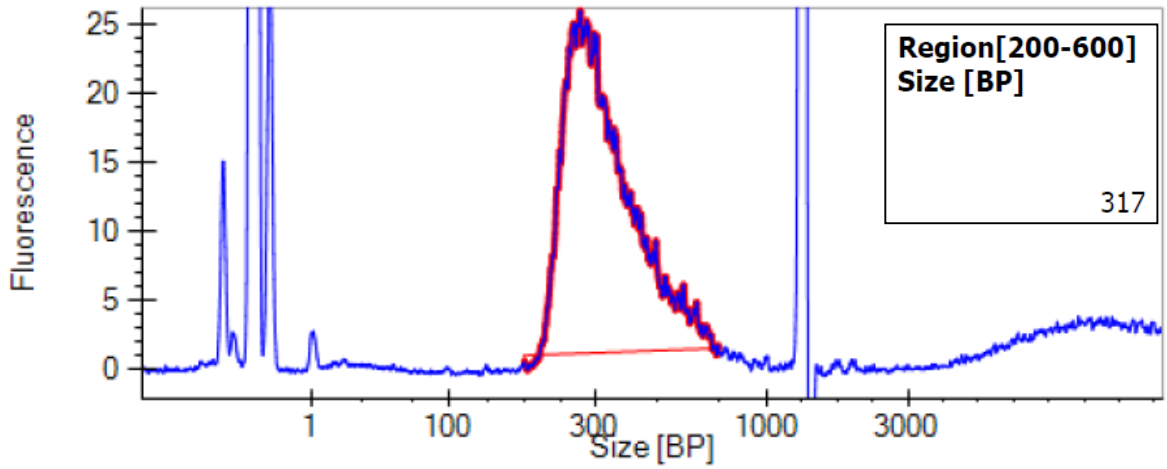
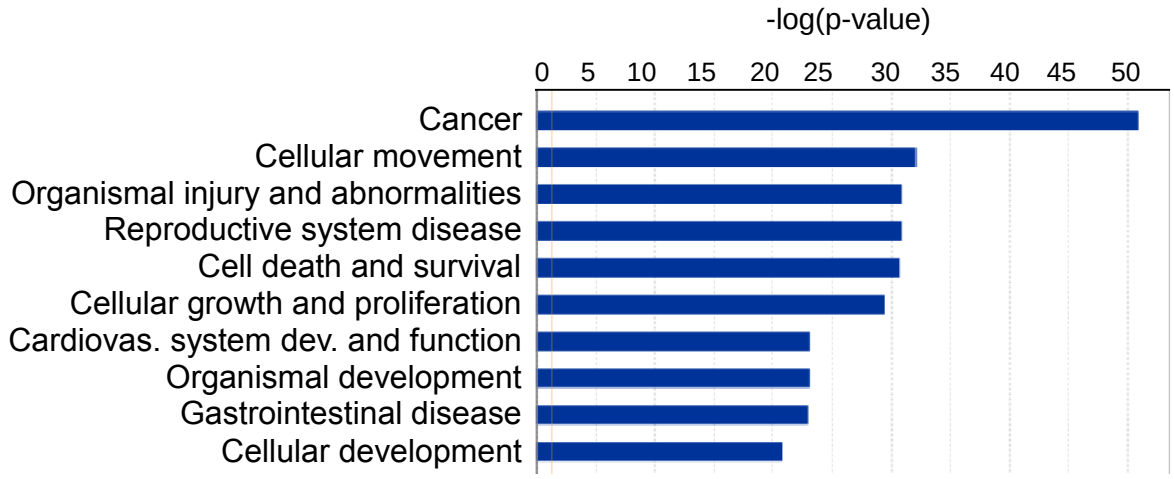


Figure 29. Representative quantification of the quality check of shControl-1's RNA library by Bioanalyzer electrophoresis run. (Conducted by Weill Cornell Medical College epigenomics core)

Illumina HiSeq2500 to generate 50 bp single-end reads was utilized for next generation sequencing (NGS). Around 18 million reads were acquired from sequencing of each sample that yielded in around 800 megabases. Around 83% of those reads passed filter (PF) quality check. Around 93% of those sequenced bases were equal or above Q score of 30. Mean quality score of the PF reads were around 37. The results are compared, averaged and analyzed for statistically differentially expressed genes by our collaborator Dr. Zeynep Hulya Gumus (Mount Sinai Hospital, US). As proof-of-principle, KDM2B expression levels were downregulated in shKDM2B cells compared to shControl down to ~33% (adjusted p-value 7,51E-91) (**Table 4**). 2457 genes were found to be differentially expressed in shKDM2B cells. Ingenuity pathway analysis of these genes for categories of diseases and functions revealed that three cell death and survival categories, two of them scoring the highest, scored high in activation states (**Figure 30**).


-log(p-value)
0 5 10 15 20 25 30 35 40 45 50
Cancer
Cellular movement
Organismal injury and abnormalities
Reproductive system disease
Cell death and survival
Cellular growth and proliferation
Cardiovas. system dev. and function
Organismal development
Gastrointestinal disease
Cellular development

Category	Diseases or Functions Annotation	p-Value	Predicted Activation State	Activation z-score	# Molecules
Cell Death and Survival	necrosis	2.15E-31	Increased	2.782	685
Cell Death and Survival	cell death	1.69E-28	Increased	2.85	786
Cancer, Organismal Injury and Abnormalities, Reproductive System Disease	mammary tumor	8.98E-26	Increased	2.481	321
Cellular Development	differentiation of cells	1.69E-21	Increased	2.468	433
Cell Death and Survival	cell survival	2.37E-21	Increased	2.849	393
Cell Death and Survival	cell viability	1.72E-20	Increased	2.766	364
Organismal Survival	organismal death	3.76E-19	Decreased	-2.051	338
Cell Death and Survival	cell death of tumor cell lines	3.81E-19	Increased	2.251	415
Cellular Assembly and Organization, Cellular Function and Maintenance	organization of cytoplasm	5.71E-19	Increased	2.195	277
Cellular Assembly and Organization, Cellular Function and Maintenance	organization of cytoskeleton	1.84E-18	Increased	2.144	274
Cellular Assembly and Organization, Cellular Function and Maintenance	microtubule dynamics	1.18E-15	Increased	2.515	244

Figure 30. A list of the diseases and functions that changed significantly between shKDM2B and shControl cells. First, a list of differentially expressed genes between shControl and shKDM2B cells from RNA-Seq data was generated using a Fold Change>1.5, p-value <0.05 criteria and then used as an input for Ingenuity Pathway Analysis (IPA) software (licensed use of Ingenuity®Systems, www.ingenuity.com). (Conducted by Dr. Zeynep H. Gümüş)

KDM2B regulates expression of apoptosis related genes

As we were particularly interested in the cell death phenotype associated with shKDM2B cells, we focused our attention into cell-death related genes differentially expressed in RNA-seq experiments. As also evident from the Ingenuity Diseases and Function Analyses of the RNA-seq data, Cell Death and Survival functions were particularly changed in shKDM2B cells compared to shControl cells. 8 out of the top 15 functions were categorized in Cell Death and Survival (**Figure 30**). From the genes associated with cell death and survival, we focused on a list of apoptosis-related genes that can affect the outcome of TRAIL induced apoptosis, when deregulated. When this list was generated from the differentially expressed and filtered genes, and ranked according to fold-change, we observed that the most significant change was on Harakiri (HRK) gene. It is a BH-3 only Bcl-2 family member that can antagonize anti-apoptotic proteins Bcl-2 and Bcl-xL, whose function in GBM is not well defined [104]. HRK's 16-fold upregulation was unmatched among the other apoptosis key players (**Table 4**). To validate the differential expression observed in RNA-seq data, we designed gene-specific primers and performed q-RT-PCR (**Table 2**). Differential expression of all apoptosis-related genes were validated (**Figure 31**). We observed a trend of upregulation of pro-apoptotic genes such as Caspase-7 and Card16 and downregulation of certain anti-apoptotic genes such as Mcl-1.

These results suggest that misregulation of the apoptotic machinery could be due to direct deregulation of target loci due to loss of KDM2B contact with chromatin regulatory regions or indirect regulation.

Gene Symbol	Entrez Gene Name	Ensembl ID	Fold Change	adjusted p-value
KDM2B	lysine (K)-specific demethylase 2B	ENSG00000089094	-3,049	7,51E-91
HRK	harakiri, BCL2 interacting protein	ENSG00000135116	16,055	2,35E-04
CARD16	caspase recruitment domain family, member 16	ENSG00000204397	3,754	6,96E-16
DAPK1	death-associated protein kinase 1	ENSG00000196730	3,751	1,95E-03
TNFAIP2	tumor necrosis factor, alpha-induced protein 2	ENSG00000185215	3,575	7,6E-255
BMF	Bcl2 modifying factor	ENSG00000104081	3,284	5,43E-09
CASP1	caspase 1, apoptosis-related cysteine peptidase	ENSG00000137752	2,429	1,14E-22
BCL2L11	BCL2-like 11 (apoptosis facilitator)	ENSG00000153094	2,24	1,56E-05
TNFRSF11B	tumor necrosis factor receptor superfamily, member 11b	ENSG00000164761	2,19	1,15E-17
TNFRSF14	tumor necrosis factor receptor superfamily, member 14	ENSG00000157873	2,16	2,39E-18
TNFRSF10A	tumor necrosis factor receptor superfamily, member 10a	ENSG00000104689	1,94	1,66E-03
TNFRSF10C	tumor necrosis factor receptor superfamily, member 10c, decoy without an intracellular domain	ENSG00000173535	1,935	6,67E-12
CASP7	caspase 7, apoptosis-related cysteine peptidase	ENSG00000165806	1,856	3,74E-19
BAK1	BCL2-antagonist/killer 1	ENSG00000030110	1,724	4,01E-14
APAF1	apoptotic peptidase activating factor 1	ENSG00000120868	1,665	3,93E-13
CARD14	caspase recruitment domain family, member 14	ENSG00000141527	1,632	5,39E-02
XAF1	XIAP associated factor 1	ENSG00000132530	1,618	1,61E-02
BCL2L2	BCL2-like 2	ENSG00000129473	1,486	3,86E-12
BCL10	B-cell CLL/lymphoma 10	ENSG00000142867	-1,457	2,02E-05
CASP3	caspase 3, apoptosis-related cysteine peptidase	ENSG00000164305	-1,506	7,99E-15
BNIP2	BCL2/adenovirus E1B 19kDa interacting protein 2	ENSG00000140299	-1,6	5,58E-33
BCL9	B-cell CLL/lymphoma 9	ENSG00000116128	-1,748	5,68E-26
TRIAP1	TP53 regulated inhibitor of apoptosis 1	ENSG00000170855	-1,85	1,20E-18
TNFRSF1B	tumor necrosis factor receptor superfamily, member 1B	ENSG00000028137	-2,109	5,51E-91
MCL1	myeloid cell leukemia 1	ENSG00000143384	-2,323	2,6E-228
BCL11B	B-cell CLL/lymphoma 11B (zinc finger protein)	ENSG00000127152	-3,463	3,78E-10
BCL2A1	BCL2-related protein A1	ENSG00000140379	-6,184	1,49E-17

able 4. Custom gene list of the differentially expressed apoptosis-related genes from RNA-Seq data.

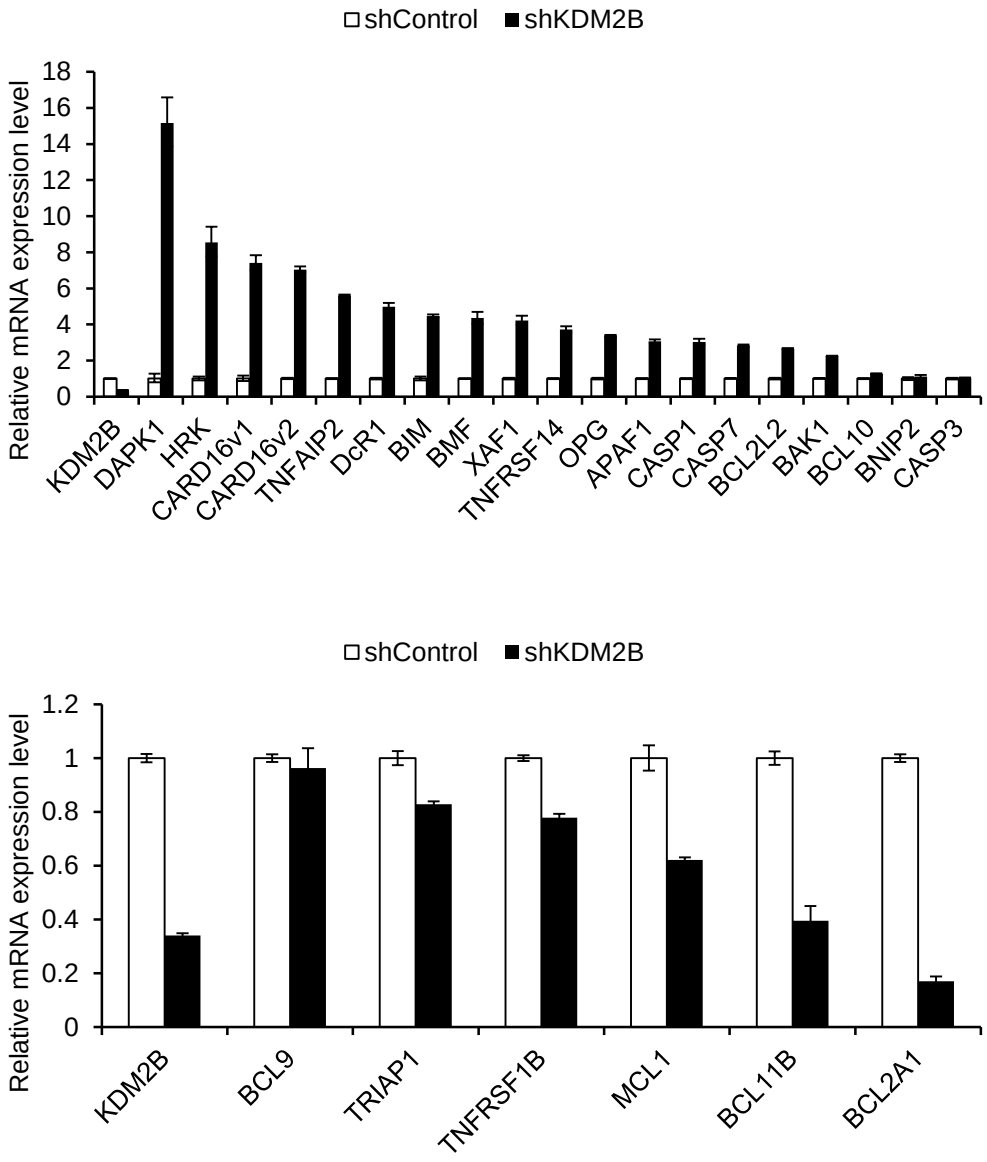


Figure 31. q-RT-PCR validation of the up-regulated (upper) and down-regulated (lower) apoptosis-related genes from the custom apoptosis gene list are plotted. (Conducted by Selena Kazancıoğlu)

Loss of Harakiri (HRK) partially reverses the shKDM2B phenotype

As HRK was the top upregulated gene upon KDM2B loss, and its function in GBMs is less-well known, we directed our focus on HRK and assessed its functional role in KDM2B-loss induced apoptosis. To test whether knockdown of HRK could reverse the observed phenotype, we designed shRNAs targeting HRK (in collaboration with Ezgi Kaya, Koç University). As expected, silencing of HRK via shRNA (knockdown down to 40%) conferred TRAIL-resistance to cells and led to significant partial recovery from TRAIL-induced death in shKDM2B cells (**Figure 32**). These results suggest that HRK might be a downstream

regulated gene of KDM2B and might facilitate TRAIL-response in GBM cells. In order to test whether HRK is a direct target of KDM2B at the chromatin level, we performed Chromatin Immunoprecipitation experiments and have preliminary evidence to suggest a direct interaction (**Please see Appendix III**).

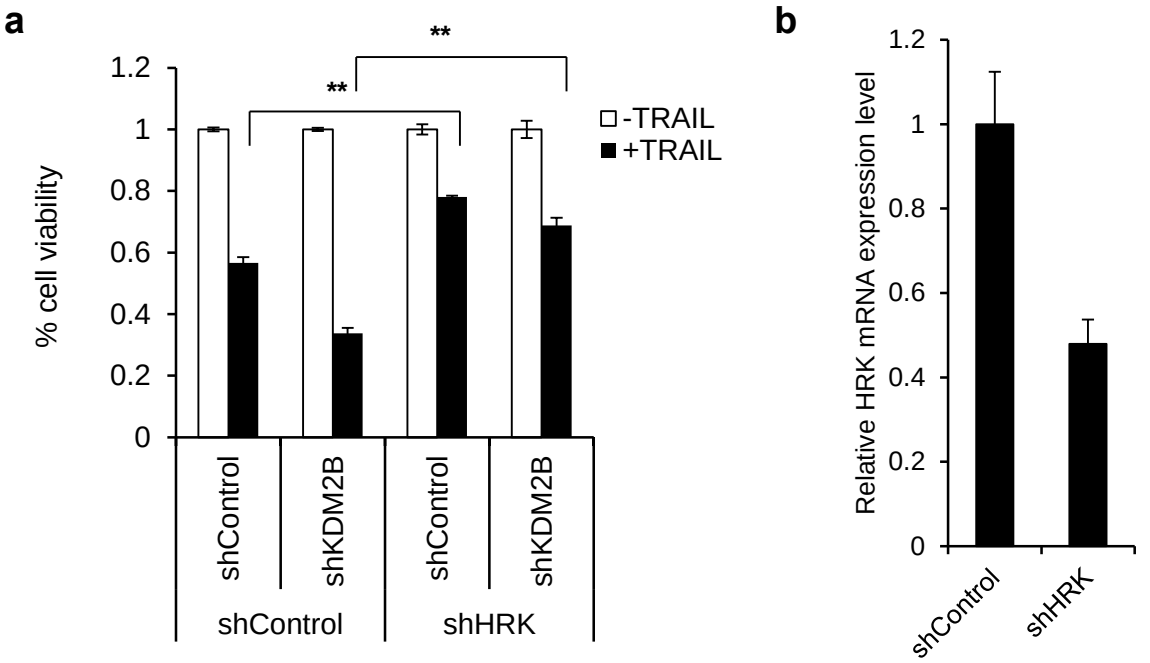


Figure 32. (a) Knockdown of the top gene, Harakiri (HRK), recovers the phenotype as assessed by cell viability analyses of shControl and shKDM2B cells after treatment with 100 ng/mL TRAIL. (b) qPCR analysis of HRK in shControl and shHRK cells. (*,**,*** denotes P<0.05, p<0.01, p<0.001, t-test) (shHRK was cloned and packaged by Ezgi Kaya)

Co-silencing of H3K36-specific HMTs partially rescues the phenotype

There were four H3K36-specific HMTs used in the shRNA screen. Namely, they are SETD2, NSD1, ASH1L and SMYD2 [60]. Since they conduct exactly the opposite enzymatic activity of KDM2B's, we wanted to see how apoptotic response of GBM cells would be regulated when they are silenced alone or in a combination of 4. We observed that loss of each one of four shRNAs significantly increased cell viability upon TRAIL treatment, as compared to shControl (**Figure 33a**). We were able to confirm the knockdowns of each one of the shRNAs at transcriptional level (**Figure 33b**). As expected, single knockout of none of the HMTs or KDM2B resulted in a global change of H3K36me2 or H3K36me3 levels (**Figure 33c**). More interestingly, co-silencing of all 4 HMTs together combined with KDM2B

knockdown significantly rescued the observed shKDM2B phenotype as assessed by TRAIL treatment and cell viability assay (**Figure 33d**).

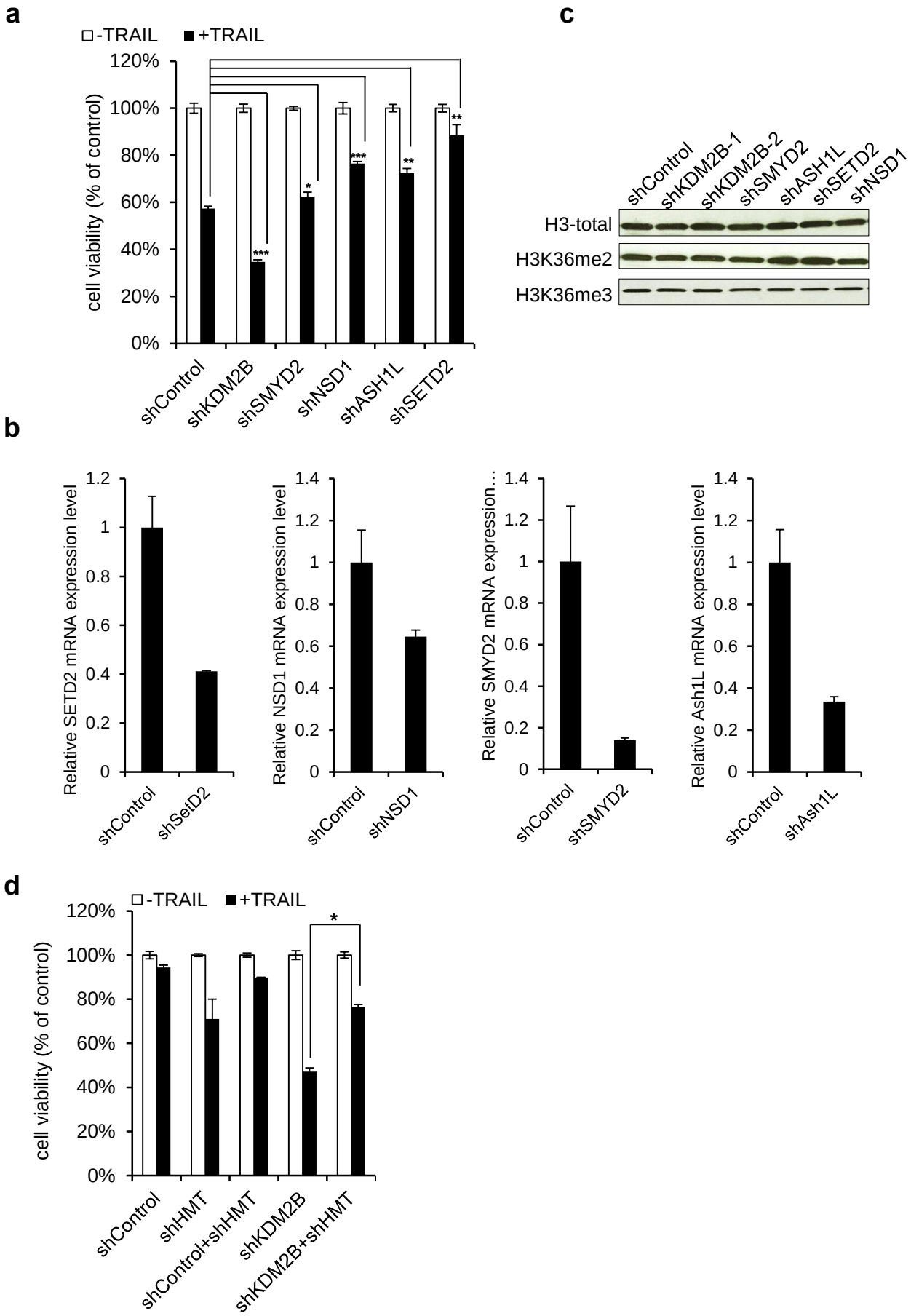

a
-TRAIL
+TRAIL
cell viability (% of control)
120%
100%
80%
60%
40%
20%
0%
shControl
shKDM2B
shSMYD2
shNSD1
shASH1L
shSETD2
c
shControl
shKDM2B-1
shKDM2B-2
shSMYD2
shASH1L
shSETD2
shNSD1
H3-total
H3K36me2
H3K36me3
b
Relative SETD2 mRNA expression level
shControl
shSetD2
Relative NSD1 mRNA expression level
shControl
shNSD1
Relative SMYD2 mRNA expression…
shControl
shSMYD2
Relative Ash1L mRNA expression level
shControl
shAsh1L
d
-TRAIL
+TRAIL
cell viability (% of control)
shControl
shHMT
shControl+shHMT
shKDM2B
shKDM2B+shHMT

Figure 33. (a) Viability analysis of shControl, shKDM2B, shSMYD2, shNSD1, shASH1L and shSETD2 cells after 100 ng/mL TRAIL treatment. (b) qRT-PCR analysis of SETD2, NSD1, SMYD2 and ASH1L in transduced cells. (c) Western blot analysis of total-H3, H3K36me2 and H3K36me3 in the histone extracts from shControl, shKDM2B, shSMYD2, shASH1L, shSETD2 and shNSD1 cells. (d) Viabillity analysis of shControl, shKDM2B, shHMT (shSETD2, shNSD1, shSMYD2 and shASH1L co-infected) cells and their combinations after 100 ng/mL TRAIL treatment. (*,**,*** denotes P<0.05, p<0.01, p<0.001, t-test)

Loss of KDM2B slows down cell proliferation *in vitro* in long-term

To assess the effect of KDM2B loss on GBM cell growth in long terms, we performed real-time cell analysis (RTCA) of shControl and shKDM2B cells for 200 hours. We observed that knockdown of KDM2B reduces proliferation rate of GBM cells *in vitro* (**Figure 34**), as opposed to the previous short-term RTCA showing no change in 24 hours.

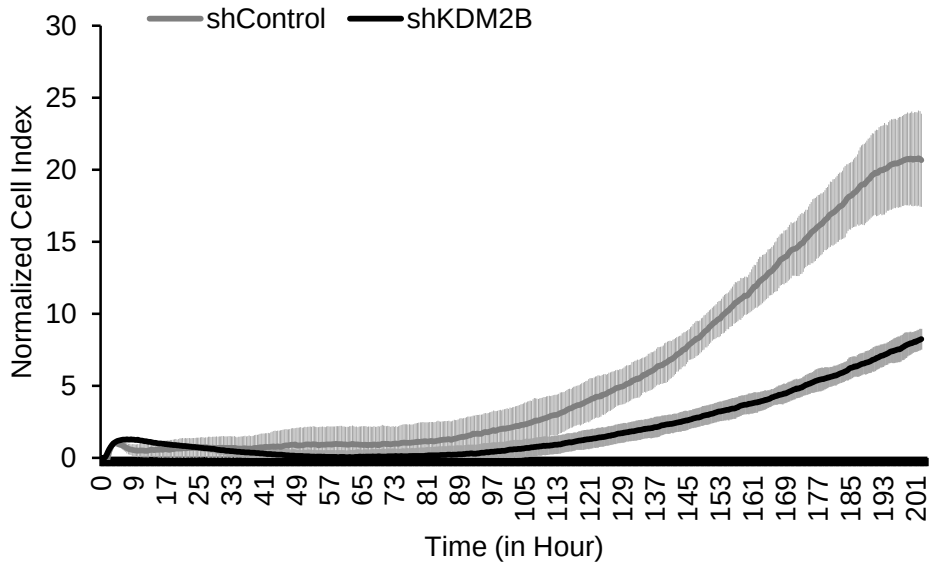


Figure 34. shControl and shKDM2B cells are seeded as 1000 cell per well and their growth dynamics are assessed by xCELLigence real time cell analyzer for 202 hours (n=6 wells for each group).

Loss of KDM2B attenuates tumor growth *in vivo*

To examine whether loss of KDM2B also affects tumor growth in vivo, we first engineered shControl and shKDM2B cells to express both firefly luciferase (Fluc) and mCherry in a single construct (FMC). The bioluminescence activity of increasing number of

shControl and shKDM2B cells were similar *in vitro* (**Figure 35a**). Subcutaneous injection of the cells in immunocompromised mice and long-term analysis of tumor-growth for 30 days revealed that loss of KDM2B also attenuates tumor growth *in vivo* (**Figure 35b-c**).

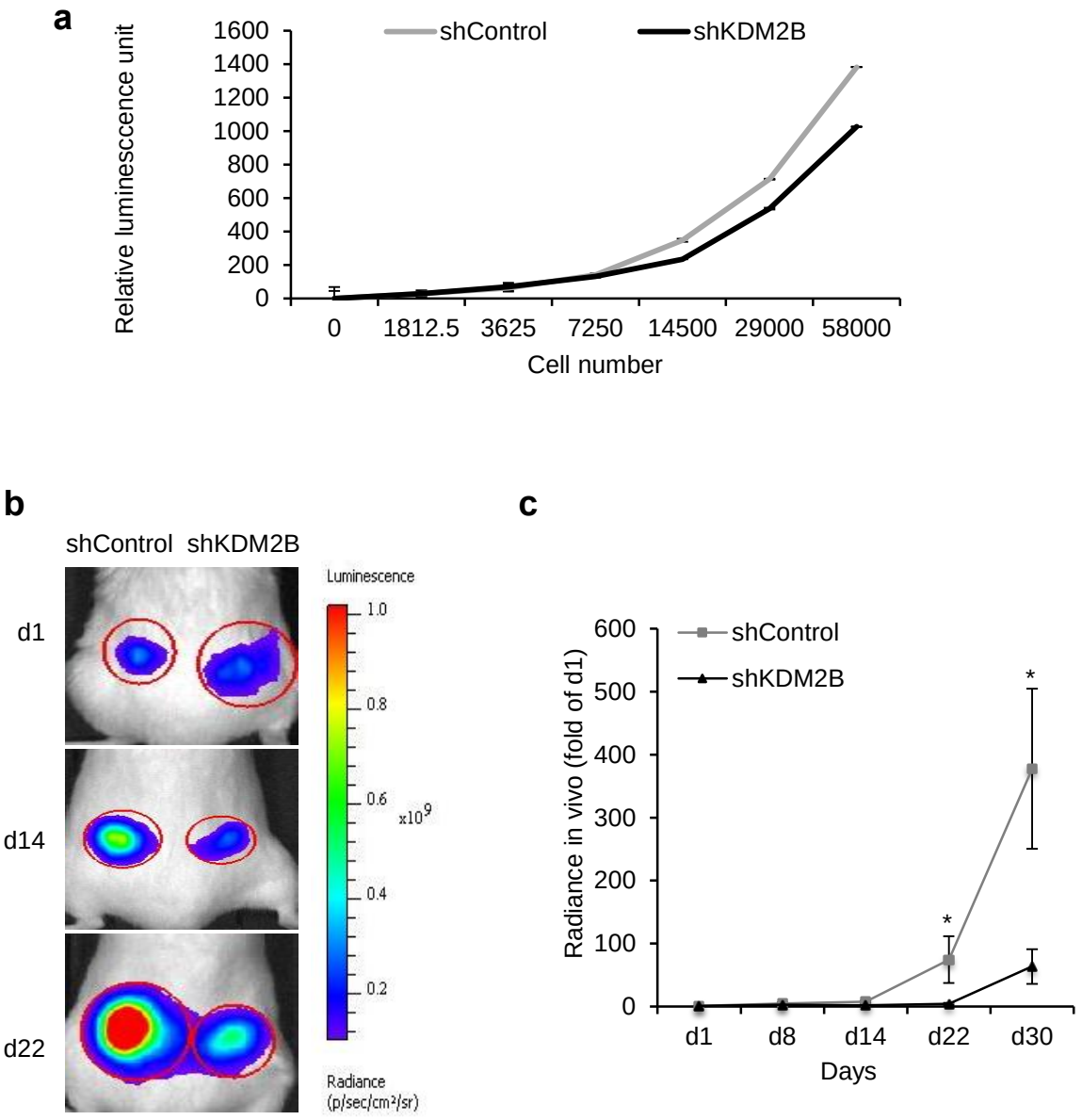


Figure 35. (a) shControl and shKDM2B cells are infected with viruses carrying Firefly luciferase(Fluc)-mCherry (FMC) constructs and their in vitro bioluminescent signal capacities are compared and plotted. (b) 1,5x10^6 cells of shControl-FMC and shKDM2B-FMC are injected subcutenously into NOD/SCID mice and assesed for tumor growth dynamics for 30 days (c). (n=7 tumors/ group) (The experiments were performed with Ahmet Cingöz).

Immunoflourescence and histological analysis of the removed tumors showed that loss of KDM2B led to reduced angiogenic capacity of the tumors as assessed by regular

H&E and VEGF stainings (**Figure 36**). Moreover, there were annexin-V positive tumor cells in shKDM2B tumors, but not in controls. These results suggest that the observed reduction in tumor growth in shKDM2B tumors could be due to decreased angiogenesis and increased basal levels of apoptosis.

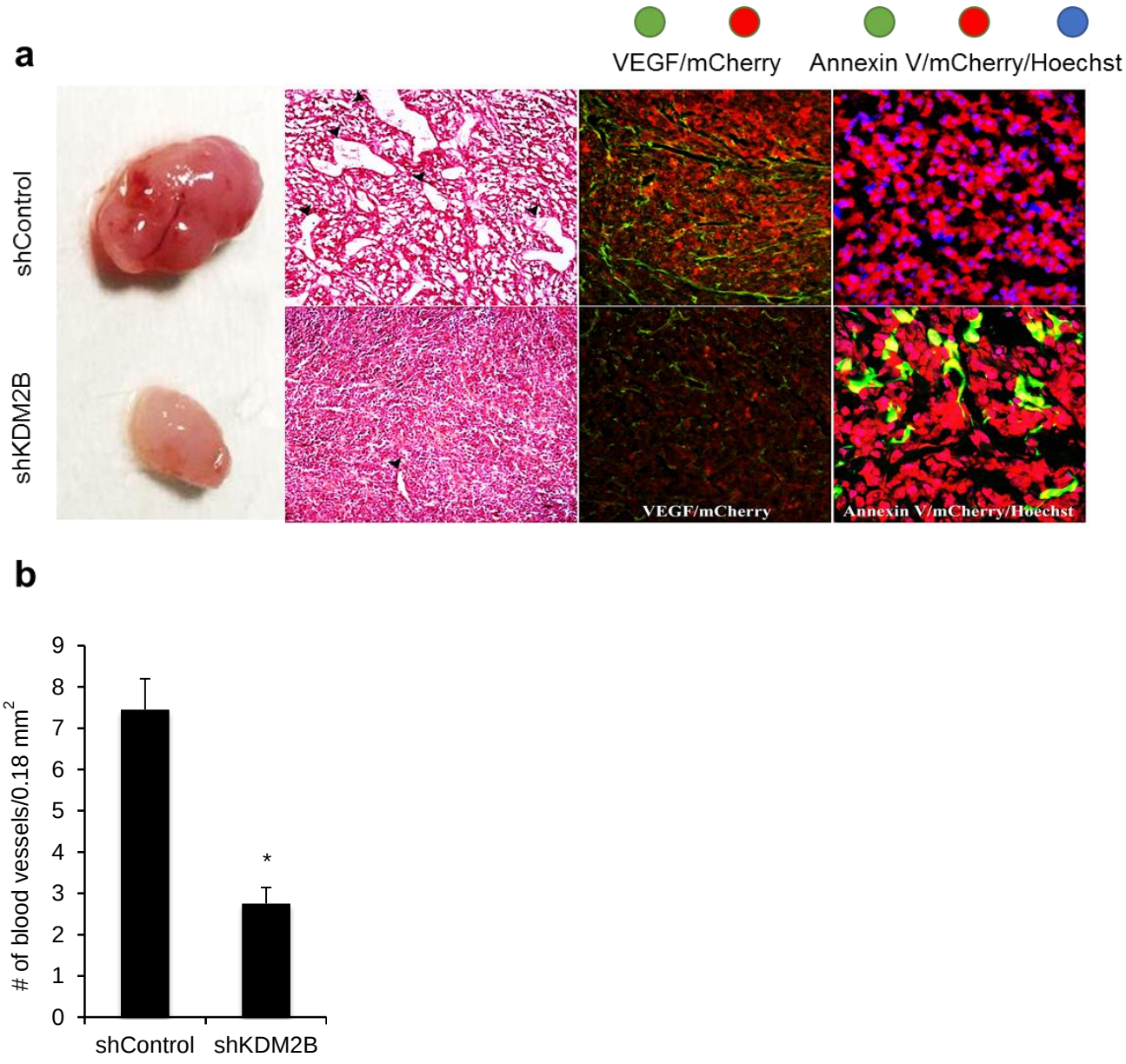


Figure 36. **(a)** Removed tumors are sectioned and stained with H&E, anti-VEGF and Annexin V. **(b)** Number of blood vessels per 18 mm2 are counted and plotted. (n=3)

Chapter 4

Discussion

Here in this thesis, we have shown that knockdown of a specific CME can lead to sensitization of an aggressive GBM cell line. KDM2B and RING1A are identified by an shRNA screen where a custom pool of 48 CMEs are silenced one by one by more than one shRNA targeting the same enzyme. 125 shRNAs targeting selected DNMTs, HDMs, HMTs, MCBPs, PRC1/2 members and few transcription factors were utilized in the screen. Among 125 shRNAs, some CME hits were inconsistent meaning that each one of its shRNAs resulted in a dissimilar phenotype. The reason for that could be poorly designed shRNAs, resulting in higher off-targets and inefficient knockdown of the target gene. There were only 2 shRNAs whose knockdown were toxic by itself. They were removed from the percent cell death analysis of the screen. RING1A is E3 ubiquitin ligase component of PRC1 conducting H2AK119ub [105]. KDM2B is a H3K36-specific HDM. There is vast data in literature introducing KDM2B and RING1B as interacting partners [73,86]. It is interesting to note that KDM2B by its F-box domain can serve as U3 ubiquiting ligase substrate specifier for RING domain E3 ubiquitin ligases [106]. It was compelling to see that at least one of the shRNAs targeting the H3K36-specific HMTs, namely SETD2, NSD1, SMYD2, ASH1L, conducting the exact opposite enzymatic activity of KDM2B, were found in the opposite section of the screen. This could explain the partial phenotype recovery of shKDM2B upon combined loss of all four H3K36-specific HMTs. Another interesting point deducted from the screen is that both of the inconsistent top hits, shG9A and shSUV39H2, were targeting H3K9 specific methyltransferases. The potential relationship between the reduction of global active mark of H3K9me3 and TRAIL sensitization could be revealed by further analysis.

RNAi systems has been shown to be masked and hindered by cellular compensation mechanisms to recover the effects of an shRNA [98]. Upon KDM2B knockdown, no collateral silencing was observed within KDM family, especially in its homologue KDM2A. This suggests that shKDM2B was specifically targeting KDM2B in KDM family. There were a trend of mild upregulation of almost all other KDM family members. Further analysis are needed to asses the implications of that.

Although literature suggests that KDM2B can carry out demethylation of H3K4me3, H3K36me2 and H3K36me3, most consensus is on its H3K36me2 specific activity [82]. In our experiments, consistent with other groups' findings, we also observed that ectopic KDM2B expression lead to observable reduction in global H3K36me2 levels, whereas did not change H3K36me3 levels [70]. Parallel with the previously published data, we also did not observe a

global change in H3K36me2/3 levels upon knockdown of KDM2B [72]. Multi CMEs regulating methylation and demethylation of H3K36 can be accounted for these observations. Knockdown of a single player in this axis is not expected to disrupt the balance to have an observable global change.

To assess the contextuality of shKDM2B phenotype in U87MG cells, other primary and secondary GBM cell lines should be tested. In our hands, KDM2B inhibition did not always lead to augmented TRAIL response in some other GBM lines (data not shown). This suggests that there are cellular variations in dependencies on epigenetic machineries. U87MG cells have wildtype diploid p53 and the observed sensitization could be p53-dependent [107]. Indeed, based on IPA analysis of the RNA-seq data, p53 is the top activated transcription regulator upon KDM2B loss (data not shown). P53 can undergo acetylation and methylation modifications. Evidences suggest that LSD1, a HDM, does demethylate p53 and suppress its pro-apoptotic functions [108,109]. And we already discussed in literature review that KDM2B loss is a known activator of p53 and Rb apoptosis and senescence regulating proteins [81]. Considering U87MG cells have wildtype p53 copies, it is encouraging to hypothesize that shKDM2B induced senescence-like morphological changes and reduced viability could be parallel and regulated together through p53. Further, literature shows that KDM2B indeed directly interacts with Arf/Ink4 locus in mouse to keep the locus suppressed and prevents cellular senescence [81,82]. In parallel, KDM2B knockdown leads to cellular senescence and its overexpression leads to immortalization and increased reprogramming efficiency in mouse embryonic cells [82]. Intrigued by these facts, we conducted B-galactosidase staining, and PI staining followed by flow cytometer. Although the results were preliminary, they were encouraging. We observed enhanced B-gal staining in shKDM2B cells with more flat morphologies (Appendix I and V). Further studies are needed to assess the implications of that and relationship between KDM2B loss and activation of p53.

Forced KDM2B expression also does not result in acquired resistance to TRAIL in TRAIL-sensitive GBM cell lines (Appendix I). CMEs have genome wide binding capacities and dynamics, thus we hypothesize that protein levels of CMEs are stringently regulated and even minor changes in their levels can alter the phenotype, stochastic model of iPSC generation [110]. Consistent with the hypothesis, drastic overexpression of KDM2B cells do not confer U87MG cells resistant to TRAIL. In contrast, it transforms them in a fragile state. This could explain why we failed to recover the shKDM2B sensitization by ectopic wildtype KDM2B expression. The level of knockdown is around 60% whereas the level of overexpression is more than 150 fold (Appendix I). This made it clear once again that cellular levels of a CME like KDM2B is very critical and it can lead to broad range of regulations

through genome and epigenome wide effects. A tightly regulated mammalian expression system such as tet-on/off is needed to find the narrow window where shKDM2B phenotype could be reversed by counter-overexpression of KDM2B in our hands.

It was also interesting to see that by ectopic vast expression of KDM2B by pBabe construct lead to significant upregulation of alpha-tubulin in both 293T and U87MG cells. KDM2B overexpression at such level also lead to a more neuron like morphology with more processes (Appendix I). This could be related with the aberrant morphological changes of U87MG cells, since alpha-tubulin (microtubules) is the key cytoskeletal protein regulating the shape and processes of cells. RNA-seq analysis of shKDM2B cells also reveals that the second most significantly upregulated canonical pathway is axonal guidance signaling pathway, including many tubulin family members in itself (data not shown). The relationship between morphological changes observed in shKDM2B and KDM2B-overexpressing cells and cytoskeletal dynamics could be further studied.

The RNA samples used for RNA-seq were quality checked. This was necessary due to possible problems or poor handling during RNA extraction that can lead to enzymatic degradation or mechanical shearing of the RNAs. Further, we were able to successfully validate the data from RNA-seq via q-RT-PCR.

H3K36me3 found along gene bodies are generally deemed as an active mark and has been shown to take place in regulation of alternative splicing, transcriptional elongation [60]. KDM2B loss could lead to accumulation of the active mark and stronger expression of the pro-apoptotic genes, like HRK. Further, HMT loss could lead to lessening of the H3K36me3 and downregulation of the pro-apoptotic genes that can explain the phenotype. Further chromatin immunoprecipitation (ChIP) experiments are needed to elucidate the exact machinery behind the observed phenotype. Our preliminary experiments have shown that KDM2B directly interacts with CGIs of promoter of HRK. KDM2B, in normal conditions, by its CxxC domain, could recognize and bind to CGIs of HRK. Then by its PHD domain it can scan and bind to H3K4me3 and H3K36me3 to start demethylating them. This could lead to suppression of HRK. Further, by its F-box and LRR domains, KDM2B can directly recruit RING1B and specify substrate for RING1B for ubiqutination. In turn this can recruit EZH and other PRC members to further inactivate HRK's expression via H2AK119ub and H3K27me3 modifications [57,73]. Upon loss of KDM2B, PRC complexes may fail to target HRK CGIs by themselves and thus HRK will be upregulated. CxxC and JmjC domain deleted KDM2Bs are generated and further analysis will reveal whether the hypothesis is valid or not. Further ChIP-qPCR and ChIP-seq analysis against KDM2B will clarify whether the deregulated

transcriptome is due to direct loss-of-KDM2B contact with genome or indirect, e.g. P53 driven.

We also know that HRK is dramatically upregulated in U87MG cells undergoing apoptosis. It would be very interesting to conduct ChIP experiments in TRAIL treated vs control cells to see whether TRAIL signaling leads to disassembly of KDM2B from CGIs of HRK. Another very interesting approach would be performing ChIP experiments against RING1A/B and against its corresponding suppressive mark H2AK119ub to see whether KDM2B and RING1A along with their marks colocalizes on CGIs of HRK and whether KDM2B or RING1A loss changes the histone dynamics to open the chromatin. These questions are yet remained to be answered by further experiments.

As shown in **Figure 37**, there are many genes regulating the H3K36 methylation/demethylation cascade. Our data suggested that the phenotype of shKDM2B could be counteracted by simultaneous knockdown of the H3K36-specific HMTs. Co-silencing of NSD1, ASH1L, SETD2 and SMYD2 partially recovered the shKDM2B phenotype, suggesting that the global deaccumulation of H3K36 methylation could be related with TRAIL resistance. ChIP experiments are needed to see whether KDM2B targeted apoptosis related genes are actually affected by the knockdown of the corresponding genes in terms of their H3K36 methylation patterns.

As previous studies have shown, KDM2B is known to form non-canonical complexes with PRC1 and PRC2, and it is hypothesized that its demethylation activity could be a factor regulating their recruitment to the target loci [74]. This is due to inhibition of PRC2 binding on target loci in the presence of active marks such as di- or tri-methylated H3K36 [111]. The fact that RING1A/B is a major component of PRC1 catalyzing mono-ubiqutination of H2AK119 and being one of our sensitizer hits, it is tempting to hypothesize that the phenotype of loss of KDM2B could be along KDM2B-PRC1 axis. H2AK119 is regarded as a silencing mark, as PRC1 itself is a well-studied and characterized suppressive complex. Though some studies suggest that PRC1 requires H3K27me3 mark, catalyzed by EZH2 component of PRC1, to bind and function on genome, we did not get EZH2 as a hit in this study. This is in parallel with the studies showing that PRC2 and PRC1 can work in a mutually exclusive manner [80,112]. We did not observe a synergistic effect when shRING1A is combined with shKDM2B in U87MG cells, suggesting the observed sensitization phenotypes are already in the same axis. More studies should be conducted to show the relationship between apoptotic response of shKDM2B and shRING1A/B cells.

KDM2B phenotype in vitro in short-term does not suggest a drop in cell proliferation, but over time, slower growth pattern emerges both in vitro and in vivo. As our data suggests

(Appendix V), this could be due to shKDM2B-induced cellular senescence. Consistent with that IPA analysis of the RNA-seq data revealed that all cell cycle progression pathways were downregulated in shKDM2B cells (data not shown). Senescence regulation of KDM2B indeed has been well-characterized in mouse cells. KDM2B overexpression is also shown to improve reprogramming efficiency into iPSCs. To see whether in our case KDM2B directly regulates with human Ink4/Arf locus and keeps it suppressed in normal conditions, further ChIP and loss of function analysis are needed.

Whether KDM2B is a proto-oncogene or a tumor suppressor has been debated and has not been clarified. The observations that KDM2B loss reduces the proliferative capacity of tumor cells both in vitro and in vivo along with inhibited angiogenic capacity and elevated basal levels of intratumor apoptosis, suggest that in U87MG cell line KDM2B acts as a proto-oncogene inducing tumorigenesis. Discovery of specific small-drug inhibitors against KDM2B could be promising for certain fraction of GBM patients.

Collaborating with Professor Udo Oppermann from University of Oxford, we also checked whether a pan-JmjC probe would sensitize U87MG cells to TRAIL. However, data suggested that a pan inhibitor of demethylases would not work and a specific KDM2B inhibitor is required (data not shown). To take our findings one step closer to therapeutic application, we will test KDM2B loss in orthotropic mice models, in which cells will be injected intracranially. We plan to combine previously shown promising TRAIL-secreting armed neural stem cells with tumor homing capacities, with our findings to see whether KDM2B loss would result in enhanced tumor death in orthotropic models as well [113,114].

It is clear that KDM2B loss leads to sensitization of U87MG GBM cells to TRAIL induced apoptosis and reduced proliferation in long term. However it is not clear yet whether other chemotherapeutic drugs that activate apoptosis can be combined with shKDM2B to synergize. Performing experiments with such drugs can shed more light into shKDM2B-induced sensitization, such as the relationship between intrinsic and extrinsic arms of apoptosis and between intact p53 and DNA damage inducing drugs.

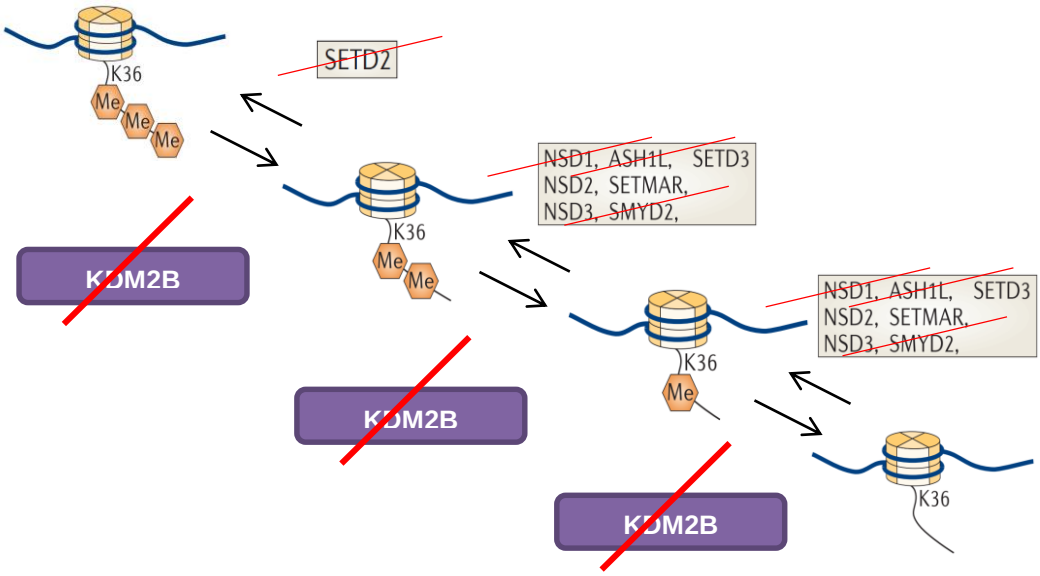


Figure 37. Schematic representation of H3K36 demethylation and methylation cascade. Red lines on enzymes indicate knockdown of the corresponding enzymes.

Appendix I

Cloning and validation of KDM2B overexpression constructs

cDNA of human KDM2B (long isoform) and KDM2A in pCAG-puro backbone were kindly supplied to us by Professor Udo Oppermann from University of Oxford. KDM2B in the mammalian expression construct has 2x Strep-tag II and 1x FLAG-tag cloned to its N-terminus. The 4167 bp KDM2B ORF is flanked by EcoRI cut sites (**Figure 38**). Expression of pCAG-KDM2B and pCAG-KDM2A were validated by transfection of 293Ts followed by q-RT-PCR (**Figure 39**) and by western blotting (**Figure 41).**

KDM2B was cloned into the viral vectors utilizing the EcoRI cut sites. We first decided to clone KDM2B into lentiviral pLenti-PGK-puro (w529-2) (addgene plasmid #19068) and lentiviral pLenti-PGK-neo (w531-1) (addgene plasmid #19067) destination vectors in order to have broader options of antibiotic selection (considering that our shRNAs have puro resistance cassette). This was also required since U87MG cells were hard to transfect. We achieved cloning by first cloning KDM2B into the pENTR1A no ccDB (w48-1) (addgene plasmid #17398) gateway entry vector, and then into the destination vectors by using Gateway LR Clonase II system (Invitrogen, USA).

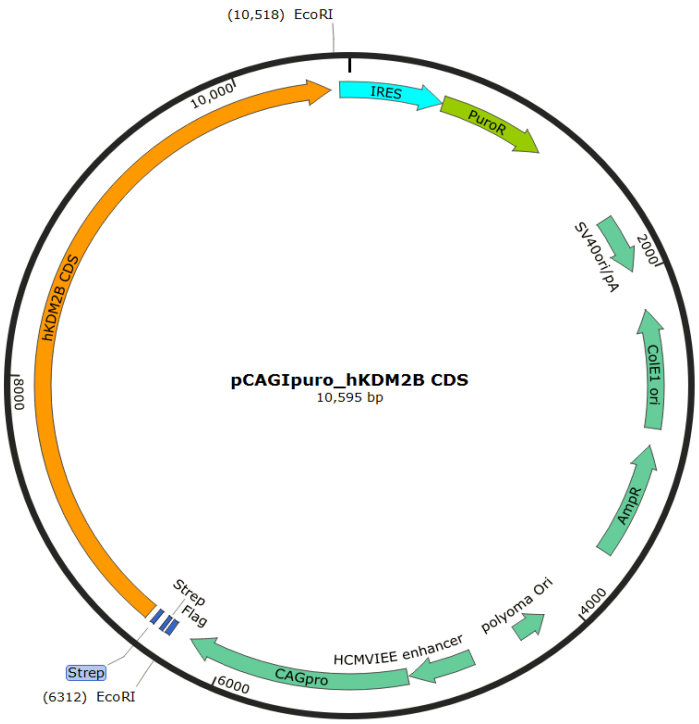


Figure 38. Plasmid map of pCAG-hKDM2B reflecting its features and EcoRI cut sites

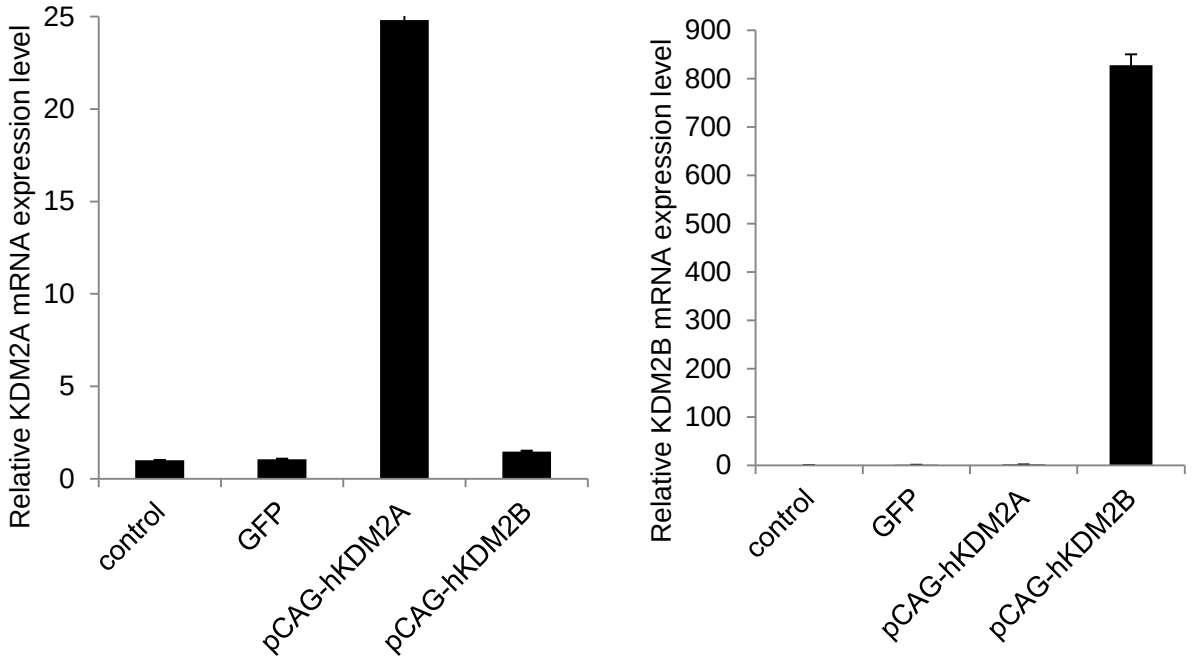


Figure 39. q-RT-PCR analysis of pCAG-hKDM2A and pCAG-hKDM2B constructs in transfected 293T cells.

Transfection of 293T cells with pLenti-KDM2B constructs showed ~150 fold upregulation of KDM2B at transcriptional level (**Figure 40**) and translational level (**Figure 41**).

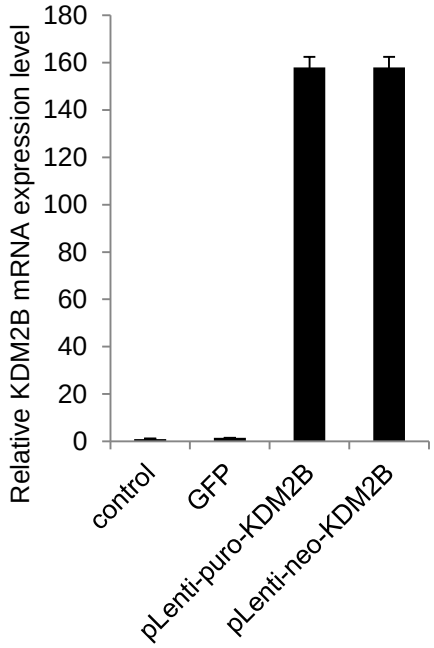


Figure 40. q-RT-PCR analysis of pLenti-KDM2B constructs transfected into 293T cells.

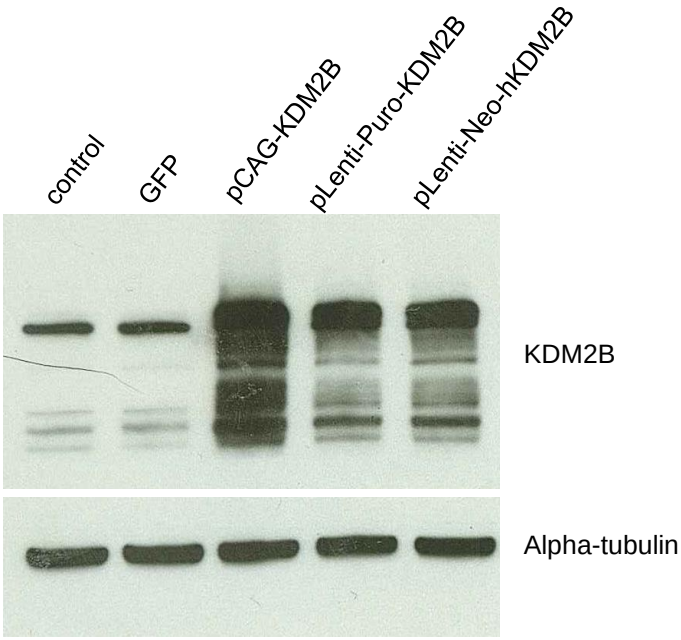


Figure 41. Western blot analysis of pCAG-hKDM2B, pLenti-PGK-Puro-hKDM2B and pLenti-PGK-Neo-hKDM2B constructs in transfected 293T cells.

Next, we packaged the viral particles carrying pLenti-KDM2B constructs. However, infection of U87MG cells by the viral particles failed to display the same level of upregulation of KDM2B in U87MG cells as assessed by q-RT-PCR and western blotting (**Figure 42**). Titration of the viral particles were within normal range. Hence, the observed low amount of KDM2B upregulation was not due to low MOI. However, upon careful analysis, we came to realize that the length of DNA between LTR sequences, that is going to be packaged into viral particles, were around 9 kb in total due to large size of KDM2B (**Figure 43**). 9 kb long DNA could be lowering the packaging efficiency or disrupting the intact DNA. Therefore, we decided to change strategy and clone KDM2B into a retroviral vector of pBabe-Puro. The cloned vector yielded in ~7 kb long DNA that was going to be packaged into viral particles (**Figure 44**). First pBabe-KDM2B construct was transfected into 293T cells (**Figure 45**). Then, it was packaged into retroviral particles and U87MG cells were infected with them (**Figure 45**). Dramatic upregulation of KDM2B was already apparent from direct morphological transformation of U87MG cells starting from post-infection day 1 (**Figure 46**). Interestingly, U87MG cells upon dramatic upregulation of KDM2B, started to have fragile and branched morphology resembling primary neuron cultures. They started showing reduced viability and proliferation. They were sensitized to TRAIL induced apoptosis as well (**Figure 47**).

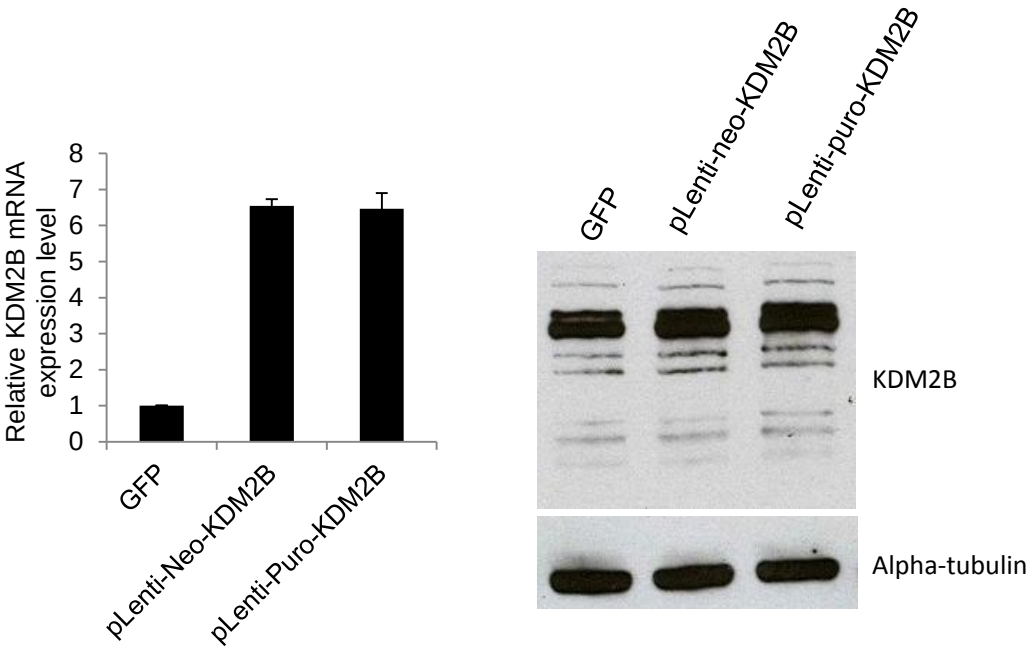


Figure 42. q-RT-PCR and western blot analysis of pLenti-KDM2B constructs transduced into U87MG cells.

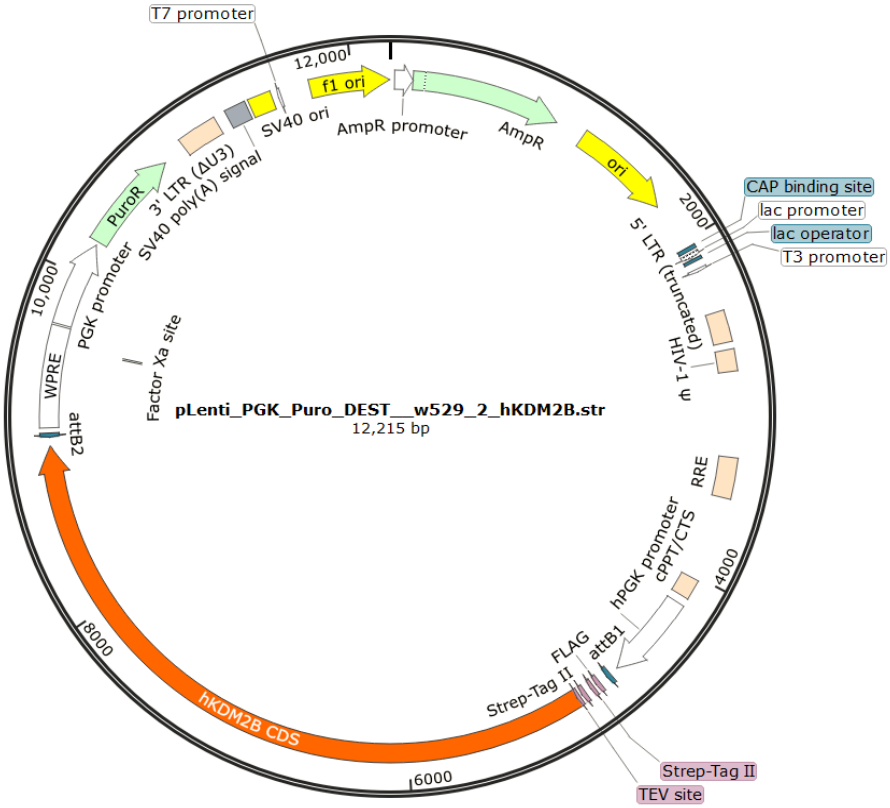


Figure 43. Plasmid map of pLenti-PGK-Puro-DEST vector with KDM2B cloned in it.

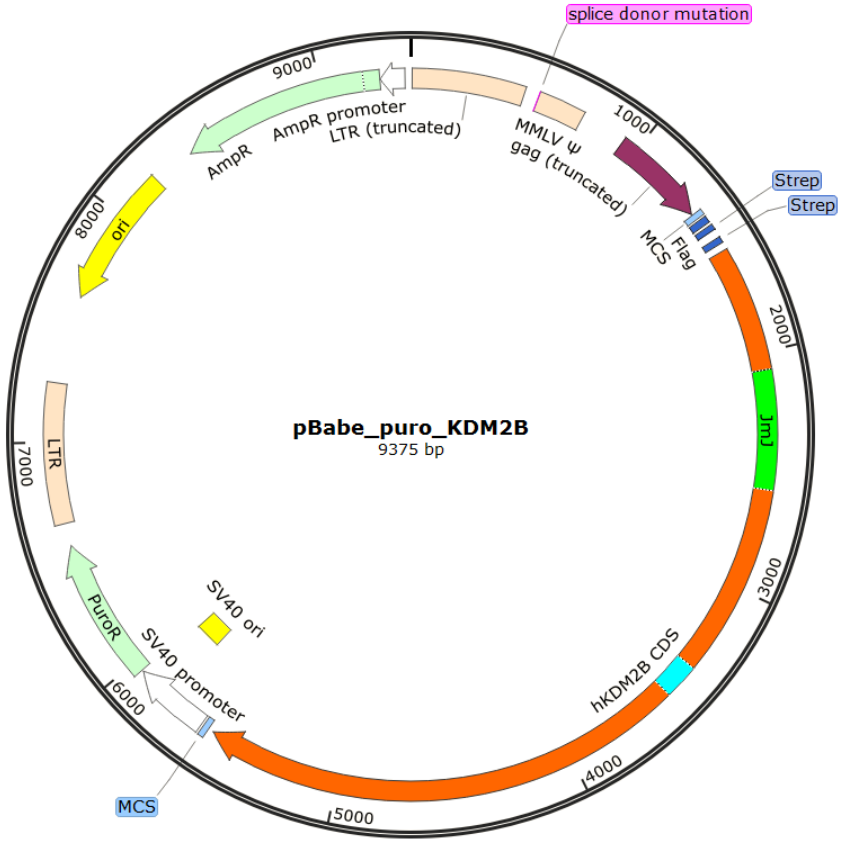


Figure 44. Plasmid map of retroviral pBabe-puro-KDM2B vector.

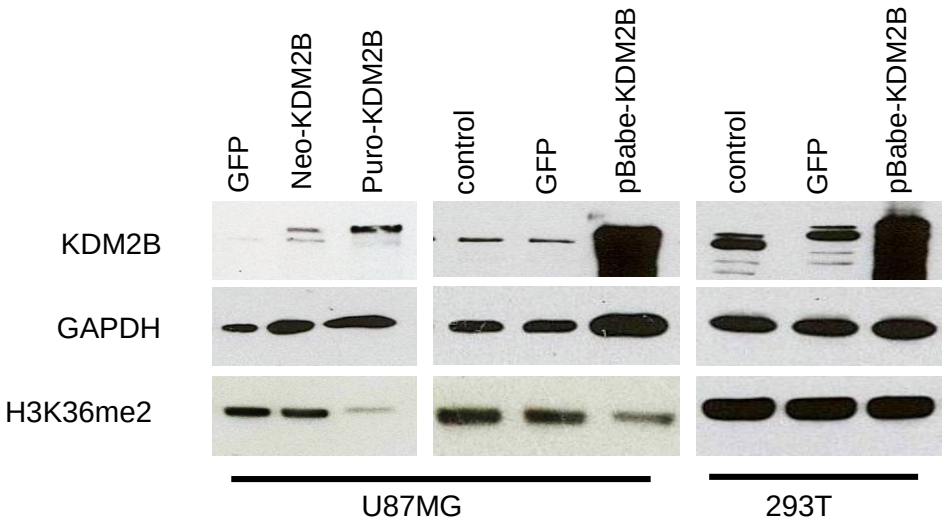


Figure 45. Western blot analysis of 293T cells transfected, and U87MG cells infected, with pBabe-KDM2B construct.

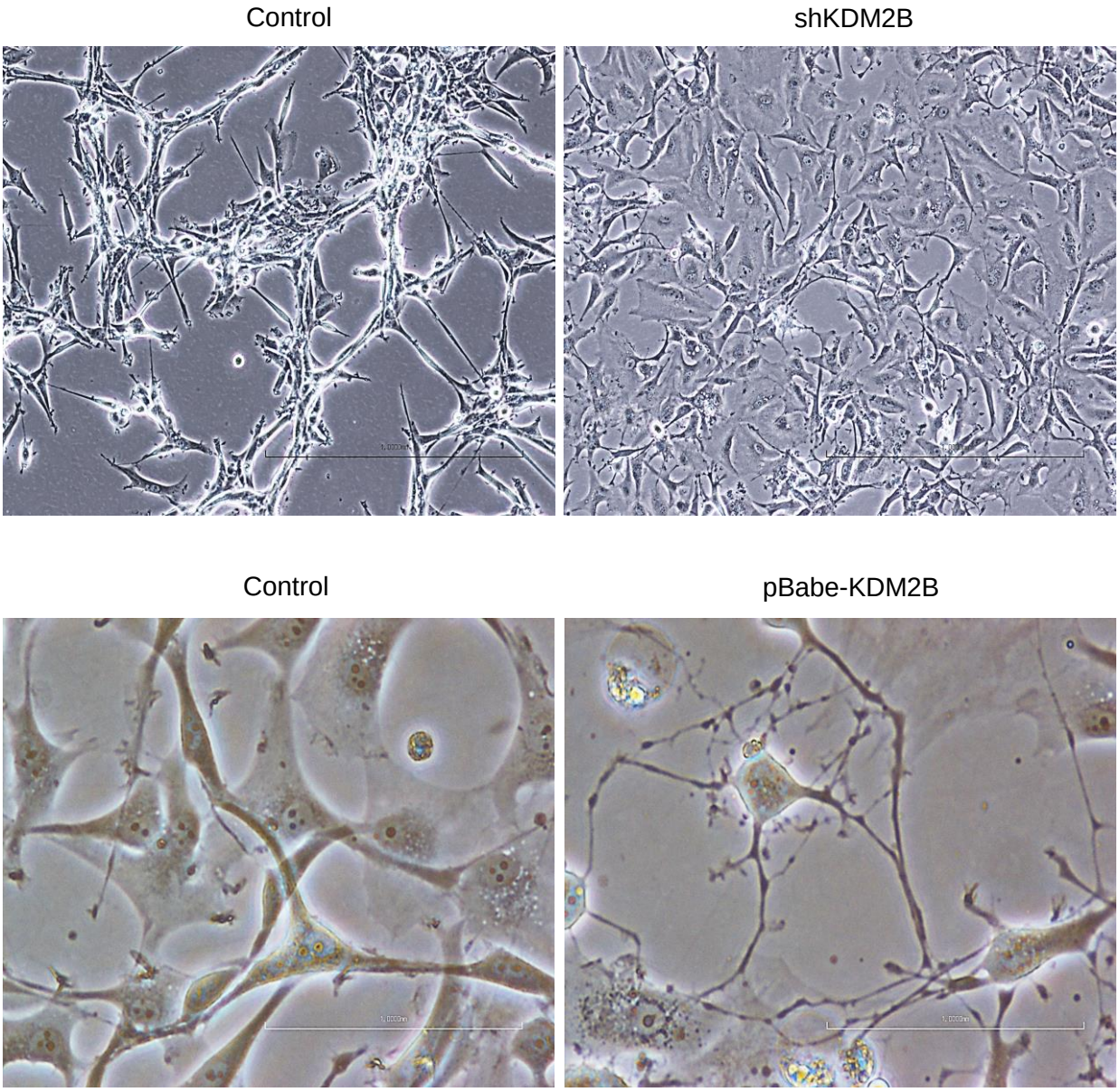


Figure 46. Brightfield microscopy images of control, shKDM2B and pBabe-KDM2B U87MG cells.

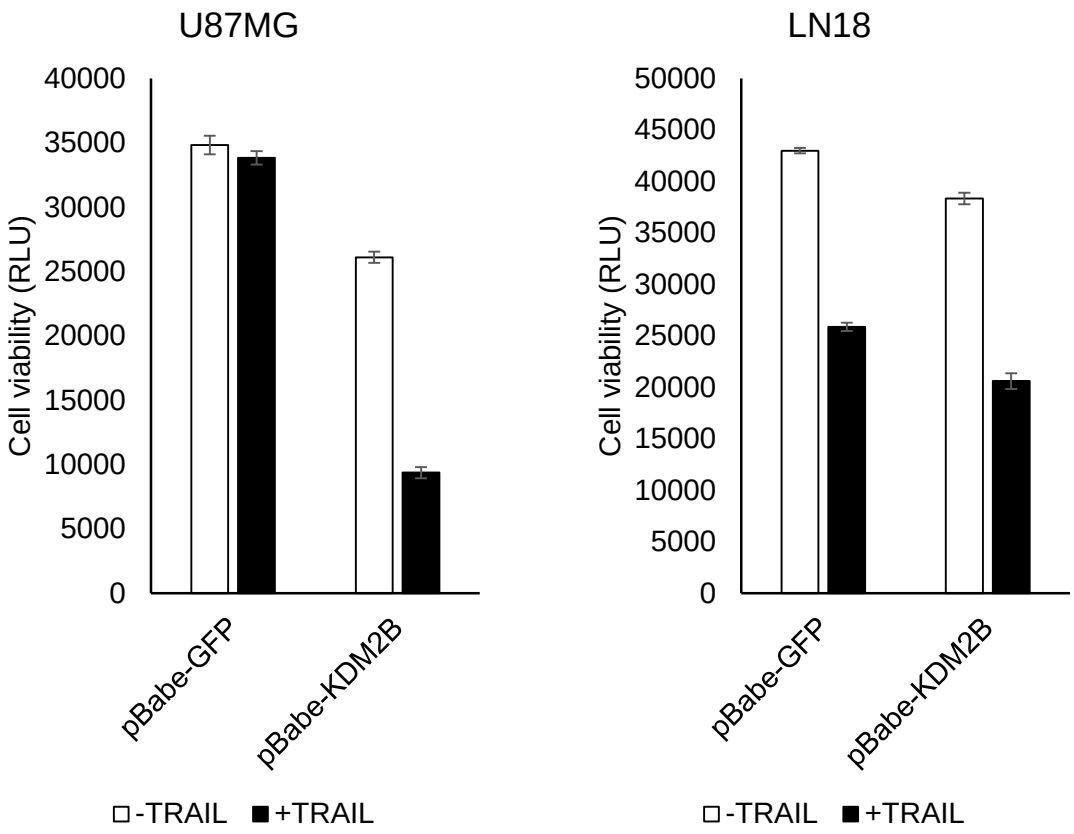


Figure 47. Cell viability analysis of U87MG and LN18 cells overexpressing KDM2B by the pBabe construct.

Generation of RNAi resistant and domain deleted KDM2B overexpression vectors

By the help of FLAG-tag found in N-terminus of KDM2B in our constructs, we were able to detect the exogenous transgene expression by anti-FLAG (FLAG M2 mouse monoclonal antibody, Sigma-Aldrich) western blotting (**Figure 48**). To further reveal what domains of KDM2B are necessary or sufficient to induce a phenotype, we also generated domain deletion mutants of pBabe-KDM2B construct by utilizing Q5 Site-Directed Mutagenesis Kit (NEB). A CxxC-ZF domain deleted, that cannot bind to DNA, and a JmJ domain deleted, that is catalytically dead, clones were generated by performing reverse PCRs by back-to-back primer sets (**Figure 49**). The clones were validated by sequencing and further will be validated by anti-FLAG western blot analysis to see the expected band shifts. shKDM2B-resistant mutated version of pBabe-KDM2B is also being generated by site-

directed mutagenesis to confer our constructs RNAi-resistant to be able to recover shKDM2B phenotype in future studies.

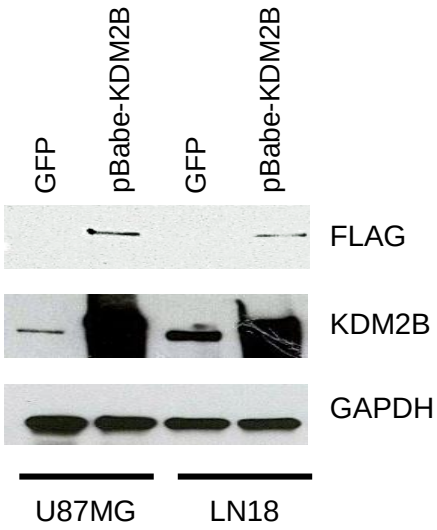


Figure 48. Western blotting analysis of pBabe-KDM2B by anti-FLAG antibody.

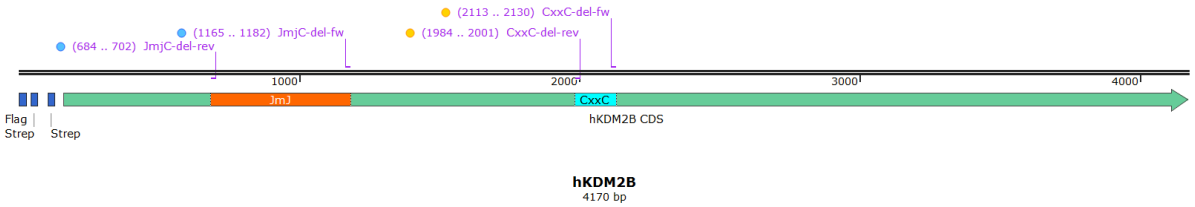


Figure 49. Reverse-PCR strategy followed for deleting domains in KDM2B and mutating shKDM2B binding sites

CRISPR-induced knock-out of KDM2B in GBM cells

To characterize the effect of KDM2B loss further, and to see whether complete loss of KDM2B leads to more sensitization of cancer cells, we decided to utilize CRISPR system. We designed two gRNAs (via http://crispr.mit.edu/) (**Table 5**) targeting exon 2 and exon 4 of KDM2B (**Figure 50**). The gRNAs were intentionally designed to target existing restriction sites in the exons so that we could assess the efficiency of indel formation in the whole population.

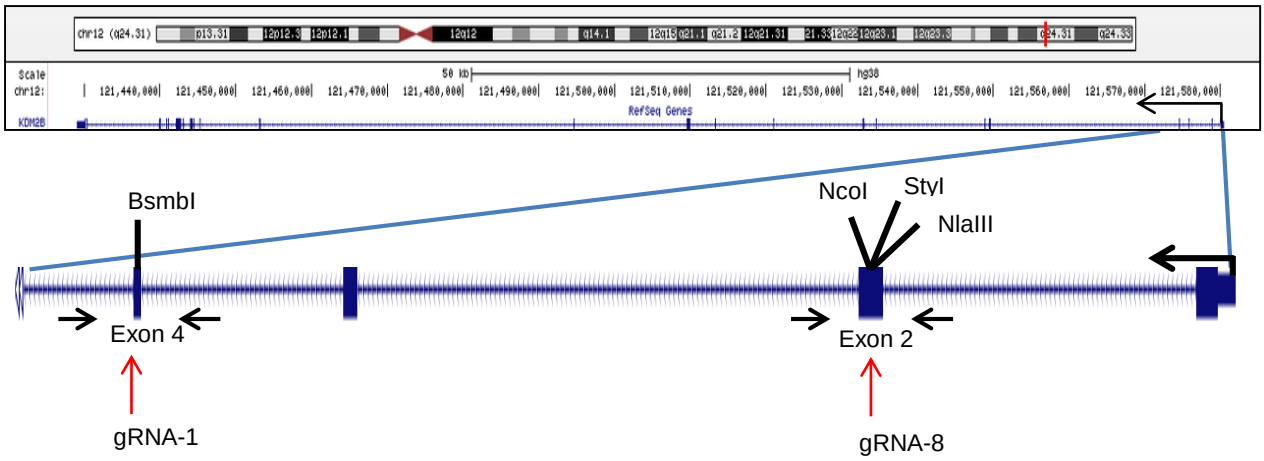


Figure 50. Genomic map of human KDM2B in chromosome 12, revealing the regions targeted by gRNAs and their corresponding potentially disrupted restriction sites upon Cas9-induced indel formations.

Both strands of gRNAs were ordered as single stranded oligos having BsmBI compatible ends. They were then cloned into lentiCRISPR backbone (pXPR_001) (**Figure 51**) following Zhang Lab's protocol [115]. The cloned construct was then packaged into lentiviral particles. U87MG cells were infected with the viruses and selected.

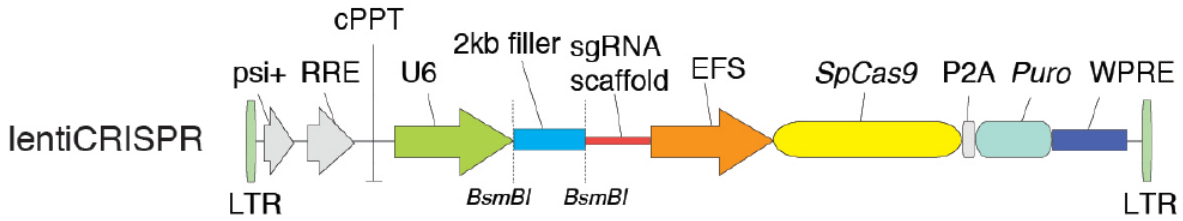


Figure 51. Plasmid map of pXPR_001 lentiCRISPR lentiviral vector.

Indel formation efficiency of the gRNAs in infected U87 cells are then checked by diagnostic cut of genomic DNA amplicons of the targeted regions (**Figure 52**). 10 days post-infection showed that majority of the genomic loci in the heterogeneous population underwent indel formation. Then we checked the level of knockout in the population by western blot analysis. Although we observed a time-dependent decline in the population levels of KDM2B (**Figure 53**), it is clear that we need to perform single cell cloning followed by genotyping, in order to have a uniform KDM2B knockout population.

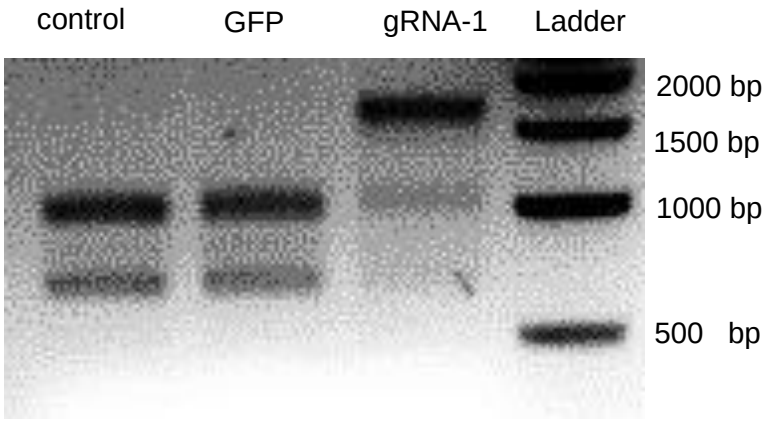


Figure 52. Diagnostic cut of exon 4 at day 10 after infection.

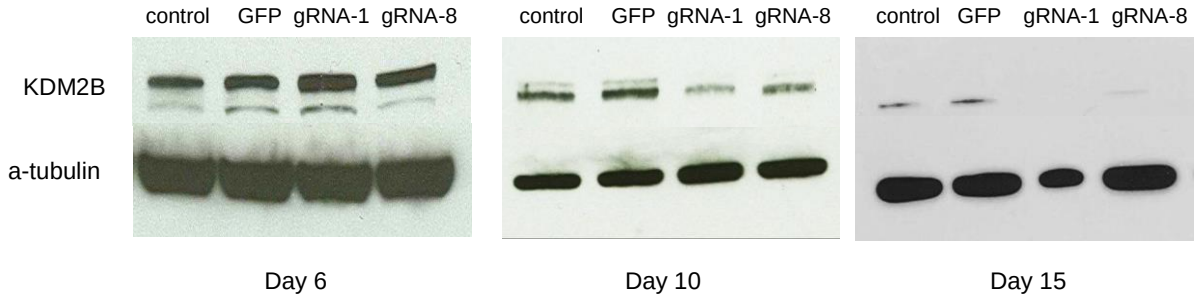


Figure 53. Western blot analysis of KDM2B in different time points in heterogeneous U87MG population infected with lentiviral gRNAs.

oligo name	*sequence*
2B_E2G8_for	CACCGACTTCGTGCACGCCATGGA
2B_E2G8_rev	AAACTCCATGGCGTGCACGAAGTC
2B_E2G8_gPCR_for	CTTGTGGGGAGATGAGGCAG
2B_E2G8_gPCR_rev	TAAGGGGGCATCGTCCCAAA
2B_E2G8_seq_for	CTCAGCCCTTCCATTTCAGC
2B_E2G8_seq_rev	TGAACCCAGTTCCAGCCAG
2B_E4G1_for	AAACAGACGTCAAACTCCTAGTGGC
2B_E4G1_rev	CACCGCCACTAGGAGTTTGACGTCT
2B_E4G1_gPCR_for	CTGACCCACCCCAGTTACAC
2B_E4G1_gPCR_rev	CTTGTACCCACCAAGAGGGC
2B_E4G1_seq_for	TGCCCCTCCACTATGTCTGT
2B_E4G1_seq_rev	GAACCCCAAGGAAGCAGGAG

Table 5. List of DNA sequences of gRNA oligos for cloning, gDNA primers used for diagnostic validations and gDNA sequencing primers for indel analysis.

Appendix II

Validation of RING1A as another hit in the shRNA screen

RING1A, an E3-ubiquitin ligase, the major component of PRC1 catalyzing ubiqutination of H2AK119, is the second consistent hit we obtained from the shRNA screen assessing the CMEs regulating TRAIL response of GBM cells. We first validated its knockdown by two separate shRNAs used in the screen (**Figure 54**). Secondly, we assessed effects of shRING1As on response of GBM cells to TRAIL, alone or in combination of shKDM2B (**Figure 55**). shRING1A-1 failed to give a repeated phenotype, whereas we observed significant sensitization of GBMs with shRING1A-2. We did not observe a synergistic effect when shRING1A is combined with shKDM2B, suggesting the observed sensitization phenotypes are already in the same axis. Further analysis by chromatin immunoprecipitation of RING1A/B and their corresponding suppressive mark H2AK119, along with ChIP against KDM2B, need to be performed to delineate the relationship between them.

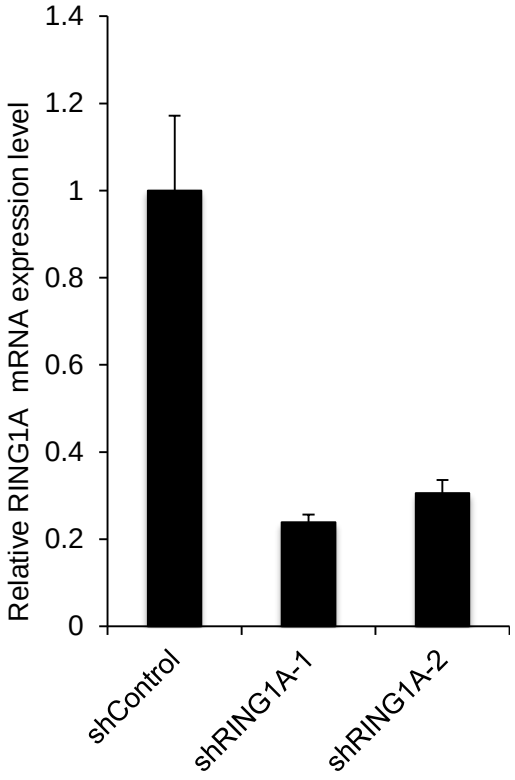


Figure 54. q-RT-PCR analysis of RING1A in infected GBM cells.

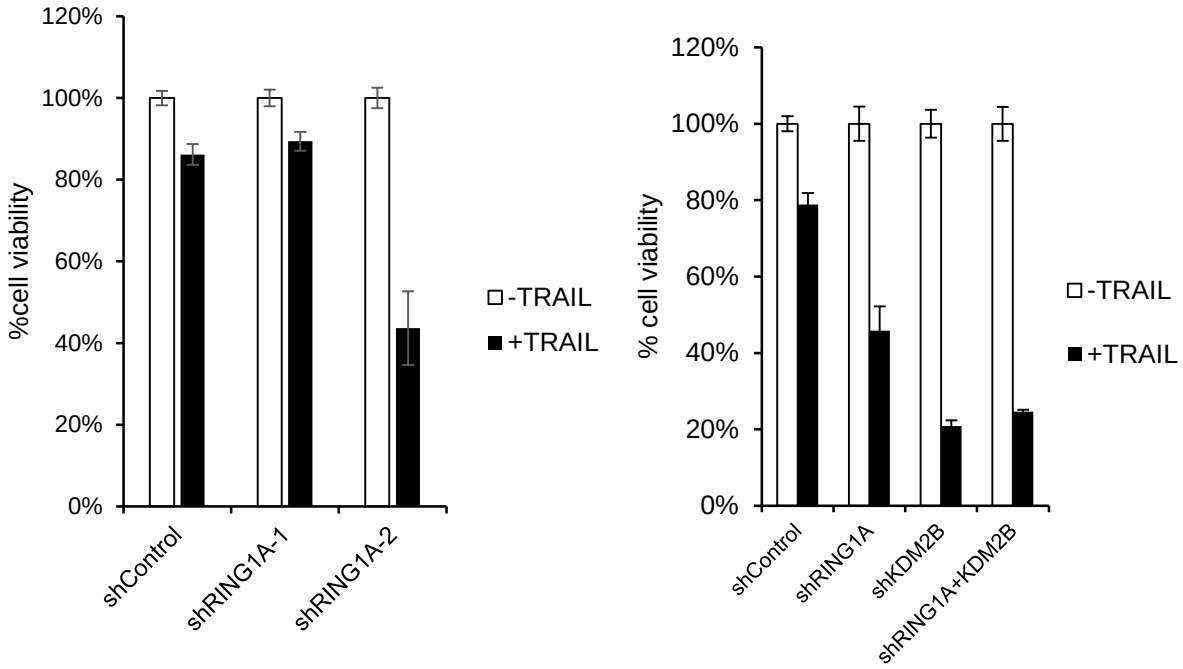


Figure 55. Cell viability analysis of RING1, KDM2B and combination silenced GBM cells upon TRAIL treatment

Appendix III

KDM2B interacts with CpG Islands of HRK

CxxC-ZF domain, by its zinc finger structure, allows KDM2B interact specifically with non-methylated CGIs found throughout genome [100]. We wanted to see whether KDM2B directly interacts with the deregulated apoptosis related genes. Hence, we conducted chromatin immunoprecipitation against KDM2B in U87MG cells and ran q-RT-PCR analysis to see fold enrichment of KDM2B on CGIs of HRK, our top deregulated gene as shown by RNA-seq analysis. We preliminarily observed that KDM2B interacts with CGIs of HRK, as compared to a control region bearing no known epigenetic modifications (**Figure 56**). The observed upregulation of HRK upon KDM2B loss could be due to the direct derepression of HRK, in the absence of KDM2B suppressing HRK's expression in normal conditions.

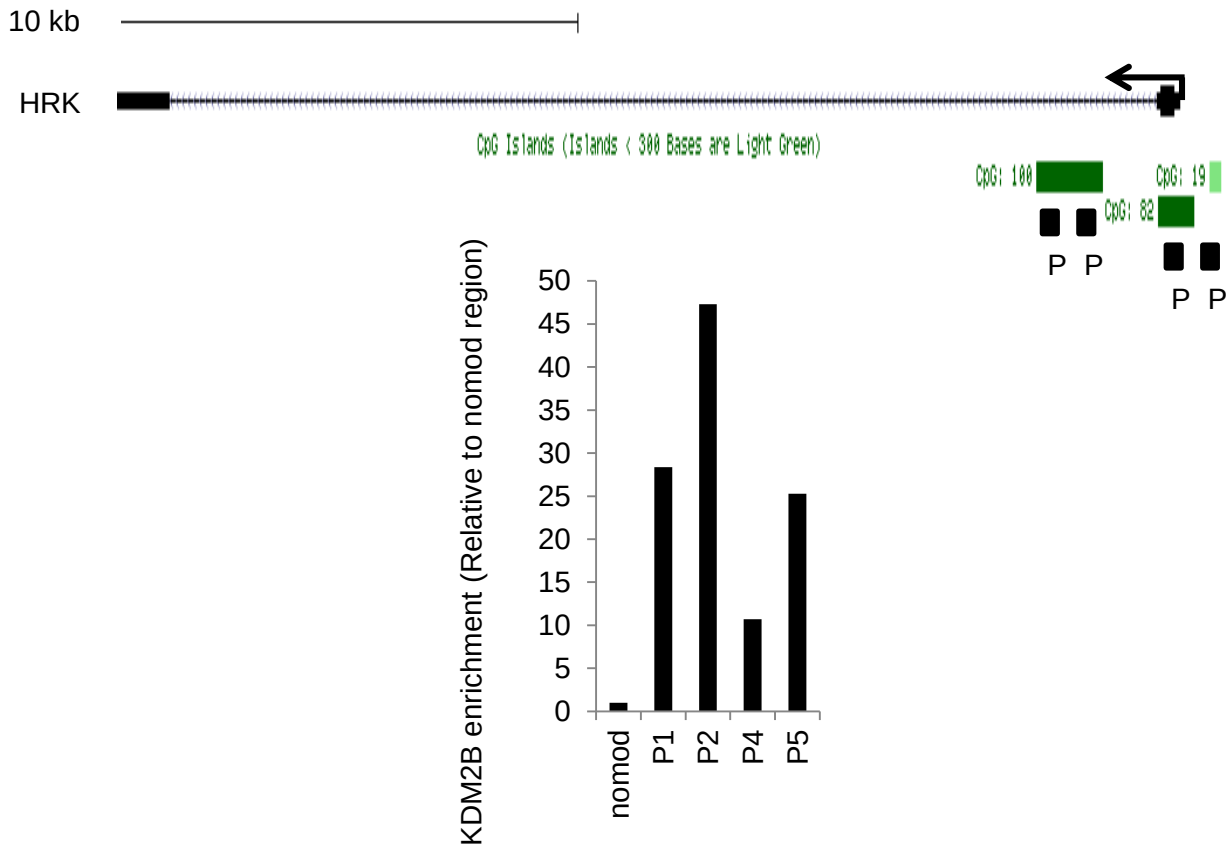


Figure 56. ChIP-qPCR analysis of CGIs of HRK against KDM2B

Appendix IV

Bcl-2 protects shKDM2B cells from TRAIL induced apoptosis

Bcl-2 is the main anti-apoptotic gatekeeper of the intrinsic apoptosis pathway [40]. It is found in the mitochondrial membrane act as an anti-apoptotic major player to keep cytochrome c in mitochondria. We wanted to see whether shKDM2B induced TRAIL sensitivity could be blocked by blocking of intrinsic apoptotic pathway. We observed that Bcl-2 overexpression was sufficient to protect almost all shKDM2B cells from TRAIL-induced apoptosis (**Figure 57**) as assessed by cell viability assay and fluorescent microscopy.

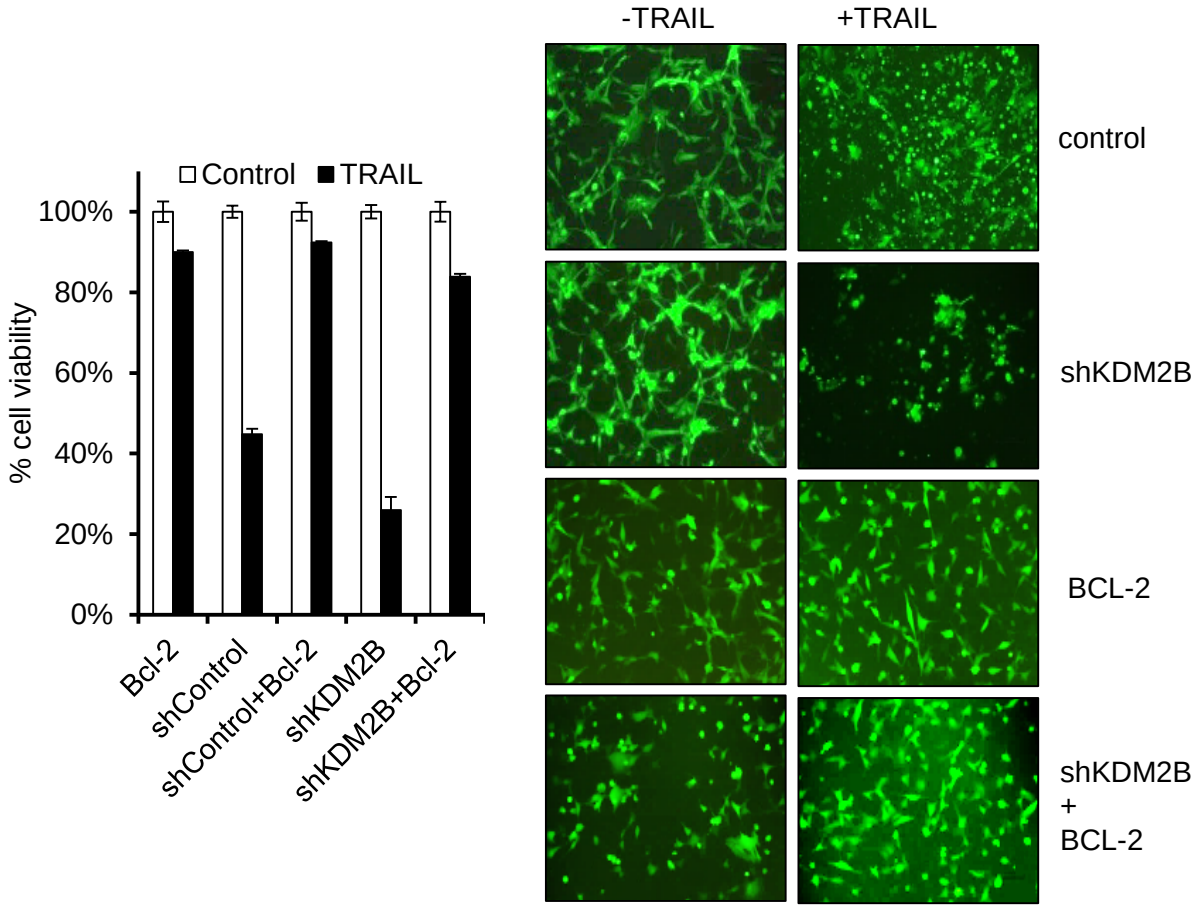


Figure 57. Cell viability analysis of BCL-2 over expressing shControl and shKDM2B GBM cells (left) and representative fluorescent images of the cells (right).

Appendix V

KDM2B and its regulation of senescence induced morphology

shKDM2B GBM cells (as shown in **Figure 46**) obtain flatter and larger morphology, compared to shControl cells. They loose their processes and become more epithelial-like cells (less motile and displaying reduced formation of clumps and foci in vitro). We observed the same phenotype in vivo in shKDM2B tumors as well. They were less spaced and more flat compared to shControl cells. In addition, they displayed increased basal levels of apoptosis. We failed to observe a change in cell cycle dynamics of shKDM2B cell population, however we were able to observe more senescence-induced beta-galactosidase expression in shKDM2B cells (**Figure 58-59**). Cell cycle analysis by PI staining should be repeated, since H202 control failed to work as well.

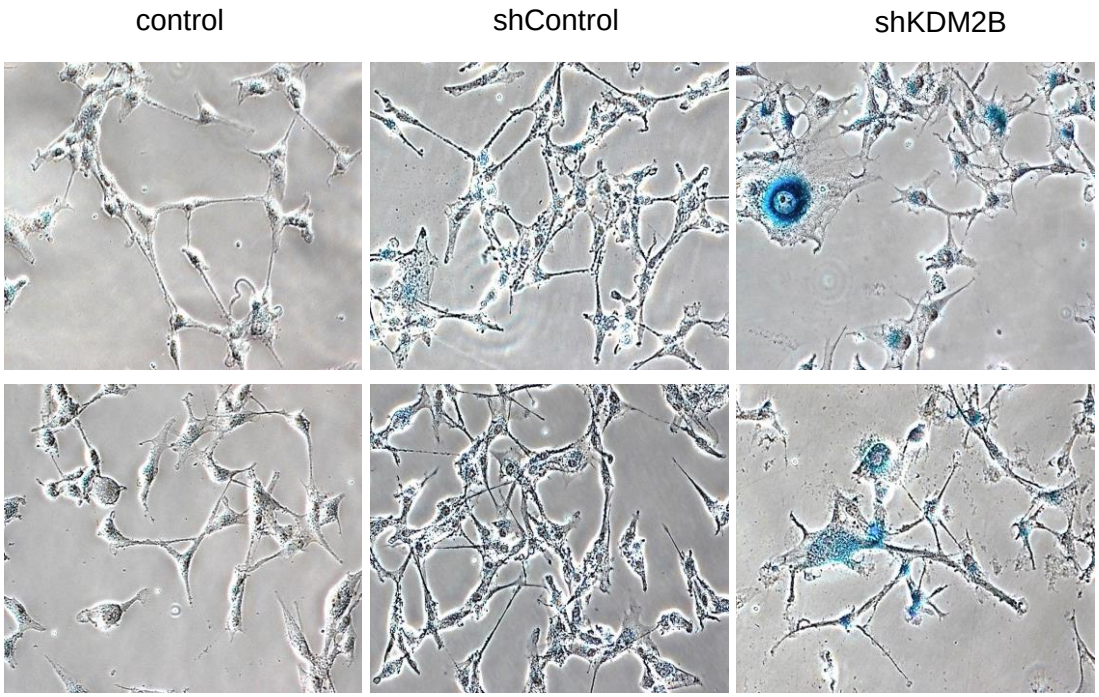


Figure 58. Representative images of X-gal staining of control, shControl and shKDM2B cells.

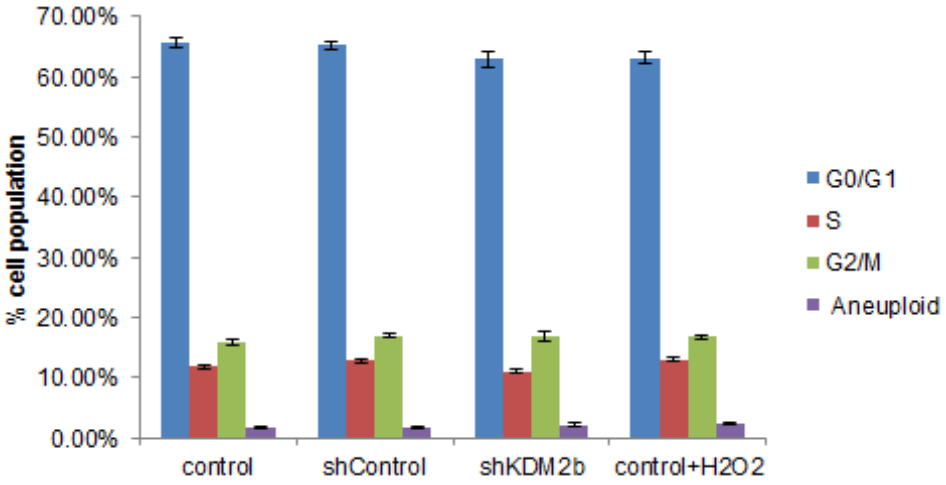


Figure 59. Cell cycle analysis of shKDM2B cells by flow cytometry

Appendix VI

Entinostat (MS-275) treatment downregulates KDM2B and upregulates HRK

Several histone deacetylase inhibitors (HDACi) have been approved by FDA and several of them are still in pre-clinical and clinical trials [116]. MS-275, one of such HDACi, has been shown by different research teams that it can sensitize GBMs to anti-cancer agents, such as TRAIL [87,117]. Different mechanisms has been shown and proposed for MS-275's sensitization, such as DR4/5 upregulation. However, the exact behind the sensitization mechanism has not yet been elucidated. Therefore, we wanted to test whether MS-275 sensitization could be related with KDM2B levels. We were surprised to see that upon MS-275 treatment, although cell were viable, KDM2B mRNA levels were downregulated to ~45 percent (n=3), whereas HRK levels were 2-3 time upregulated (n=2) (**Figure 60**).

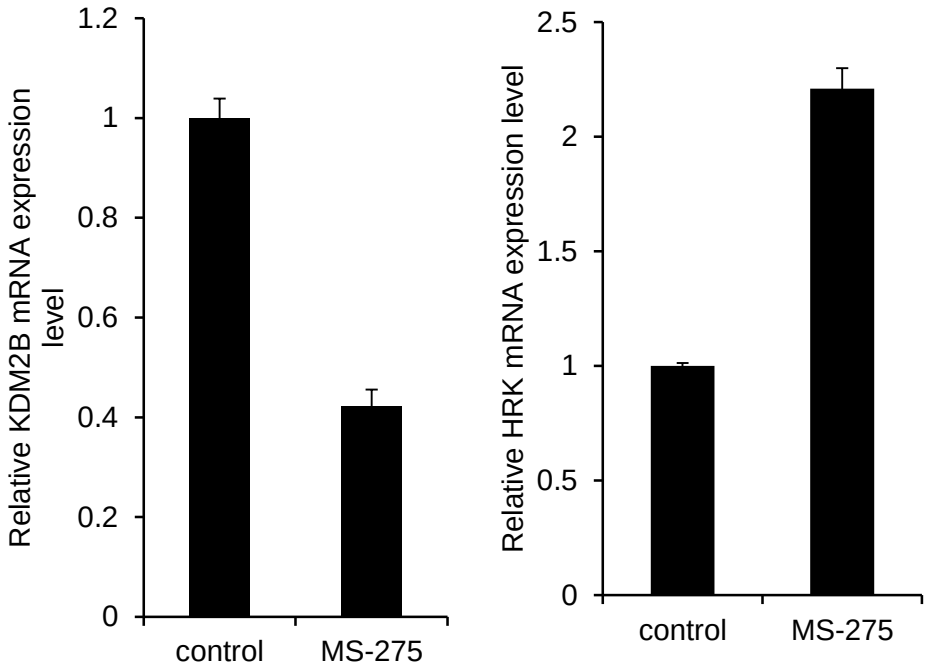


Figure 60. q-RT-PCR analysis of HRK and KDM2B in GBM cells treated with control medium or 5 uM MS-275 for 24 hours . KDM2B and HRK mRNA relative to GAPDH mRNA was calculated and relative expression was determined with ΔΔCt method.

Bibliography

[1] F.B. Furnari, T. Fenton, R.M. Bachoo, A. Mukasa, J.M. Stommel, A. Stegh, et al., Malignant astrocytic glioma: Genetics, biology, and paths to treatment, Genes Dev. 21 (2007) 2683–2710. doi:10.1101/gad.1596707.

[2] T.K. Owonikoko, J. Arbiser, A. Zelnak, H.-K.G. Shu, H. Shim, A.M. Robin, et al., Current approaches to the treatment of metastatic brain tumours., Nat. Rev. Clin. Oncol. 11 (2014) 203–22. doi:10.1038/nrclinonc.2014.25.

[3] D. Antonios, Extra-axial brain tumors, Eur. Radiol. 15 (2005) 453–467. doi:10.1007/s00330-004-2557-0.

[4] J.A. Schwartzbaum, J.L. Fisher, K.D. Aldape, M. Wrensch, Epidemiology and molecular pathology of glioma., Nat. Clin. Pract. Neurol. 2 (2006) 494–503; quiz 1 p following 516. doi:10.1038/ncpneuro0289.

[5] D.J. MacKenzie, A Classification of the Tumours of the Glioma Group on a Histogenetic Basis With a Correlated Study of Prognosis, Can. Med. Assoc. J. 16 (1926) 872. http://www.ncbi.nlm.nih.gov/pmc/articles/PMC1709238/ (accessed June 17, 2015).

[6] C. Jones, L. Perryman, D. Hargrave, Paediatric and adult malignant glioma: close relatives or distant cousins?, Nat. Rev. Clin. Oncol. 9 (2012) 400–13. doi:10.1038/nrclinonc.2012.87.

[7] D.N. Louis, H. Ohgaki, O.D. Wiestler, W.K. Cavenee, P.C. Burger, A. Jouvet, et al., The 2007 WHO classification of tumours of the central nervous system., Acta Neuropathol. 114 (2007) 97–109. doi:10.1007/s00401-007-0243-4.

[8] Y. Rong, D.L. Durden, E.G. Van Meir, D.J. Brat, “Pseudopalisading” necrosis in glioblastoma: a familiar morphologic feature that links vascular pathology, hypoxia, and angiogenesis., J. Neuropathol. Exp. Neurol. 65 (2006) 529–39. http://www.ncbi.nlm.nih.gov/pubmed/16783163 (accessed June 17, 2015).

[9] M.-D.-M. Inda, R. Bonavia, J. Seoane, Glioblastoma multiforme: a look inside its heterogeneous nature., Cancers (Basel). 6 (2014) 226–39. doi:10.3390/cancers6010226.

[10] S. Sathornsumetee, J.N. Rich, Designer therapies for glioblastoma multiforme, Ann. N. Y. Acad. Sci. 1142 (2008) 108–132. doi:10.1196/annals.1444.009.

[11] P.Y. Wen, S. Kesari, Malignant gliomas in adults., N. Engl. J. Med. 359 (2008) 1850; author reply 1850. doi:10.1056/NEJMc086380.

[12] A. Arcos, L. Romero, R. Serramito, J.M. Santín, A. Prieto, M. Gelabert, et al., Multicentric glioblastoma multiforme . Report of 3 cases , clinical and pathological study and literature review, 3 (2012) 211–215.

[13] A. Moiyadi, P. Syed, S. Srivastava, Fluorescence-guided surgery of malignant gliomas based on 5-aminolevulinic acid: paradigm shifts but not a panacea., Nat. Rev. Cancer. 14 (2014) 146. doi:10.1038/nrc3566-c1.

[14] R.K. Jain, E. di Tomaso, D.G. Duda, J.S. Loeffler, a G. Sorensen, T.T. Batchelor, Angiogenesis in brain tumours., Nat. Rev. Neurosci. 8 (2007) 610–22. doi:10.1038/nrn2175.

[15] G. Iacob, E.B. Dinca, Current data and strategy in glioblastoma multiforme., J. Med. Life. 2 (2009) 386–93. http://www.pubmedcentral.nih.gov/articlerender.fcgi?artid=3019011&tool=pmcentrez&rendertype=abstract (accessed June 18, 2015).

[16] M.S. Ahluwalia, Chemotherapy for Brain Tumors, Sixth Edit, Elsevier Inc., 2012. doi:10.1016/B978-1-4160-6839-6.10007-3.

[17] A. Noack, S. Noack, A. Hoffmann, K. Maalouf, M. Buettner, P.-O. Couraud, et al., Drug-induced trafficking of p-glycoprotein in human brain capillary endothelial cells as demonstrated by exposure to mitomycin C., PLoS One. 9 (2014) e88154. doi:10.1371/journal.pone.0088154.

[18] J. Zhou, K.-B. Atsina, B.T. Himes, G.W. Strohbehn, W.M. Saltzman, Novel delivery strategies for glioblastoma., Cancer J. 18 (2012) 89–99. doi:10.1097/PPO.0b013e318244d8ae.

[19] A.E. Pegg, M.E. Dolan, R.C. Moschel, Structure, function, and inhibition of O6-alkylguanine-DNA alkyltransferase., Prog. Nucleic Acid Res. Mol. Biol. 51 (1995) 167–223. http://www.ncbi.nlm.nih.gov/pubmed/7659775 (accessed June 18, 2015).

[20] E. Jesien-Lewandowicz, D. Jesionek-Kupnicka, I. Zawlik, M. Szybka, D. Kulczycka-Wojdala, P. Rieske, et al., High incidence of MGMT promoter methylation in primary glioblastomas without correlation with TP53 gene mutations., Cancer Genet. Cytogenet. 188 (2009) 77–82. doi:10.1016/j.cancergencyto.2008.09.015.

[21] R. Martínez, Beyond Genetics in Glioma Pathways: The Ever-Increasing Crosstalk between Epigenomic and Genomic Events, J. Signal Transduct. 2012 (2012) 1–9. doi:10.1155/2012/519807.

[22] The Cancer Genome Atlas Research Network, Comprehensive genomic characterization defines human glioblastoma genes and core pathways., Nature. 455 (2008) 1061–8. doi:10.1038/nature07385.

[23] Y. Chen, F. Hu, Y. Zhou, W. Chen, H. Shao, Y. Zhang, MGMT promoter methylation and glioblastoma prognosis: a systematic review and meta-analysis., Arch. Med. Res. 44 (2013) 281–90. doi:10.1016/j.arcmed.2013.04.004.

[24] B.E. Johnson, T. Mazor, C. Hong, M. Barnes, K. Aihara, C.Y. McLean, et al., Mutational analysis reveals the origin and therapy-driven evolution of recurrent glioma., Science. 343 (2014) 189–93. doi:10.1126/science.1239947.

[25] A.L. Cohen, S.L. Holmen, H. Colman, IDH1 and IDH2 mutations in gliomas., Curr. Neurol. Neurosci. Rep. 13 (2013) 345. doi:10.1007/s11910-013-0345-4.

[26] M.R. Gilbert, Y. Liu, J. Neltner, H. Pu, A. Morris, M. Sunkara, et al., Autophagy and oxidative stress in gliomas with IDH1 mutations., Acta Neuropathol. 127 (2014) 221–33. doi:10.1007/s00401-013-1194-6.

[27] S. Turcan, D. Rohle, A. Goenka, L. a Walsh, F. Fang, E. Yilmaz, et al., IDH1 mutation is sufficient to establish the glioma hypermethylator phenotype., Nature. 483 (2012) 479–83. doi:10.1038/nature10866.

[28] Q. SongTao, Y. Lei, G. Si, D. YanQing, H. HuiXia, Z. XueLin, et al., IDH mutations predict longer survival and response to temozolomide in secondary glioblastoma., Cancer Sci. 103 (2012) 269–73. doi:10.1111/j.1349-7006.2011.02134.x.

[29] G.P. Pfeifer, S. Kadam, S.-G. Jin, 5-hydroxymethylcytosine and its potential roles in development and cancer., Epigenetics Chromatin. 6 (2013) 10. doi:10.1186/1756-8935-6-10.

[30] D. Kanduc, A. Mittelman, R. Serpico, E. Sinigaglia, A.A. Sinha, C. Natale, et al., Cell death: apoptosis versus necrosis (review)., Int. J. Oncol. 21 (2002) 165–70. http://www.ncbi.nlm.nih.gov/pubmed/12063564 (accessed April 24, 2015).

[31] P. Meier, A. Finch, G. Evan, Apoptosis in development., Nature. 407 (2000) 796–801. doi:10.1038/35037734.

[32] J.C. Martinou, M. Dubois-Dauphin, J.K. Staple, I. Rodriguez, H. Frankowski, M. Missotten, et al., Overexpression of BCL-2 in transgenic mice protects neurons from naturally occurring cell death and experimental ischemia., Neuron. 13 (1994) 1017–30. http://www.ncbi.nlm.nih.gov/pubmed/7946326 (accessed June 18, 2015).

[33] R. Merino, Y. Gañán, D. Macias, J. Rodríguez-León, J.M. Hurle, Bone morphogenetic proteins regulate interdigital cell death in the avian embryo., Ann. N. Y. Acad. Sci. 887 (1999) 120–32. http://www.ncbi.nlm.nih.gov/pubmed/10668469 (accessed June 18, 2015).

[34] T.T. Rohn, E. Head, W.H. Nesse, C.W. Cotman, D.H. Cribbs, Activation of caspase-8 in the Alzheimer's disease brain., Neurobiol. Dis. 8 (2001) 1006–1016. doi:10.1006/nbdi.2001.0449.

[35] C.R. Casella, T.H. Finkel, Mechanisms of lymphocyte killing by HIV., Curr. Opin. Hematol. 4 (1997) 24–31. doi:10.1097/00062752-199704010-00005.

[36] D. Hanahan, R.A. Weinberg, The hallmarks of cancer., Cell. 100 (2000) 57–70. http://www.ncbi.nlm.nih.gov/pubmed/10647931 (accessed July 10, 2014).

[37] T.J. Fan, L.H. Han, R.S. Cong, J. Liang, Caspase family proteases and apoptosis, Acta Biochim. Biophys. Sin. (Shanghai). 37 (2005) 719–727. doi:10.1111/j.1745-7270.2005.00108.x.

[38] E.M. Michalak, A. Villunger, J.M. Adams, A. Strasser, In several cell types tumour suppressor p53 induces apoptosis largely via Puma but Noxa can contribute., Cell Death Differ. 15 (2008) 1019–1029. doi:10.1038/cdd.2008.16.

[39] A. Letai, Pharmacological manipulation of Bcl-2 family members to control cell death., J. Clin. Invest. 115 (2005) 2648–2655. doi:10.1172/JCI26250.

[40] L. Coultas, A. Strasser, The role of the Bcl-2 protein family in cancer, Semin. Cancer Biol. 13 (2003) 115–123. doi:10.1016/S1044-579X(02)00129-3.

[41] A.M. Chinnaiyan, The apoptosome: heart and soul of the cell death machine., Neoplasia. 1 (1999) 5–15.

[42] G. van Loo, X. Saelens, M. van Gurp, M. MacFarlane, S.J. Martin, P. Vandenabeele, The role of mitochondrial factors in apoptosis: a Russian roulette with more than one bullet., Cell Death Differ. 9 (2002) 1031–1042. doi:10.1038/sj.cdd.4401088.

[43] S. Nagata, Apoptotic DNA fragmentation., Exp. Cell Res. 256 (2000) 12–18. doi:10.1006/excr.2000.4834.

[44] A. Ashkenazi, Directing cancer cells to self-destruct with pro-apoptotic receptor agonists., Nat. Rev. Drug Discov. 7 (2008) 1001–12. doi:10.1038/nrd2637.

[45] S. Fulda, Tumor resistance to apoptosis, Int. J. Cancer. 124 (2009) 511–515. doi:10.1002/ijc.24064.

[46] A. Ashkenazi, Targeting death and decoy receptors of the tumour-necrosis factor superfamily., Nat. Rev. Cancer. 2 (2002) 420–30. doi:10.1038/nrc821.

[47] C. Plass, S.M. Pfister, A.M. Lindroth, O. Bogatyrova, R. Claus, P. Lichter, Mutations in regulators of the epigenome and their connections to global chromatin patterns in cancer., Nat. Rev. Genet. 14 (2013) 765–80. doi:10.1038/nrg3554.

[48] L. Liu, X. Yu, X. Guo, Z. Tian, M. Su, Y. Long, et al., miR-143 is downregulated in cervical cancer and promotes apoptosis and inhibits tumor formation by targeting Bcl-2., Mol. Med. Rep. 5 (2012) 753–60. doi:10.3892/mmr.2011.696.

[49] F. Ji, H. Zhang, Y. Wang, M. Li, W. Xu, Y. Kang, et al., MicroRNA-133a, downregulated in osteosarcoma, suppresses proliferation and promotes apoptosis by targeting Bcl-xL and Mcl-1., Bone. 56 (2013) 220–6. doi:10.1016/j.bone.2013.05.020.

[50] M.M. van Noesel, S. van Bezouw, G.S. Salomons, P.A. Voûte, R. Pieters, S.B. Baylin, et al., Tumor-specific down-regulation of the tumor necrosis factor-related apoptosis-inducing ligand decoy receptors DcR1 and DcR2 is associated with dense promoter hypermethylation., Cancer Res. 62 (2002) 2157–61. http://www.ncbi.nlm.nih.gov/pubmed/11929838 (accessed June 18, 2015).

[51] I. Petak, R.P. Danam, D.M. Tillman, R. Vernes, S.R. Howell, L. Berczi, et al., Hypermethylation of the gene promoter and enhancer region can regulate Fas expression and sensitivity in colon carcinoma., Cell Death Differ. 10 (2003) 211–7. doi:10.1038/sj.cdd.4401132.

[52] M.L. Suvà, N. Riggi, B.E. Bernstein, Epigenetic reprogramming in cancer., Science. 339 (2013) 1567–70. doi:10.1126/science.1230184.

[53] D. Hanahan, R.A. Weinberg, Hallmarks of cancer: The next generation, Cell. 144 (2011) 646–674. doi:10.1016/j.cell.2011.02.013.

[54] K. Grønbæk, C. Hother, P. a. Jones, Epigenetic changes in cancer, Apmis. 115 (2007) 1039–1059. doi:10.1111/j.1600-0463.2007.apm_636.xml.x.

[55] C.L. Peterson, M.-A. Laniel, Histones and histone modifications., Curr. Biol. 14 (2004) R546–51. doi:10.1016/j.cub.2004.07.007.

[56] S.M. Kooistra, K. Helin, Molecular mechanisms and potential functions of histone demethylases., Nat. Rev. Mol. Cell Biol. 13 (2012) 297–311. doi:10.1038/nrm3327.

[57] A. Janzer, K. Stamm, A. Becker, A. Zimmer, R. Buettner, J. Kirfel, The H3K4me3 histone demethylase Fbxl10 is a regulator of chemokine expression, cellular morphology, and the metabolome of fibroblasts, J. Biol. Chem. 287 (2012) 30984–92. doi:10.1074/jbc.M112.341040.

[58] L. Morey, A. Santanach, L. Di Croce, Pluripotency and epigenetic factors in mouse embryonic stem cell fate regulation., Mol. Cell. Biol. (2015) MCB.00266–15–. doi:10.1128/MCB.00266-15.

[59] T. Ueda, A. Nagamachi, K. Takubo, N. Yamasaki, H. Matsui, A. Kanai, et al., Fbxl10 overexpression in murine hematopoietic stem cells induces leukemia involving metabolic activation and upregulation of Nsg2., Blood. 125 (2015) 3437–46. doi:10.1182/blood-2014-03-562694.

[60] E.J. Wagner, P.B. Carpenter, A. Manuscript, Understanding te language of Lys36 methylation at histone H3, Nat. Rev. Mol. Cell Biol. 29 (2012) 997–1003. doi:10.1016/j.biotechadv.2011.08.021.Secreted.

[61] M. Rodríguez-Paredes, M. Esteller, Cancer epigenetics reaches mainstream oncology., Nat. Med. 17 (2011) 330–9. doi:10.1038/nm.2305.

[62] V.O. Kaminskyyy, O. V. Surovay, A. Vaculova, B. Zhivotovsky, Combined inhibition of DNA methyltransferase and histone deacetylase restores caspase-8 expression and sensitizes SCLC cells to TRAIL, Carcinogenesis. 32 (2011) 1450–1458. doi:10.1093/carcin/bgr135.

[63] D. Rotili, A. Mai, Targeting Histone Demethylases: A New Avenue for the Fight against Cancer., Genes Cancer. 2 (2011) 663–79. doi:10.1177/1947601911417976.

[64] X.-S. Shu, L. Li, Q. Tao, Chromatin regulators with tumor suppressor properties and their alterations in human cancers., Epigenomics. 4 (2012) 537–49. doi:10.2217/epi.12.50.

[65] S.-H. Song, S.-W. Han, Y.-J. Bang, Epigenetic-based therapies in cancer: progress to date., Drugs. 71 (2011) 2391–403. doi:10.2165/11596690-000000000-00000.

[66] K. Helin, D. Dhanak, Chromatin proteins and modifications as drug targets., Nature. 502 (2013) 480–8. doi:10.1038/nature12751.

[67] R. Thakur, D.P. Mishra, Modulation of cell death pathways in cancer stem cells: Targeting histone demethylases, Adv. Biosci. Biotechnol. 03 (2012) 720–730. doi:10.4236/abb.2012.326093.

[68] Y. He, I. Korboukh, J. Jin, J. Huang, Targeting protein lysine methylation and demethylation in cancers, Acta Biochim. Biophys. Sin. (Shanghai). 44 (2011) 70–79. doi:10.1093/abbs/gmr109.

[69] R. Thakur, Modulation of cell death pathways in cancer stem cells: Targeting histone demethylases, Adv. Biosci. Biotechnol. 03 (2012) 720–730. doi:10.4236/abb.2012.326093.

[70] G. Liang, J. He, Y. Zhang, Kdm2b promotes induced pluripotent stem cell generation by facilitating gene activation early in reprogramming., Nat. Cell Biol. 14 (2012) 457–66. doi:10.1038/ncb2483.

[71] C. Sánchez, I. Sánchez, J. a a Demmers, P. Rodriguez, J. Strouboulis, M. Vidal, Proteomics analysis of Ring1B/Rnf2 interactors identifies a novel complex with the Fbxl10/Jhdm1B histone demethylase and the Bcl6 interacting corepressor., Mol. Cell. Proteomics. 6 (2007) 820–34. doi:10.1074/mcp.M600275-MCP200.

[72] A.M. Farcas, N.P. Blackledge, I. Sudbery, H.K. Long, J.F. McGouran, N.R. Rose, et al., KDM2B links the Polycomb Repressive Complex 1 (PRC1) to recognition of CpG islands., Elife. 1 (2012) e00205. doi:10.7554/eLife.00205.

[73] X. Wu, J.V. Johansen, K. Helin, Fbxl10/Kdm2b recruits polycomb repressive complex 1 to CpG islands and regulates H2A ubiquitylation., Mol. Cell. 49 (2013) 1134–46. doi:10.1016/j.molcel.2013.01.016.

[74] N.P. Blackledge, A.M. Farcas, T. Kondo, H.W. King, J.F. McGouran, L.L.P. Hanssen, et al., Variant PRC1 complex-dependent H2A ubiquitylation drives PRC2 recruitment and polycomb domain formation, Cell. 157 (2014) 1445–1459. doi:10.1016/j.cell.2014.05.004.

[75] J. He, L. Shen, M. Wan, O. Taranova, H. Wu, Y. Zhang, Kdm2b maintains murine embryonic stem cell status by recruiting PRC1 complex to CpG islands of developmental genes., Nat. Cell Biol. 15 (2013) 373–84. doi:10.1038/ncb2702.

[76] T. Suzuki, K. Minehata, K. Akagi, N.A. Jenkins, N.G. Copeland, Tumor suppressor gene identification using retroviral insertional mutagenesis in Blm-deficient mice., EMBO J. 25 (2006) 3422–31. doi:10.1038/sj.emboj.7601215.

[77] R. Pfau, A. Tzatsos, S.C. Kampranis, O.B. Serebrennikova, S.E. Bear, P.N. Tsichlis, Members of a family of JmjC domain-containing oncoproteins immortalize embryonic fibroblasts via a JmjC domain-dependent process., Proc. Natl. Acad. Sci. U. S. A. 105 (2008) 1907–12. doi:10.1073/pnas.0711865105.

[78] D. Frescas, D. Guardavaccaro, F. Bassermann, R. Koyama-Nasu, M. Pagano, JHDM1B/FBXL10 is a nucleolar protein that represses transcription of ribosomal RNA genes., Nature. 450 (2007) 309–13. doi:10.1038/nature06255.

[79] J. He, A.T. Nguyen, Y. Zhang, KDM2b/JHDM1b, an H3K36me2-specific demethylase, is required for initiation and maintenance of acute myeloid leukemia., Blood. 117 (2011) 3869–80. doi:10.1182/blood-2010-10-312736.

[80] A. Tzatsos, P. Paskaleva, F. Ferrari, V. Deshpande, S. Stoykova, G. Contino, et al., KDM2B promotes pancreatic cancer via Polycomb-dependent and -independent transcriptional programs, (2013). doi:10.1172/JCI64535.function.

[81] J. He, E.M. Kallin, Y.-I. Tsukada, Y. Zhang, The H3K36 demethylase Jhdm1b/Kdm2b regulates cell proliferation and senescence through p15(Ink4b)., Nat. Struct. Mol. Biol. 15 (2008) 1169–75. doi:10.1038/nsmb.1499.

[82] A. Tzatsos, R. Pfau, S.C. Kampranis, P.N. Tsichlis, Ndy1 / KDM2B immortalizes mouse embryonic fibroblasts by repressing the Ink4a / Arf locus, Sci. York. 106 (2009) 2641–2646. doi:10.1073/pnas.0813139106.

[83] A. Tzatsos, P. Paskaleva, S. Lymperi, G. Contino, S. Stoykova, Z. Chen, et al., Lysine-specific demethylase 2b (KDM2B)-let-7-enhancer of zester homolog 2 (EZH2) pathway regulates cell cycle progression and senescence in primary cells, J. Biol. Chem. 286 (2011) 33061–33069. doi:10.1074/jbc.M111.257667.

[84] E. Karoopongse, C. Yeung, J. Byon, A. Ramakrishnan, Z.J. Holman, P.Y.Z. Jiang, et al., The KDM2B- Let-7b -EZH2 Axis in Myelodysplastic Syndromes as a Target for Combined Epigenetic Therapy, PLoS One. 9 (2014) e107817. doi:10.1371/journal.pone.0107817.

[85] R. Gao, R. Dong, J. Du, P. Ma, S. Wang, Z. Fan, Depletion of histone demethylase KDM2A inhibited cell proliferation of stem cells from apical papilla by de-repression of p15INK4B and p27Kip1., Mol. Cell. Biochem. 379 (2013) 115–22. doi:10.1007/s11010-013-1633-7.

[86] F. Kottakis, P. Foltopoulou, I. Sanidas, P. Keller, A. Wronski, B.T. Dake, et al., NDY1/KDM2B functions as a master regulator of polycomb complexes and controls self-renewal of breast cancer stem cells, Cancer Res. 74 (2014) 3935–3946. doi:10.1158/0008-5472.CAN-13-2733.

[87] T. Bagci-Onder, A. Agarwal, D. Flusberg, S. Wanningen, P. Sorger, K. Shah, Real-time imaging of the dynamics of death receptors and therapeutics that overcome TRAIL resistance in tumors., Oncogene. 32 (2013) 2818–27. doi:10.1038/onc.2012.304.

[88] T. Bagci-Onder, H. Wakimoto, M. Anderegg, C. Cameron, K. Shah, A dual PI3K/mTOR inhibitor, PI-103, cooperates with stem cell-delivered TRAIL in experimental glioma models., Cancer Res. 71 (2011) 154–63. doi:10.1158/0008-5472.CAN-10-1601.

[89] S.H. Kim, K. Kim, J.G. Kwagh, D.T. Dicker, M. Herlyn, A.K. Rustgi, et al., Death induction by recombinant native TRAIL and its prevention by a caspase 9 inhibitor in primary human esophageal epithelial cells, J. Biol. Chem. 279 (2004) 40044–40052. doi:10.1074/jbc.M404541200.

[90] T.T. Onder, N. Kara, A. Cherry, A.U. Sinha, N. Zhu, K.M. Bernt, et al., Chromatin-modifying enzymes as modulators of reprogramming, Nature. 483 (2012) 598–602. doi:10.1038/nature10953.

[91] Abcam, Histone extraction protocol for western blot, (n.d.). http://www.abcam.com/protocols/histone-extraction-protocol-for-western-blot (accessed January 1, 2015).

[92] D. Kim, G. Pertea, C. Trapnell, H. Pimentel, R. Kelley, S.L. Salzberg, TopHat2: accurate alignment of transcriptomes in the presence of insertions, deletions and gene fusions., Genome Biol. 14 (2013) R36. doi:10.1186/gb-2013-14-4-r36.

[93] M. Lawrence, W. Huber, H. Pagès, P. Aboyoun, M. Carlson, R. Gentleman, et al., Software for Computing and Annotating Genomic Ranges, PLoS Comput. Biol. 9 (2013). doi:10.1371/journal.pcbi.1003118.

[94] S. Anders, W. Huber, Differential expression analysis for sequence count data., Genome Biol. 11 (2010) R106. doi:10.1186/gb-2010-11-10-r106.

[95] M. Adli, B.E. Bernstein, Whole-genome chromatin profiling from limited numbers of cells using nano-ChIP-seq., Nat. Protoc. 6 (2011) 1656–68. doi:10.1038/nprot.2011.402.

[96] Y. Tomaru, C. Simon, A.R. Forrest, H. Miura, A. Kubosaki, Y. Hayashizaki, et al., Regulatory interdependence of myeloid transcription factors revealed by Matrix RNAi analysis., Genome Biol. 10 (2009) R121. doi:10.1186/gb-2009-10-11-r121.

[97] M. D'Antonio, R.F. Guerra, M. Cereda, S. Marchesi, F. Montani, F. Nicassio, et al., Recessive cancer genes engage in negative genetic interactions with their functional paralogs., Cell Rep. 5 (2013) 1519–26. doi:10.1016/j.celrep.2013.11.033.

[98] P. Kitzmann, J. Schwirz, C. Schmitt-Engel, G. Bucher, RNAi phenotypes are influenced by the genetic background of the injected strain., BMC Genomics. 14 (2013) 5. doi:10.1186/1471-2164-14-5.

[99] S. Fulda, K.-M. Debatin, Extrinsic versus intrinsic apoptosis pathways in anticancer chemotherapy., Oncogene. 25 (2006) 4798–811. doi:10.1038/sj.onc.1209608.

[100] H.K. Long, N.P. Blackledge, R.J. Klose, ZF-CxxC domain-containing proteins, CpG islands and the chromatin connection., Biochem. Soc. Trans. 41 (2013) 727–40. doi:10.1042/BST20130028.

[101] O. Mueller, A. Schroeder, RNA Integrity Number (RIN) – Standardization of RNA Quality Control Application, Nano. (2004) 1–8.

[102] A. Schroeder, O. Mueller, S. Stocker, R. Salowsky, M. Leiber, M. Gassmann, et al., The RIN: an RNA integrity number for assigning integrity values to RNA measurements., BMC Mol. Biol. 7 (2006) 3. doi:10.1186/1471-2199-7-3.

[103] UCI Genomics High Throughput Facility, Illumina HT DNA Sequencing Guidelines, (n.d.). http://ghtf.biochem.uci.edu/content/illumina-guidelines (accessed June 19, 2015).

[104] N. Inohara, L. Ding, S. Chen, G. Núñez, Harakiri, a novel regulator of cell death, encodes a protein that activates apoptosis and interacts selectively with survival-promoting proteins Bcl-2 and Bcl-X(L), EMBO J. 16 (1997) 1686–1694. doi:10.1093/emboj/16.7.1686.

[105] M. Vidal, Role of polycomb proteins Ring1A and Ring1B in the epigenetic regulation of gene expression, Int. J. Dev. Biol. 53 (2009) 355–370. doi:10.1387/ijdb.082690mv.

[106] Z. Wang, P. Liu, H. Inuzuka, W. Wei, Roles of F-box proteins in cancer., Nat. Rev. Cancer. 14 (2014) 233–47. doi:10.1038/nrc3700.

[107] B. Badie, C.S. Goh, J. Klaver, H. Herweijer, D.A. Boothman, Combined radiation and p53 gene therapy of malignant glioma cells., Cancer Gene Ther. 6 155–62. doi:10.1038/sj.cgt.7700009.

[108] J. Huang, R. Sengupta, A.B. Espejo, M.G. Lee, J.A. Dorsey, M. Richter, et al., p53 is regulated by the lysine demethylase LSD1., Nature. 449 (2007) 105–8. doi:10.1038/nature06092.

[109] R. Hamamoto, V. Saloura, Y. Nakamura, Critical roles of non-histone protein lysine methylation in human tumorigenesis, Nat. Rev. Cancer. 15 (2015) 110–124. doi:10.1038/nrc3884.

[110] S. Yamanaka, Elite and stochastic models for induced pluripotent stem cell generation., Nature. 460 (2009) 49–52. doi:10.1038/nature08180.

[111] Y.D. Benoit, K.B. Laursen, M.S. Witherspoon, S.M. Lipkin, L.J. Gudas, Inhibition of PRC2 histone methyltransferase activity increases TRAIL-mediated apoptosis sensitivity in human colon cancer cells., J. Cell. Physiol. 228 (2013) 764–72. doi:10.1002/jcp.24224.

[112] M. Ku, R.P. Koche, E. Rheinbay, E.M. Mendenhall, M. Endoh, T.S. Mikkelsen, et al., Genomewide analysis of PRC1 and PRC2 occupancy identifies two classes of bivalent domains., PLoS Genet. 4 (2008) e1000242. doi:10.1371/journal.pgen.1000242.

[113] T. Bagci-Onder, Neural Stem Cells as Therapeutic Delivery Vehicles for Malignant Brain Tumors, in: K. Turksen (Ed.), Stem Cells Curr. Challenges New Dir., Springer New York, New York, NY, 2013: pp. 253–278. doi:10.1007/978-1-4614-8066-2.

[114] T. Bagci-Onder, W. Du, J.-L. Figueiredo, J. Martinez-Quintanilla, K. Shah, Targeting breast to brain metastatic tumours with death receptor ligand expressing therapeutic stem cells, Brain. 138 (2015) 1710–1721. doi:10.1093/brain/awv094.

[115] O. Shalem, N.E. Sanjana, E. Hartenian, X. Shi, D. a Scott, T.S. Mikkelsen, et al., Genome-scale CRISPR-Cas9 knockout screening in human cells., Science. 343 (2014) 84–7. doi:10.1126/science.1247005.

[116] H.-J. Kim, S.-C. Bae, Histone deacetylase inhibitors: molecular mechanisms of action and clinical trials as anti-cancer drugs., Am. J. Transl. Res. 3 (2011) 166–79. http://www.pubmedcentral.nih.gov/articlerender.fcgi?artid=3056563&tool=pmcentrez&rendertype=abstract (accessed June 19, 2015).

[117] A. Bangert, S. Häcker, S. Cristofanon, K.-M. Debatin, S. Fulda, Chemosensitization of glioblastoma cells by the histone deacetylase inhibitor MS275., Anticancer. Drugs. 22 (2011) 494–9. doi:10.1097/CAD.0b013e32834631e0.

Vita

İbrahim Çağrı Kurt was born in Istanbul, Turkey in 1990. He attended Kadiköy Anatolian High school in İstanbul between 2004 and 2009. In 2011, as a junior undergraduate he had the privilege to study at University of California Santa Cruz, USA for a year. In 2013, he received his Bachelor of Science degree in Molecular Biology and Genetics from Bilkent University in Ankara, Turkey. In 2013, he started his Research and Teaching assistant position in Koç University School of Medicine as a part of Graduate School of Science and Engineering Master of Science program.